


11-16-2009

PEGylation of Niosomes

John A. Elliott

University of South Florida

Follow this and additional works at: <http://scholarcommons.usf.edu/etd>

 Part of the [American Studies Commons](#), [Biomedical Engineering and Bioengineering Commons](#), and the [Chemical Engineering Commons](#)

Scholar Commons Citation

Elliott, John A., "PEGylation of Niosomes" (2009). *Graduate Theses and Dissertations*.
<http://scholarcommons.usf.edu/etd/3448>

This Dissertation is brought to you for free and open access by the Graduate School at Scholar Commons. It has been accepted for inclusion in Graduate Theses and Dissertations by an authorized administrator of Scholar Commons. For more information, please contact scholarcommons@usf.edu.

PEGylation of Niosomes

by

John A. Elliott

A dissertation submitted in partial fulfillment
of the requirements for the degree of
Doctor of Philosophy
Department of Chemical and Biomedical Engineering
College of Engineering
University of South Florida

Co-Major Professor: Michael VanAuker, Ph.D.

Co-Major Professor: Mark Jaroszeski, Ph.D.

Joel Strom, M.D.

Nathan Gallant, Ph.D.

Ryan Toomey, Ph.D.

Karl Muffly, Ph.D.

John Wolan, Ph.D.

Date of Approval:

November 16, 2009

Keywords: targeted drug delivery, polyethylene glycol, nanoparticle, liposome,
inflammation

© Copyright 2010 , John Elliott

Dedication

I would like to dedicate this document to my wife Jill and my two children Tyler and Claire as well as all those who have inspired me in the past and those who I hope to encourage making a positive impact on the scientific community.

Acknowledgments

I would like to acknowledge Dr. Brenda Flam and Dr. Elizabeth Hood for being great mentors and for all the encouragement and help I have received from them over the course of my research. A special acknowledgement is in order for all of my committee members and especially, Drs. VanAuker, Muffly and Strom for their guidance and support during this process. I would also like to acknowledge the faculty and staff at USF Health for the use of their facilities and all of the technical support they have provided.

Table of Contents

List of Tables	iii
List of Figures	iv
Abstract	viii
1. Project Background.....	1
1.1.0 Drug Delivery Introduction	4
1.1.1 Basics of Pharmacokinetics	4
1.1.2 Compartment Models.....	6
1.2.0 Introduction to the Cardiovascular System.....	8
1.2.1 Blood.....	8
1.2.2 Heart.....	11
1.2.3 Circulation.....	12
1.3.0 Cell Introduction	13
1.3.1 Endothelial Cells.....	14
1.3.2 Endothelial Cell Mass Transport	16
1.3.3 Endocytosis.....	19
1.4.0 Cell Surface Receptors.....	20
1.4.1 Proteins	24
1.4.2 Antibodies.....	24
1.4.2.1 Immunoglobulin G	26
1.4.2.2 Monoclonal Antibodies	28
1.4.3 CD44 Receptor.....	29
1.4.4 Intercellular Adhesion Molecule (ICAM)	30
1.4.5 Vascular Cellular Adhesion Molecule (VCAM)	31
1.5.0 Cytokines and Inflammation.....	32
1.5.1 Tumor Necrosis Factor Alpha.....	33
1.5.2 Interleukin 1	34
1.6.0 Cardiovascular Disease.....	34
2. Construction and Characterization of Modified Vesicle Design	37
2.1.0 Amphiphiles.....	37
2.1.1 Non-Ionic Surfactants	39
2.1.2 Cholesterol	40
2.2.0 Polyethylene Glycol.....	41
2.3.0 Molecule Synthesis	42
2.3.1 Functionalized Non-Ionic Surfactant.....	43
2.3.2 Functionalized Cholesterol	46
2.4.0 Vesicle Synthesis	47

2.4.1	Thin Film Formation and Hydration.....	48
2.4.2	Vesicle Extrusion.....	48
2.4.3	Size Exclusion Chromatography	
	Introduction.....	49
2.4.3.1	SEC Volumetric Theory	50
2.4.3.2	SEC Methods	51
2.4.4	Antibody Conjugation.....	53
2.5.0	Vesicle Metrology.....	54
2.5.1	Thin Layer Chromatography Introduction.....	54
2.5.1.1	Thin Layer Chromatography Methods.....	55
2.5.1.2	Thin Layer Chromatography Results.....	57
2.5.2	Fluorescent Microscopy.....	58
2.5.3	Flow Cytometry	61
2.5.4	Transmission Electron Microscopy	65
2.5.5	Dynamic Light Scattering.....	69
3.	Evaluation of Receptor-Conjugated Vesicles.....	73
3.1.0	Cell Culture.....	73
3.2.0	Fixed Cell Binding.....	74
3.3.0	Live Cell Binding.....	77
3.3.1	Multiwell Plate Experiments.....	77
3.3.2	Confocal Laser Scanning Microscopy	80
3.3.3	Transmission Electron Microscopy	89
3.4.0	pH Sensitive Dye Study.....	92
3.5.0	Vesicle Binding in Flow	95
4.	Enhancement of the Modified Vesicle Designs for Targeted Delivery in Vivo	97
4.1.0	Multi Well Plate Imaging.....	97
4.2.0	Phantom Mouse Imaging	99
5.	Discussion and Future Direction.....	103
5.1.0	Vesicle Design and Manufacturing.....	103
5.2.0	Experimental Conclusions	107
5.3.0	Future Directions	109
	References	111
	Bibliography	125
	Appendices	127
	Appendix A: Transmission Electron Microscopy Notes	128
	About The Author.....	End Page

List of Tables

Table 1.0	Project Aims.....	3
Table 1.1	Physical Properties of Blood.....	9
Table 1.2	Blood Cell Types	10
Table 1.3	Endothelial Transport Equations [36].....	17
Table 1.4	Integral Membrane Protein Types	21
Table 1.5	Common Cell Adhesion Molecules (CAMs).....	22
Table 1.6	Human Immunoglobulin Types	26
Table 2.0	Immuno-niosome Materials	43
Table 2.1	TLC Materials.....	55
Table 2.2	5% PEG Sample Event Population.....	63
Table 2.3	5% PEG Sample Median Distribution	63
Table 2.4	10% Functionalized Cholesterol Median Population	64
Table 2.5	Transmission Electron Microscopy Materials	65
Table 3.0	Static Binding Results.....	77
Table 3.1	Injury Binding Results	83

List of Figures

Figure 1.0	PEGylated Immuno-niosome.....	3
Figure 1.1	Simple Compartmental Model.....	7
Figure 1.2	Endothelial Cell on Aortic Valve (arterial).....	15
Figure 1.3	Immunoglobulin G (IgG).....	28
Figure 1.4	CD44 Genomic Sequence and Receptor Structure [82,83]	29
Figure 1.5	ICAM-1.....	31
Figure 1.6	VCAM-1	32
Figure 2.0	Hydrodynamic Shell of a Surfactant Molecule.....	38
Figure 2.1	Molecules: Span 60 and Tween 61	40
Figure 2.2	Cholesterol	40
Figure 2.3	Polyethylene Glycol (PEG).....	41
Figure 2.4	PEGylated Surfactant Synthesis	45
Figure 2.5	Functionalized Cholesterol Synthesis	47
Figure 2.6	Size Exclusion Chromatography.....	50
Figure 2.7	Size Exclusion Chromatography Elution Profile.....	51
Figure 2.8	Elution Profile from 2 ml Sample Size	52
Figure 2.9	Elution Profile from 500 ul Sample Size	53
Figure 2.10	Antibody Conjugation.....	54
Figure 2.11	TLC Image Analysis	57
Figure 2.12	Atorvastatin Standards	58

Figure 2.13	Jablonski Diagram	59
Figure 2.14	PEGylated FITC Conjugated Immuno-niosomes	60
Figure 2.15	FITC Conjugated Immuno-niosomes Using Functionalized Cholesterol	60
Figure 2.16	5% PEG Sample Forward Scatter Distribution.....	62
Figure 2.17	5% PEG Sample Particle Size Distribution	62
Figure 2.18	5% PEG Sample Dynamic Light Scattering Data.....	63
Figure 2.19	10% Functionalized Cholesterol Forward Scatter Distribution	64
Figure 2.20	10% Functionalized Cholesterol Sample Dynamic Light Scattering Data.....	65
Figure 2.21	TEM of Bulk Solution	67
Figure 2.22	TEM of Extruded 5% PEGylated Niosomes	68
Figure 2.23	TEM of 5% PEGylated FeO-Loaded Niosomes.....	68
Figure 2.24	Dynamic Light Scattering	69
Figure 2.25	Niosome Sample Correlation Data	71
Figure 2.26	Data from Stability Comparison Study on Day90	72
Figure 3.0	Fixed Cell Binding: 10% Tween Fluorescein-loaded IN (CD44, KM201).....	76
Figure 3.1	Fixed Cell Binding: 5% PEG Fluorescein-loaded IN (CD44, KM201).....	76
Figure 3.2	Nonspecific Binding Results.....	79
Figure 3.3	Live Binding Performances	80
Figure 3.4	One Hour Scratch Injury ICAM (200X Magnification)	82
Figure 3.5	Graph of Fluorescent Intensity from Region of Interest 1	82
Figure 3.6	Injury Model Region of Interest (200X Magnification)	83

Figure 3.7	(A) 4 Hour PEGylated CD44 Immuno-niosomes, (B) Control, 4 Hour PEGylated CD44 Immuno-niosomes, (630X Magnification)	85
Figure 3.8	(A) 3 Hour PEGylated CD44 Immuno-niosomes, (B) Control, 3 Hour PEGylated CD44 Immuno-niosomes, (630X Magnification)	85
Figure 3.9	(A) 2 Hour PEGylated CD44 Immuno-niosomes, (B) Control, 2 Hour PEGylated CD44 Immuno-niosomes, (630X Magnification)	86
Figure 3.10	(A) 1 Hour PEGylated CD44 Immuno-niosomes, (B) Control, 1 Hour PEGylated CD44 Immuno-niosomes, (630X Magnification)	86
Figure 3.11	(A-D) Z-stack of the 1-4 Hour PEGylated CD44 Immuno-niosomes, (630X Magnification)	87
Figure 3.12	(A) 4 Hour PEGylated VCAM-1 Immuno-niosomes, (B) Control, 4 Hour PEGylated VCAM-1 Immuno-niosomes, (630X Magnification)	88
Figure 3.13	(A) 4 Hour ICAM Cholesterol Immuno-niosomes, (B) Control, 4 Hour ICAM Cholesterol Immuno-niosomes (630X Magnification)	89
Figure 3.14	Gold Loaded, Internalized Immuno-niosomes	91
Figure 3.15	Gold Loaded Immuno-niosome Bound to Cell Membrane	92
Figure 3.16	Fluorescence Spectra of 1 μ M SNARF-4 in PBS, pH 5.45 to 7.2	93
Figure 3.17	Spectrum of SNARF-4 Loaded Span 60 Niosomes at pH 7.2	94
Figure 3.18	Spectrum of Cholesterol	95
Figure 3.19	Flow Cell	95
Figure 3.20	PEGylated CD44 Conjugated Immuno-niosomes Bound to Endothelial Cells Under Flow Conditions (400x Magnification)	96
Figure 4.0	IRDye 800CW Bulk Solutions	97
Figure 4.1	IRDye 800CW Reference Samples	98
Figure 4.2	4nmol IRDye 800CW Loaded 5% PEGylated Niosomes	99
Figure 4.3	IRDye 800CW Pipette Standards for Phantom Mouse	100

Figure 4.4	Minimum Detection Limits with Epi-illumination	101
Figure 4.5	Phantom Mouse Imaged Under Trans-illumination	102

PEGylation of Niosomes

John A. Elliott

ABSTRACT

The research presented in this dissertation describes the creation and characterization of a novel antibody-vesicle conjugate modified with polyethylene glycol (PEG) that possesses enhanced binding to and uptake by inflammation-activated endothelial cells with improved storage stability and longer shelf-life and potential reduction in immunogenic potential compared to previous designs.

Targeted drug delivery provides an effective means of delivering therapeutic concentrations of a drug to the site or organ of action. The drug is delivered using a niosome, a vesicle with an aqueous core and a bilayer membrane composed of non-ionic surfactants and cholesterol. Antibodies that recognize specific cell antigens are attached to the niosome to complete the targeting molecule, an immuno-niosome (IN). When functionalized PEG, a water soluble, biologically inert polymer, is attached to proteins, it can protect the protein, increasing its half-life in vivo. The immuno-niosome synthesis process is modified to include PEG incorporation into the niosome membrane, a process known as PEGylation.

Since the vasculature connects the entire body, immuno-niosomes targeted to endothelial cells were used. When endothelial cells are activated during disease, stress and injury, certain receptors are expressed and upregulated. One such receptor, CD44, is upregulated in response to vascular inflammation associated with atherosclerosis.

The research hypothesis is that the addition of polyethylene glycol to the drug delivery vesicle (immuno-niosome) using cyanuric chloride linking chemistry will improve colloidal stability and binding performance of the PEGylated immuno-niosomes to endothelial cell surface receptors expressed during an inflammatory response. The research presented in this dissertation provides the following evidence to support this hypothesis:

- Construction and characterization of a modified drug delivery vesicle using non-ionic surfactants conjugated with PEG and functionalized with antibodies against endothelial cell surface receptors (PEGylated immuno-niosomes) improves the colloidal stability over previously designed vesicles.
- Binding of PEGylated CD44-IN to activated endothelial cells is improved over previously designed vesicles.
- Binding of PEGylated CD44-IN to activated endothelial cells under physiological conditions (flow) is demonstrated.
- Uptake of PEGylated immuno-niosomes by activated or injured endothelial cells is demonstrated using confocal microscopy.

1. Project Background

Generally, the most effective and least toxic method of delivery of a therapeutic agent is targeting directly to the site of action. Therefore, methods to enhance and improve the design of targeted delivery vesicles are increasingly important to avoid the deleterious health and drug dilution effects associated with systemic administration. In 1965 Bangham et al., described the liposome, a self-assembly bilayer phospholipid vesicle composed of the cell membrane materials [1-3]. They determined that ions encapsulated within the liposomes could diffuse out, similar to the process of particle diffusion across a cell or biological membrane. Then, in the 1970's, Gregoriadis determined that liposomes could be used to encapsulate proteins, chemotherapeutic drugs and other therapeutic agents [4]. Also, in the 1970's, scientists in the cosmetics industry developed niosomes, bilayer membrane vesicles composed of non-ionic surfactants [5, 6]. Since the phospholipids in liposomes are prone to oxidation, niosomes offer better stability and shelf-life [7]. Next, with the advent of monoclonal antibody production in 1975 by Schwaber and Cohen [8], targeting specific sites located on cellular targets became feasible. Additionally, the grafting of small molecular weight drug molecules to polymer chains, e.g. polyethylene glycol (PEG), was reported to alter the immunological properties of the molecule [9] and also reduce renal excretion of the molecule [10, 11]. Therefore, to improve the delivery vesicle (niosome) circulation time and provide colloidal stability, a biodegradable polymer chain made from polyethylene glycol is attached to the niosome surface, a process known as PEGylation. The hydrophilic PEG

chain attracts water molecules to the vesicle surface and this hydration inhibits plasma protein attachment. Allen et al. and others have shown that PEGylation inhibits reticuloendothelial system uptake and provides a site for antibody conjugation that is extended away from the vesicle surface [12-15]. During the vesicle production process, the functionalized surfactant, PEG, is incorporated into the membrane of the niosome. Antibodies targeted to a specific cell surface receptor are conjugated to the terminal end of the PEG chain, creating the immuno-niosome [16, 17]. In many disease states, e.g. trauma, atherosclerosis, infection and inflammation, specific receptors are expressed on the endothelial cell surface [18, 19]. For example, when exposed to cytokines and abnormal shear stress, endothelial cells become activated, initiate an inflammatory response and express cellular adhesion molecules [20]. Cellular adhesion molecules are transmembrane glycoproteins involved in leukocyte recruitment, adhesion and transmigration, thus making them potential targets for targeted delivery vesicles [20-23]. In particular, CD44, a smooth muscle and endothelial cell surface receptor, is involved in inflammation-mediated processes, making it an attractive therapeutic target [24]. CD44 plays a critical role in inflammation associated with atherosclerosis, the buildup of plaque causing hardening of the arteries and progression to heart disease. Blocking antigen binding to the activated cell surface CD44 can reduce evidence of inflammation [18]. CD44 is also a potential target for solid tumor cells that express the cell surface receptor and in some metastatic cancers where elevated levels of soluble CD44 can be found in the circulation [25-28]. PEGylated immuno-niosomes are antibody-conjugated targeted delivery vesicles made from PEGylated non-ionic surfactants, shown in figure 1.0.

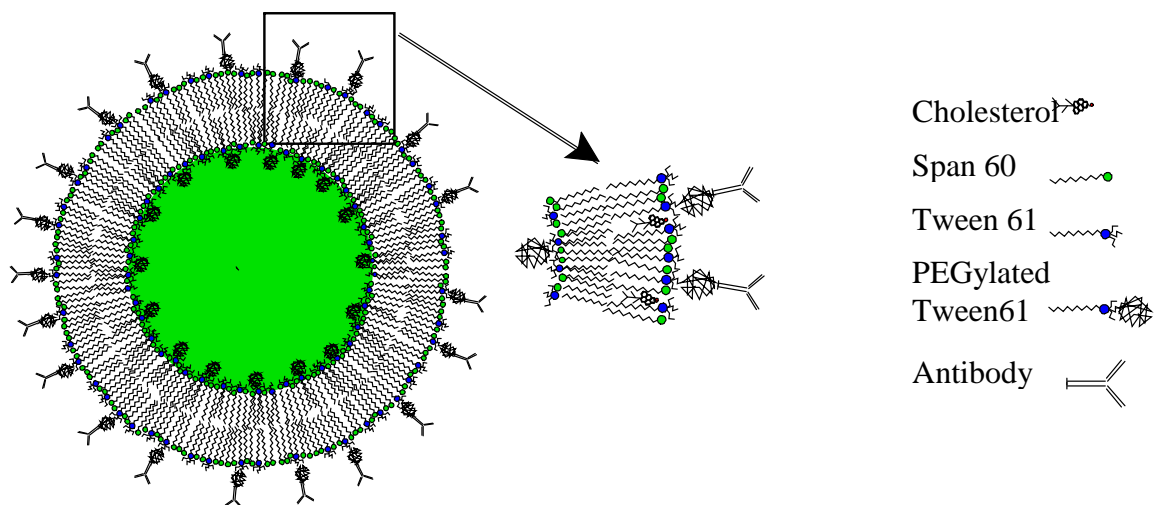


Figure 1.0 PEGylated Immuno-niosome

The research hypothesis is that the addition of polyethylene glycol to the targeted delivery vesicle (niosome) using cyanuric chloride linking chemistry will improve the colloidal stability and binding performance of the PEGylated immuno-niosomes to endothelial cell surface receptors expressed during an inflammatory response. Through successful completion of the proposed aims in table 1.0, we provide a stable targeted delivery vesicle, the PEGylated immuno-niosome, capable of delivering therapeutic agents to specific cellular sites with high specificity.

Table 1.0 Project Aims

Aim 1	Construct and characterize a modified vesicle design using non-ionic surfactants conjugated with PEG and functionalized with antibodies against endothelial cell surface receptors (PEGylated immuno-niosomes).
Aim 2	Compare and observe binding of PEGylated immuno-niosomes to endothelial cell surface inflammatory receptors.
Aim 3	Develop vesicle designs and techniques for in vivo delivery and imaging of the PEGylated immuno-niosomes.

1.1.0 Drug Delivery Introduction

Design of a targeted drug delivery molecule requires knowledge of biology, transport phenomena and pharmacokinetics. Integrating the knowledge derived from these fields provides the foundation for modern research and development of most drug delivery vesicles and conjugates. Therapeutic agents can be delivered by various routes, e.g. oral, ocular, rectal, bronchial, transdermal and systemic. Most of the methods use the cardiovascular system for distribution and removal of the agent once it has entered the body. The cardiovascular system provides the driving force and infrastructure for the distribution of the therapeutic agent throughout the body. Depending on the location of the targeted site, distribution is carried out by diffusive and convective forces. When the blood is used to transport material through the body, the point of first contact for the targeting vesicle is the membrane of the endothelial cell surface.

1.1.1 Basics of Pharmacokinetics

Pharmacokinetics is the study of how the body distributes, absorbs, metabolizes, and clears a drug after administration while pharmacodynamics describes the biochemical and physiological effects of the drug on the body. The basic overview of the process of pharmacokinetics is described by the acronym LADME which represents Liberation (L), Absorption (A), Distribution (D), Metabolism (M) and Excretion (E). These processes are not discreet as some can take place simultaneously. For example, simple compartment models can be used to estimate serum levels in order to prevent the occurrence of nephrotoxicity.

Inputs and outputs are the two types of operation described by LADME.

Liberation and absorption describe input processes where liberation is the release of the

drug from its original form and absorption is the movement of the drug from its original site of administration into the blood stream. Distribution, metabolism and excretion are output operations. Distribution is where the drug diffuses or travels from the intravascular space into the tissue. Metabolism is where the drug is broken down or converted into forms that are easy to eliminate. Excretion is the elimination of the original compound or its metabolites from the body through renal, hepatic or pulmonary routes.

In the design of drug delivery molecules, the first thing to consider is how the drug is to be administered or introduced into the body. Drugs can be delivered by site specific methods such as ocular, dermal and bronchial or by broader distribution methods of delivery such as oral and intravenous routes. The dermal methods are based on adsorption through the skin by a patch that releases the drug over time. The drug is absorbed into the blood and distributed, e.g. nicotine and nitroglycerine patches. Oral methods of delivery use pills containing simple starch or gelatin binders to control release rates in the gastrointestinal tract (GI), with the latter providing a slower release rate in the stomach and intestine. A more sophisticated oral delivery method uses an osmotic pump across a polymer shell so the drug can be delivered for a longer time. The drawback to oral delivery methods is the harsh environment of the GI tract and the low absorption rates of some drugs from the GI tract into the blood. The benefit is greater compliance since typically the drugs can be taken by the patient without aid from a medical professional and without the pain or complications that can be associated with intravenous delivery methods. The route chosen for this study is the intravenous route since the entire dosage of the administered drug reaches the circulatory system where it is

then distributed throughout the body prior to clearance by hepatic, renal and proteolytic enzyme routes.

1.1.2 Compartment Models

When the drug enters the blood stream, the central volume (V_c) describes the volume of blood in the vessels. This includes any tissues that are highly perfused with blood and where the drug may distribute. The peripheral volume (V_p) describes blood in the tissues outside of the central volume. Together V_c and V_p make up the volume of distribution (V_d), which is the total fluid volume the drug is dissolved in [29]. Together, the terms V_c , V_p and V_d are used to approximate the amount of drug in the body, peak serum levels and the clearance of the drug from the body. The clearance (Cl) of the drug from the blood is another important term that describes the behavior of the drug in vivo. The rate of drug clearance is described by a constant called the elimination coefficient (k_{el}), which describes the fraction of drug eliminated per unit time. The constant is patient-specific because it is based on the capacity and functionality of specific organs that can be impacted by disease and the administered drug treatment. The clearance calculation is shown in equation 1.0.

$$Cl = k_{el} * V_d \quad \text{Equation 1.0}$$

The simplest way of characterizing a drug in the body is to use first order kinetics and a single compartment model. In reality, first order kinetics holds up for most drugs while the single compartment model works if serum samples are collected after the drug moves into the tissues. The one compartment model is used for drugs that perfuse rapidly while the two compartment model takes into account the distribution phase. When graphing the two models, the one compartment model will yield a straight line on a

logarithmic y axis. The two compartment model yields a biphasic line on the same graph, indicating the distribution phase. Some drugs, when administered by intravenous infusion over a time course, will follow a three compartment model consisting of distribution, elimination and tissue release. In encapsulated drug delivery design, the tissue release of the drug can be coordinated with the time release from the vesicles. This is a beneficial attribute of encapsulated delivery methods since drug plasma concentrations are maintained for long time periods without the initial high drug plasma concentrations associated with non-encapsulated delivery techniques.

The body can be modeled as a set of compartments connected in parallel and/or series with the blood plasma as the conduit between the organs, as shown in figure 1.1.

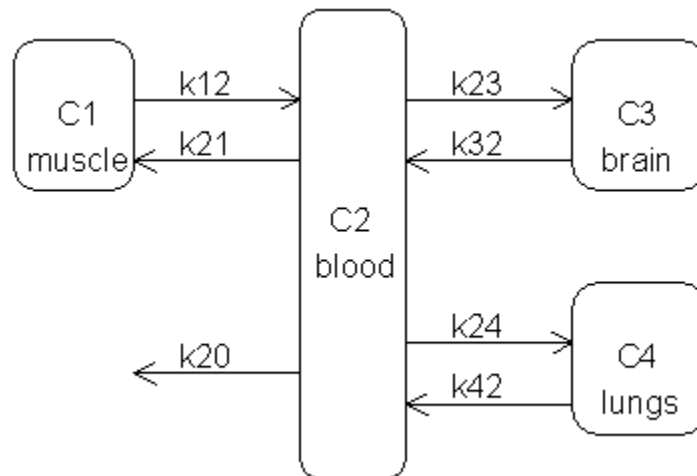


Figure 1.1 Simple Compartmental Model

With rate constants representing the coefficients for drugs entering and leaving a particular compartment (k_{12} , k_{21}), the liver and kidneys act as a sink (k_{20}) where the drug is metabolized and/or extracted from the plasma through hepatic and renal clearance. This multiple compartment model is still incomplete because there are intercellular and extracellular space interactions and intracellular compartment interactions within each organ. More advanced modeling is being investigated in order to

incorporate physiological data from experiments [30]. Another method used to characterize the drug in the body is to take into account the complex design of the vascular bed and to implement fractal analysis [31, 32].

1.2.0 Introduction to the Cardiovascular System

The major components of the cardiovascular system are the heart, vessels and blood circulated throughout the body. The entire vascular system is lined with endothelial cells providing a blood contact surface. Therefore, the cells play an active role in the cardiovascular system. The system is considered a closed loop because it is a sealed system where all the fluid is maintained and circulated within an enclosed body. It should be noted that a water cycle exists where fluids are absorbed through the GI tract, replenishing the large water content that leaves the system through renal excretion, sweat and respiratory function. The system provides transport of vital nutrients and fluids to all the organs in the human body making it an attractive avenue for drug delivery schemes. Because the operation of the cardiovascular system is essential for life, it is also a target for therapeutic intervention and treatment.

1.2.1 Blood

The fundamental role of blood is maintenance and homeostasis. It is a fluid composed of a multitude of components ranging from cells to proteins and trace minerals. Blood density is very close to pure water as shown in table 1.1, 1050 kg/m^3 compared to 1000 kg/m^3 .

Table 1.1 Physical Properties of Blood

Property	Values
Density	1050 ± 7 [kg/m ³] @ 37°C
Viscosity at shear rate	3.26 ± 0.43 [mPa*s] at shear rate of 100 [1/s] 4.37 ± 0.60 [mPa*s] at shear rate of 50 [1/s] 5.46 ± 0.84 [mPa*s] at shear rate of 1 [1/s]
pH	7.4 ± 0.05 [H ⁺]
Osmotic colloidal pressure	284 [mm H ₂ O]

The cellular component of blood can be divided into three main groups with subtypes as shown in table 1.2. The three main cell types are erythrocytes or red blood cells (RBC), leukocytes or white blood cells (WBC) and thrombocytes or platelets. Whole blood contains all the cellular and fluid components. Plasma contains the whole blood soluble factors only, with the cells separated out by centrifugation. Once whole blood has clotted, the remaining liquid component is serum. It is similar to plasma except that it lacks the clotting factors. The plasma makes up approximately 55% of the blood by volume and carries nutrients, proteins and trace minerals and acts as a pH buffer. The plasma is composed primarily of water and contains numerous low molecular weight organic and inorganic materials and about 7% protein, e.g. albumin, fibrinogen and four major groups of globulins.

Table 1.2 Blood Cell Types

Type	Sub Type	Function
Erythrocytes	Red Blood Cells	Carry oxygen to tissues in the body.
Leukocytes	Neutrophil	Bacterial and fungal targeting.
	Eosinophil	Parasite targeting and allergy mechanisms.
	Basophil	Contains histamine and heparin, involved in specific inflammatory and allergic processes.
	Lymphocytes (Natural Killer cell) (B cell and T cell)	NK cells remove tumors and viral-infected cells by cytokine induced apoptosis. B and T cells are frontline agents in the adaptive immune system.
	Monocyte	Replenish macrophages and fight infection.
Thrombocytes	Platelets	Regulation in blood clotting and inflammation.

A Newtonian fluid is described as a fluid that is non-compressible. The viscosity is a function of temperature and pressure only and is described by Newton's Law of Viscosity where the shear stress τ_{xy} is a function of the velocity profile $\frac{dv_y}{dx}$ multiplied by a constant of proportionality μ as shown in equation 1.1.

$$\tau_{xy} = -\mu \frac{dv_y}{dx} \quad \text{Equation 1.1}$$

Blood can be approximated as a Newtonian fluid when circulating in large vessels. However, when the vessel radius approaches that of capillaries, the red blood cells and plasma separate into two phases and blood can no longer be considered a Newtonian fluid. The blood flow is described as smooth (laminar) or turbulent depending on the

fluid path. In smooth flow, there are no disruptions in the axial direction and the cross sectional velocity patterns are described as plug or parabolic. In plug flow the cross sectional velocity is constant, creating high shear rates that act on the vessel wall. In plug flow it is assumed there is no boundary layer at the wall surface. When the velocity profile is parabolic, the fluid in the center of the vessel has the maximum velocity and the fluid at the wall has the slowest velocity. The parabolic profile creates conditions that can impede particles from reaching the vessel wall. This condition was first described by Segre and Silberberg in 1962. The phenomenon causes particles that are near the wall to migrate toward the axial position and particles that are in the axial position migrate toward the wall. When blood is initially ejected from the heart, it travels through the large arteries in a plug profile which becomes parabolic as the cycle continues. This effect is less pronounced as the blood travels further away from the heart into smaller vessels (not including the capillaries). Turbulent flow occurs at bifurcations and in pathological conditions such as atherosclerosis where hardening of the arteries and plaque formation disrupt the normal blood flow. Fluid flow can be described by the velocity profile, pressure drop and the wall shear stress where the difference in pressure is the driving force causing fluid flow. Blood is circulated based on the principle that a fluid flows from an area of higher pressure to lower pressure, analogous to heat flow. The ventricles in the heart contract and force the blood out, creating the driving force, so the blood will move from an area of higher to lower pressure.

1.2.2 Heart

The human heart is a four chamber pump driven by and composed of myocardial muscle tissue and it provides the driving force for blood circulation through the entire

system. The myocardial muscle tissue is surrounded by the pericardium, a tough inelastic multilayered tissue. The inner walls of the myocardium are lined with endocardial tissue composed of endothelial cells covering trabeculae. The left and right coronary arteries are positioned on the outer surface of the muscle tissue and feed blood to the myocardial muscle. To control the direction of blood flow, there are four valves, two valves that are actuated by papillary muscles and two cuspid valves that are passive and are operated by the pressure differential across the valve.

1.2.3 Circulation

The blood is returned from the body to the right atrium through two veins, the superior and inferior vena cava. Blood flows from the right atrium through a tricuspid valve into the right ventricle and is pumped through the right and left pulmonary arteries to the lungs through a semilunar valve. In the lungs, a gas exchange occurs between the air in the alveolar sacs and the lung capillaries. After this exchange process, the blood is now ready to deliver oxygen to the various tissues in the body. The oxygenated blood is returned to the heart through the right and left pulmonary veins to the left atrium. The blood traverses across the mitral valve into the left ventricle where it is ejected across the aortic valve into the aortic arch and the descending aorta. From the major arteries, the vessels continue to branch out into smaller arteries, transitioning from the arterioles to the smallest group of vessels called capillaries. The arterioles are responsible for the peripheral resistance in the cardiovascular system; this resistance is directly related to arterial pressure from the restriction of blood flowing from the arteries through the arterioles. The capillaries contain the largest total cross-sectional surface area in the body and are present in every tissue. They contain a single layer of endothelial cells

surrounded by basal lamina. Capillaries are the pathway for the delivery and exchange of oxygen, carbon dioxide and critical nutrients to the surrounding tissues in the body, making them a focus for targeted drug delivery techniques. The fluid that carries nutrients from the capillaries is collected in the lymphatic ducts. The lymphatic system is responsible for removing fluids from the tissue interstitial spaces around the body and returning those fluids to the blood stream. The blood is returned to the heart by a complementary set of vessels called veins which completes the closed loop of the cardiovascular system.

1.3.0 Cell Introduction

Cells are contained within the tissues of all living creatures. Cells can be divided into two distinct types, eukaryotes, cells with a nucleus and well-developed intracellular organelles and prokaryotes, cells without a discrete nuclear membrane. The basic structure of a cell consists of a fluid core surrounded by a bilayer lipid membrane. The internal space of eukaryotic cells, the cytoplasm, is a fluid core with membrane-bound organelles and a nucleus. The cytoplasm contains many small and large molecules and the cell transports material into the cytoplasm and between organelles using small membrane-bound vesicles. The nucleus contains the information the cell needs to function and replicate. Energy for cellular processes is generated in the mitochondrion. Mitochondria produce adenosine triphosphate (ATP) that is used as an activated energy carrier in biosynthesis reactions and is also responsible for cellular functions such as the cell cycle and growth. The nucleus is surrounded by a double layer membrane with pores that allow the transfer of material. Ribosomes within the cytosol are sites of protein synthesis where messenger RNA transcribed in the nucleus is translated into protein on

the ribosomes. An additional multifunctional cytoplasmic organelle is the endoplasmic reticulum (ER). The rough endoplasmic reticulum (RER) is coated with ribosomes. The formed proteins can be further modified on the surface of the RER. There is another part of the ER called the smooth endoplasmic reticulum (SER) that is responsible for specialized functions like lipid and steroid production. The proteins formed at the free ribosomes, RER and SER are transported to an organelle called the golgi apparatus. The golgi apparatus functions primarily as a cellular post office where the material is sorted, packaged and sent to the proper destination within the cell. Lysosomes import and recycle materials using digestive enzymes. Lysosomes have an internal pH of 4.8. Materials transported into the cell by endocytotic vacuoles are typically shuttled to an acidic vacuole called an endosome. The endosome sorts recyclable materials to the plasma membrane or delivers them to the lysosome. This transport and recycling feature is important in developing drug delivery strategies because therapeutic agents can be degraded by the acidic conditions.

1.3.1 Endothelial Cells

The vasculature is lined with a single layer of endothelial cells providing the blood contact surface in the heart, arteries, veins and lymphatic system. The endothelial cell is a subtype of the epithelium which lines human body cavities and tissue structures. One feature of the endothelial cell type is that it expresses the E-cadherin adhesion molecule on its surface. There are differences between arterial and venous endothelial cells and it has been shown that the genetic coding determines the cell phenotype [33]. In fact, different phenotypes are seen in the five different types of endothelial cells found in the heart (endocardial, coronary, arterial, capillary and lymphatic) [34]. There are

organizational/orientation differences between the endothelial cells (arterial versus ventricular) covering the aortic valve. The cells are aligned in different patterns to compensate for the physiological stresses they encounter. A transmission electron microscope image of an endothelial cell on an aortic valve is shown in figure 1.2

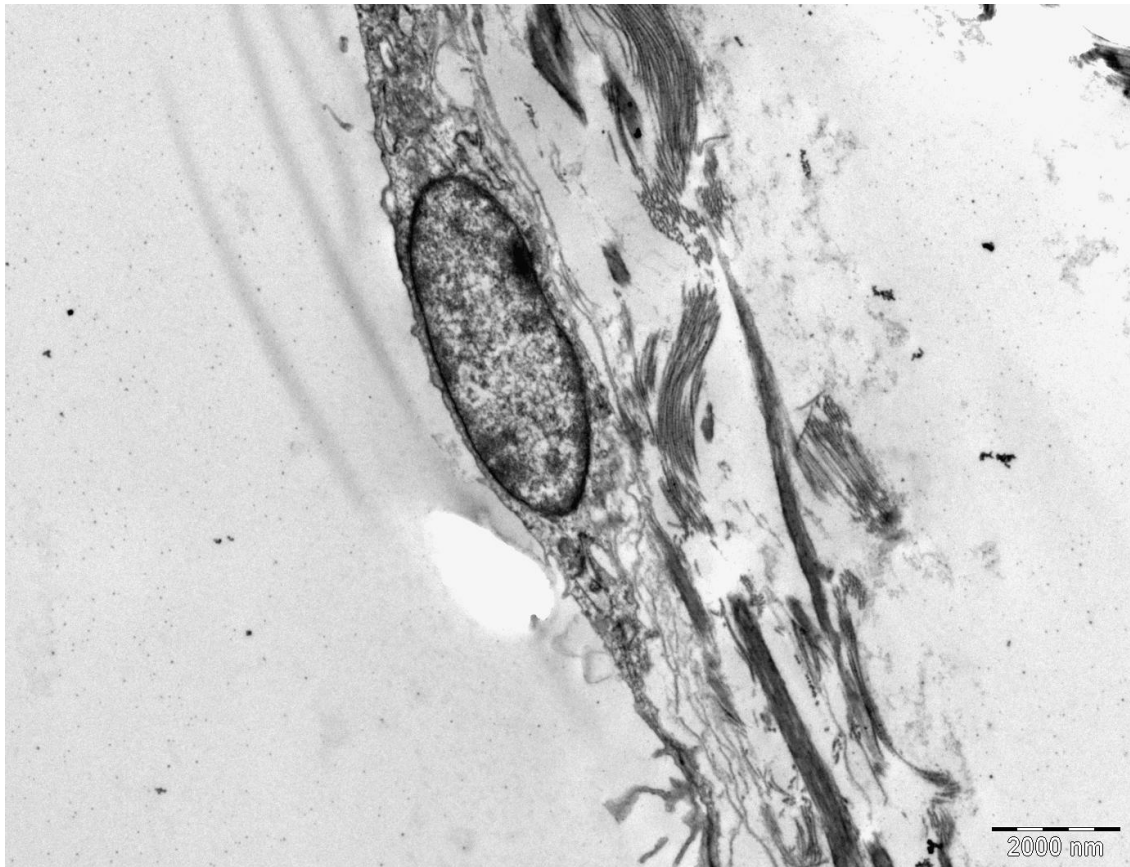


Figure 1.2 Endothelial Cell on Aortic Valve (arterial)

Variations in permeability of the endothelial cell layer in large arteries and capillaries are caused by the underlying structural components of the different vessels. The large arteries transport blood and the capillaries function to deliver vital molecules and fluids to the tissue intracellular spaces. The main arteries allow passage of oxygen and small molecules from the blood through the endothelial cells into the arterial substructure to maintain the smooth muscle cells. The lymphatic system is a low flow

system that maintains intracellular fluids and has the potential to become a target for developing anti-inflammatory treatments [35]. There are also interactions between tumor cells and the lymphatic system making it a focus for anti-cancer treatment strategies.

1.3.2 Endothelial Cell Mass Transport

For intravenous targeted drug delivery, the endothelial cell surface is the first point of contact, whether the surface of the cell is the intended site of therapy, the drug is to be transported into the cell, or the drug needs to cross the endothelial cell barrier to reach the underlying tissues. The selection of the cell surface receptor is matched to the delivery vesicle using knowledge of the receptor's temporal expression and binding affinity. The targeting strategy dictates the size and composition of the delivery vesicle to provide the behavior required in the area of interest since it may need to overcome convective forces due to blood flow momentum in great vessels or shear forces in smaller vessels. Depending on the application of the therapeutic agent, the mass transport interactions with the endothelium can be characterized as: a reactive surface, a reactive wall or a semi-permeable membrane shown in table 1.3 [36].

Table 1.3 Endothelial Transport Equations [36]

Process	Equation	Important Conditions
Reactive Surface	$C_s/C_b = 1/(1 + Da_r/Sh)$, Equation 1.2	$Da_r \ll Sh$ $Da_r \gg Sh$
Semi-Permeable Membrane	$C_s/C_b = 1/(1 + Da_c/Sh)$, Equation 1.3	$Da_c \gg Sh$
Reactive Wall	$P_{s,A}/P_{b,A} = 1 - Da_w/Sh$, Equation 1.4	$Da_r \ll Sh$ $Da_r \approx Sh$

As a reactive surface, Michaelis-Menten kinetics (MMK) are used to model the interactions at the surface. MMK describe biological reactions involving enzymes and assume the reaction is irreversible and that the product does not bind or occupy the enzyme. The Damkohler number (Da) is a ratio relating the reaction rate to the mass transport rate and the Sherwood number (Sh) is used to relate the convective and diffusive forces. When the surface concentration is equal to the concentration found in the blood stream, reactive surface equation 1.2 is reaction limited. When the Damkohler number is much greater than the Sherwood number ($Da_r \gg Sh$), the reactants are present at the wall in concentrations high enough or in excess for the reaction. The diffusive and convective forces that bring the reactants from the blood stream to the cell wall do not influence the reaction.

When the endothelium is described as a semi-permeable membrane for small molecules, equation 1.3 shows that when the Damkohler number is much larger than the Sherwood number, the system is transport limited or fluid-phase limited. In larger vessels

this means it will be more difficult for large molecules and particles to move to the endothelial surface. In contrast, smooth flow patterns will allow smaller particles to diffuse to the endothelial surface more quickly. This illustrates how a vesicle that is attached to the endothelial surface at a site of therapeutic interest can take advantage of this process. In the capillary vessels, there is a phenomenon called shear thinning that takes place. This occurs because the diameter of the red blood cell is similar to that of the vessel. The red blood cells separate from the plasma and travel down the center of the vessel and the plasma is pushed toward the wall surface creating a non-Newtonian liquid with two distinct phases. The effect of the plasma being located near the wall creates a fluid phase that the delivery vesicle will occupy when in close proximity to the binding site on the vessel wall.

At the reactive wall, there is consumption or a sink on the mass balance. The act of oxygen transport from the blood stream to the vessel wall is an important process that is required to maintain homeostasis of the vessel. Equation 1.4 shows that when the Damkohler number is much smaller than the Sherwood number, the reaction is limited by the reaction rates associated with the wall, and transport phenomena does not play an important role. As the Damkohler and Sherwood numbers approach one another, the reaction is limited by transport of the reactant to the wall, and convective and diffusive forces become important. This has been used to explain endothelial dysfunction in coronary arteries leading to a leaky vascular wall and allowing the influx of low density lipoproteins, a primary step in atherosclerotic plaque formation.

1.3.3 Endocytosis

Endocytosis is the uptake of nutrients, fluids, large and small molecules and particles in cells. There are two main pathways for endocytosis, phagocytosis and pinocytosis. Phagocytosis is described as a process where the cell engulfs large particles (>250nm) by folding its membrane around the particle. Pinocytosis is a process where a cell uptakes liquids and small molecules (<150nm) inside pits that are formed in the cell membrane and that pinch off forming vacuoles that carry the contents to various intracellular locations [37]. Phagocytosis is a process that specialized cells in the immune system use to remove pathogens and debris and is the process that macrophages use to complete housekeeping duties throughout the body. Phagocytosis is a major pathway for specialized cells like macrophages, but is rare in endothelial cells in situ. However, Muro et al. reported that endothelial cells can internalize large particles up to 5 μm in size [22]. Considering the rarity of phagocytosis in endothelial cells in vivo, it has not been a focus of most targeted delivery schemes. However, since macrophage activity is a process associated with tissue injury and inflammation, the macrophage is an attractive target for therapeutic treatment [38]. Pinocytosis and receptor-mediated pathways are also used to deliver a payload to the site of interest. Pinocytosis is a non-specific uptake of extracellular fluids and small molecules and can be used to deliver a reservoir to the cell surface. The reservoir contents are eluted into the extracellular fluid and diffusion becomes the driving force for delivery. Uptake pathways are described by four main groups: macropinocytosis, clathrin-mediated endocytosis (CME), caveolae-mediated endocytosis (CavME), and clathrin-caveolae-independent-internalization [39, 40]. CME

and CavME both provide non-specific pathways for the uptake of adsorbed molecules through invaginations found on the cell membrane.

The caveolae are small 60-80 nm plasma membrane invaginations used for endocytosis, exocytosis, transcytosis and the internal transport of macromolecules [41]. They do not have a large volume and are typically lined with receptors such as gp60, an albumin specific receptor. The CavME pathway has been well studied and provides a promising route for delivery to the endosome, caveosome and the cell nucleus [42]. The selection of these different delivery routes is based on interactions of the surface lipid rafts, integrins and proteins. Caveolae are involved in the transcytotic and exocytotic processes which are directed by secondary protein interactions.

1.4.0 Cell Surface Receptors

Targeted drug delivery can be used to target cell types based on size, charge and binding schemes using cell surface receptors and receptors found within the pits formed during pinocytosis. Cells continually express protein and carbohydrate receptors for ligands both externally on their membrane surface and internally for a variety of functions. The receptors that are expressed vary between cell types and some of them may only be up-regulated during certain stages of disease or injury, such as receptors for inflammation. Cell surface receptors may be either integral or peripherally attached to the membrane. Peripheral receptors are composed of proteins that are temporarily attached to the cell membrane and function in a regulatory manner. They are not as common as the integral types. Peripheral and integral membrane receptors are required cellular homeostasis. The functions of the receptors vary from adhesion, signaling and communication to the extracellular matrix and other cells, as well as triggering cellular

processes such as apoptosis, endocytosis and mitosis. Transmembrane receptors are integral in nature and their protein structures penetrate through the membrane into the cytoplasm for intracellular signaling. The integral membrane proteins are typically made from alpha helices and beta sheets. Integral proteins can be grouped into six categories based on how the structure interacts with the lipid membrane of the cell (table 1.4, [14]).

Table 1.4 Integral Membrane Protein Types

Type	Description
I	One helix structure with terminal amino group on the outside and carboxyl group on the inside of the cell membrane.
II	One helix structure with terminal carboxyl group on the outside and amino group on the inside of the cell membrane.
III	Multiple helix structure penetrating the cell membrane using a single polypeptide.
IV	Multiple helix structure formed by different polypeptides creating a channel through the membrane.
V	Proteins that are attached to the lipid membrane by covalently linking to lipid molecules without passing through the membrane.
VI	Single polypeptide structure that passes through the cell membrane and has a type V lipid anchor.

The delivery vesicle encounters the cell membrane surface receptor and this is the first target for most delivery schemes. A secondary interaction with peripheral receptors could provide additional targeting benefits. Inflammatory receptors are cell surface

receptors that are up-regulated by the cell during conditions of disease, injury and infection. Inflammatory receptors include the cellular adhesion molecules (CAMs) which can be expressed on the cell surface, intracellularly or within the extracellular matrices of tissues. The CAM family can be grouped into five groups based on protein type. These are: immunoglobulins, selectins, addressins, integrins and cadherins. Of these five, three have been used for targeting the arterial endothelium. The CAM groups, the immunoglobulins, selectins and cadherins, provide potential binding sites for therapeutic particle delivery (table 1.5).

Table 1.5 Common Cell Adhesion Molecules (CAMs)

Type	Name	Function
IgG	ICAM-1	InterCellular Adhesion Molecule 1 is expressed by leukocytes and endothelial cells and is responsible for leukocyte extravasation into tissues from the blood stream during an inflammatory response [43].
IgG	CD44	Is involved in cell to cell interactions and is expressed by endothelial cells during inflammation, atherosclerosis, rheumatoid arthritis and cancer [44-46].
IgG	VCAM-1	Vascular Cell Adhesion Molecule-1 is expressed by activated endothelium during inflammation. It is expressed by large and small vessels and is associated with atherosclerosis. Some melanomas use it to attach to the endothelial cell surface [47-49].

Table 1.5 (Continued)

IgG	PECAM	Platelet Endothelial Cell Adhesion Molecule is found on endothelial cells, platelets, macrophages, neutrophils and Kupffer cells. It plays an important signaling role in thrombosis and between macrophage cells and dying neutrophils [50, 51].
Selectin	E-selectin	A low affinity cell adhesion molecule expressed only by endothelial cells during inflammation. It allows leukocytes to bind in a reversible manner known as leukocyte rolling [52, 53].
Selectin	P-selectin	A cell adhesion molecule similar to E-selectin but expressed very quickly as it is stored in endothelial cells preformed and does not need to be synthesized [54, 55].
Selectin	L-selectin	A cell adhesion molecule that is associated with lymphatic endothelial cells. It functions like E-selectin and P-selectin and is used for leukocyte recruitment [56-58].
Cadherin	VE-cadherin	VE-cadherin is an intracellular adhesion molecule that is responsible for the integrity of the junctions between endothelial cells [59, 60].
Cadherin	T-cadherin H-cadherin	T-cadherin is highly expressed in the heart and aorta and is upregulated in atherosclerotic lesions and tumor penetrating blood vessels [61-63]. H-cadherin is associated with cancer and tumor development [64-67].

1.4.1 Proteins

Proteins are responsible for most of the functions that take place in a cell. They are the most complex molecules found with regard to their structure and function. They are comprised of a combination of amino acids that have side chains that give them distinct chemical functions. Polypeptides are formed when the amino acid molecules are linked together by a covalent peptide bond forming linear polymers with functional side chains. Some proteins have a negative or positive charge, some are uncharged or polar, and some are hydrophilic. The noncovalent interactions between the side chains cause the linear polypeptide sequence to take shape. Hydrogen bonds, ionic bonds and van der Waals attractions are responsible for secondary structure of the molecule. The peptides will shift to a conformation with the lowest energy level. This is determined by temperature, pH and the solvent. The two major structures that are commonly formed are the alpha helix and beta pleated sheet. Beta pleated sheet structures resemble ribbons with polypeptide chains running in the same direction in a parallel structure or an alternating direction forming an anti-parallel sheet structure. Proteins form alpha helix structures to cross the cell membrane.

1.4.2 Antibodies

The immunoglobulin superfamily (IgSF) is a large group of cell surface and soluble proteins made from amino acids that contain an immunoglobulin (Ig) domain. The Ig domains contain two layers of β pleated sheets and three to four anti-parallel polypeptide chains. The Ig structure anti-parallel beta sheets are characterized by the conserved disulfide bond that links the two sheets together. All the proteins with these immunoglobulin domains belong to the IgSF (the structures are involved with cell

recognition, binding, adhesion and receptors for antigens and cytokines). Antibodies belong to this superfamily and bind to their specific antigens with high affinity and selectivity [68]. These antibodies are used to target inflammatory receptors in the described studies. There are five different classes or isotypes of human antibodies shown in table 1.6. They contain polypeptide structures grouped into regions called chains with constant regions that are conserved and variable regions that form the binding sites for specific antigens. All five classes have the same fundamental four chain structure made from a pair of identical heavy chains and a pair of identical light chains held together as a tetramer with disulfide bonds. In 1959 Porter, showed that the antibody could be cleaved using the proteolytic enzyme papain, into three major structures that compose 90% of the original molecule (figure 1.3). He noted that two of the structures retained the ability to bind with antigen and had nearly identical chemical properties. He also noted the third fragment had very different chemical properties and did not bind with antigen. This was the first clue that immunoglobulins had a “Y” structure composed of the three groups he found after the papain digest. The two identical structures are called fragment antigen binding arms (Fab) and the third region is called fragment crystalline (Fc) [69] (figure 1.3). The five classes of antibodies each have distinct heavy chains which are used for classification, as listed in table 1.6.

Table 1.6 Human Immunoglobulin Types

Type	Heavy Chain	Description
IgA	α	Dimer that is found in mucous and breast milk provides protection from pathogen colonization [70]. Can survive conditions in the gastrointestinal tract [71].
IgD	δ	Monomer that is located on the surface of B cells and acts as an antigen receptor [72].
IgE	ϵ	Monomer that binds its Fc region to leukocytes and binds to allergens to trigger the release of histamine. [73] It also initiates an immune response to parasitic worms [74], [75].
IgG	γ	Monomer and the immunoglobulin that is responsible for the secondary immune response. Comprises 75% of the immunoglobulin found in serum[76].
IgM	μ	Pentamer immunoglobulin that is the largest and first found in the blood or in monomer form on the cell membrane [77].

1.4.2.1 Immunoglobulin G

The IgG family of antibodies comprises 75% of the antibodies found in human plasma. The four major classes of human IgG are IgG(1), IgG(2), IgG(3) and IgG(4) with IgG(1) being the most abundant of the four classes [78]. Immunoglobulin contains glycoproteins produced by specialized lymphocyte cells. These specialized lymphocytes

originate from hematopoietic stem cells and terminally differentiate into plasma cells and memory B cells. The genetic code that is developed during this maturation process is based on four genes, the variable (V), diversity (D), joining (J) and constant (C) gene. The cell line that produces IgG has the following lineage. The stem cells differentiate into pro-B cells pre-B cells, and then immature B cells. At this stage, the cells are located in the bone marrow and they are antigen independent. The cells then migrate into the spleen, tonsils and other peripheral lymphoid tissues and some become mature B cells, and collect in areas that are rich in helper T cells. These specialized areas in the tissues are known as germinal centers. When the mature B cell is activated by a helper T cell, it divides and differentiates into a centerblast by a process called somatic hypermutation. After somatic hypermutation, the precursor cell is called a centrocyte prior to becoming a plasma cell or a memory B cell. During B cell maturation, the genetic code that is responsible for the makeup of the variable binding region is determined through a process called VDJ recombination. The variable chain has three domains that are encoded by the V, D and J genes. During the VDJ recombination process, base pair changes are introduced for both heavy and light chain variable regions. In this way, the immune system is able to make a diverse group of antibodies that are able to recognize multiple antigen types.

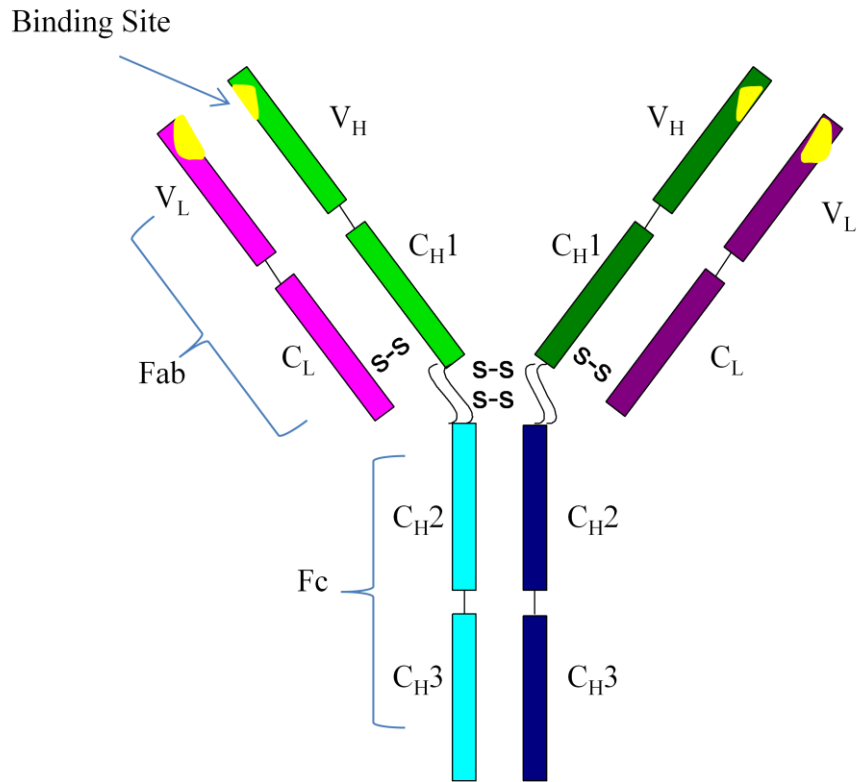


Figure 1.3 Immunoglobulin G (IgG)

1.4.2.2 Monoclonal Antibodies

The advent of methods of monoclonal antibody production in the mid 1970's was made possible by Paul Erlich's "magic bullet" concept. The technique was first described in 1973 by Schwaber and Cohen and they reported being able to produce human-mouse antibodies by fusing mouse myeloma and human peripheral lymphocytes, creating hybridomas [8, 79]. There has been controversy over this paper and Kohler and Milstein in 1975 reported production of monoclonal antibodies by fusing mouse melanoma cells with spleen cells from an immunized mouse [80]. They were recognized as the first group to produce antibodies using the hybridoma technique.

1.4.3 CD44 Receptor

CD44, shown in figure 1.4, is a cell surface receptor that remains expressed on the cell surface or that can be shed or released into circulation by enzymatic cleavage, becoming soluble CD44 [27]. CD44 is involved in many functions including cell to cell interactions with leukocytes and endothelial cells and remodeling of the extracellular matrix during cell to substrate interactions in embryonic development [81]. There are typically two forms of CD44, the standard and the variant form. A single gene with 20 exons encodes CD44, and the standard form is the most prevalent, consisting of exons 1-5, 16-18 and 20. Exons 6-15 are called variant exons v1-v10. The variant exons are spliced in different combinations in the stem portion of the receptor [82].

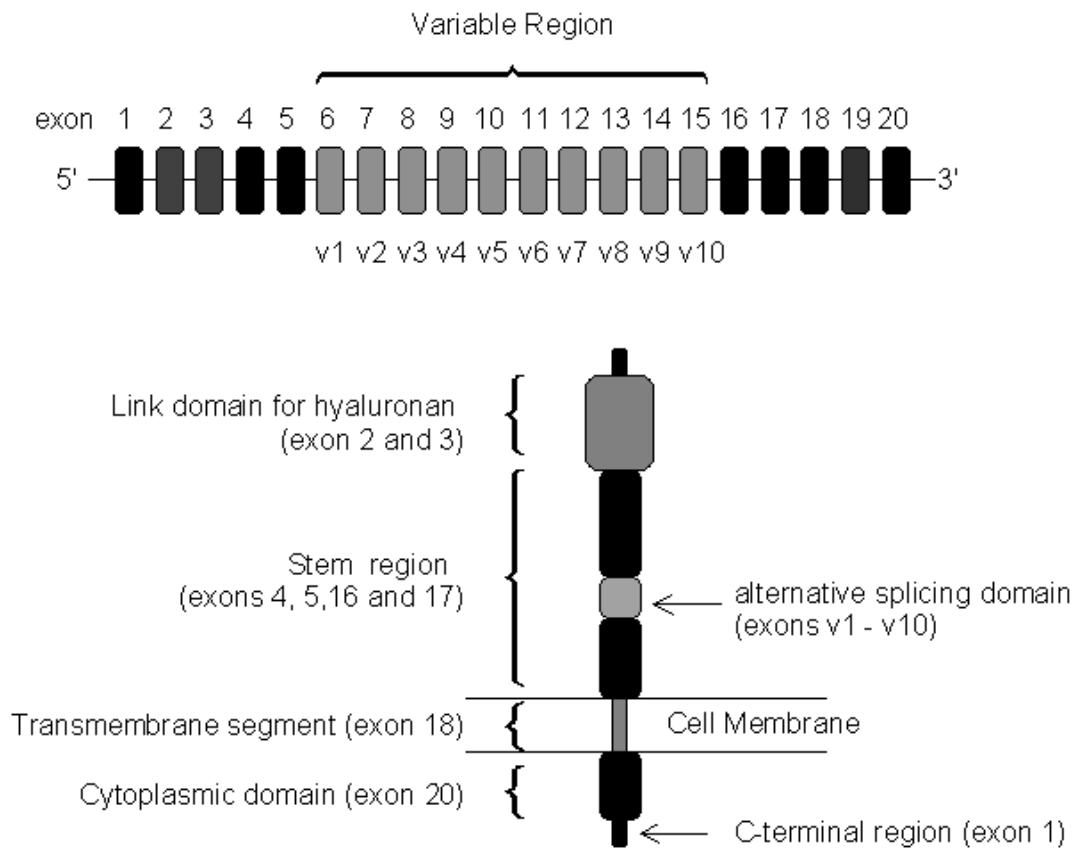


Figure 1.4 CD44 Genomic Sequence and Receptor Structure [82, 83]

CD44 is a transmembrane glycoprotein in the cellular adhesion molecule family and is the major receptor for hyaluronan [84]. CD44 is expressed by many cell types throughout the body including the keratinocytes [85] and red blood cells [86]. The CD44 receptor, expressed by both endothelial and smooth muscle cells is involved in inflammation-mediated processes, making it an attractive therapeutic target [24]. It has been shown to play a critical role in inflammation associated with atherosclerosis, and blocking binding to the CD44 receptor can reduce evidence of inflammation [18]. CD44 is also expressed on various cancer cell surfaces and has been implicated as a marker for cancer when found in high levels in its soluble form in the circulation [25, 28, 44].

1.4.4 Intercellular Adhesion Molecule (ICAM)

Intercellular adhesion molecule (ICAM) is found in three forms (ICAM-1, ICAM-2 and ICAM-3) and is part of the immunoglobulin superfamily. It is expressed by cytokine-activated vascular endothelial cells, macrophages, fibroblasts, smooth muscle cells, keratinocytes and leukocytes. The normal function of ICAM is to provide binding between endothelial cells and leukocytes during injury and infection by binding to leukocyte function association antigen (LFA) or macrophage-1 antigen (Mac-1). ICAM is also a receptor for human rhinoviruses and malaria-infected erythrocytes [87]. ICAM-1, -2 and -3 are type I transmembrane glycoproteins that are all involved in the LFA immune response [88].

ICAM-1 was first discovered in 1986 [89] followed by the discovery of ICAM-2 in 1989 [90] and finally ICAM-3 in 1992. ICAM-3 is expressed by lymphoid but not endothelial cells [91]. The ICAM-1 and ICAM-2 receptors are normally expressed in low concentrations on endothelial cells but are highly upregulated after exposure to the pro-

inflammatory cytokines, tumor necrosis factor alpha (TNF- α) and interleukin-1 (IL-1), making them an attractive binding target for drug therapy. ICAM-1 is encoded by human chromosome 19. It has a total of seven domains. Five are in the extracellular space with D1 and D3 as active binding sites [92] as shown in figure 1.5.

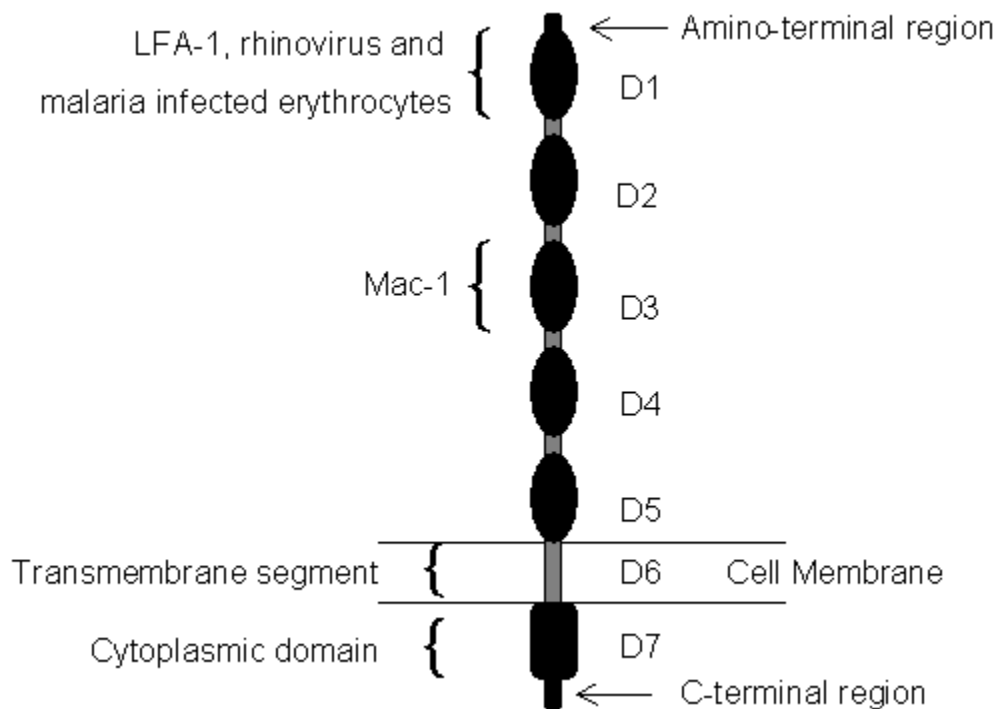


Figure 1.5 ICAM-1

1.4.5 Vascular Cellular Adhesion Molecule (VCAM)

Vascular cellular adhesion molecule (VCAM-1) is a member of the immunoglobulin superfamily and is encoded by human chromosome 1. It is expressed only by cytokine-activated endothelial cells in large and small vessels, and like ICAM-1 it binds leukocytes via the leukocyte function association antigen (LFA) [93]. It differs from CD44 and ICAM since it has two binding sites in domains 1 and 4 for very late antigen (VLA-4) expressed by T and B lymphocytes, monocytes, basophils and eosinophils [94] (figure 1.6). Metastatic melanoma cells bind to VCAM expressed on

endothelial cells [95]. It has also been shown that the adhesion molecule facilitates migration of leukocytes into the lymph nodes [96]. VCAM is upregulated at sites where arterial atherosclerotic plaques develop during the progression of this chronic disease. VCAM expression is associated with the recruitment of monocytes and macrophages that infiltrate arterial tissue and venous grafts, making it an attractive drug delivery target [97, 98].

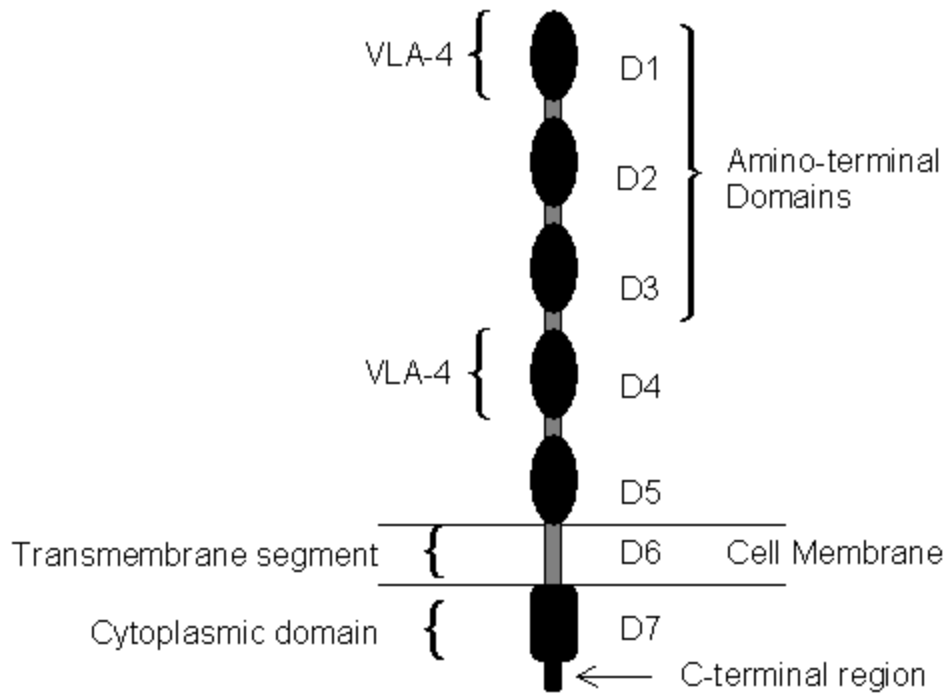


Figure 1.6 VCAM-1

1.5.0 Cytokines and Inflammation

Cytokines are extracellular signaling molecules that are required for cell-cell communication. They share several properties, which include: secreted briefly and are self limited, can be produced by multiple cell types, act on different cells types, action can be redundant and can influence the production and action of other cytokines.

Cytokine chemical signaling can be grouped into autocrine, paracrine and endocrine

action. Autocrines are chemical agents that influence or act on the cell from which it was secreted. Paracrine action is where a cytokine acts on a different type of cell than the one that secreted it in the same area of a tissue. Endocrine action is where a cytokine secreted in the blood stream is distributed into tissues by blood and extracellular fluids. Cytokines are classified into three major groups that describe their function: interleukins, lymphokines and chemokines. Interleukins were first classified as molecules that were produced by a population of blood leukocytes and that interacted with other leukocyte populations [99]. However they are produced by other cell types and many newly discovered cytokines are designated with the interleukin nomenclature to prevent naming ambiguity [100]. Lymphokines are a class of cytokines that are produced by activated T-lymphocytes in response to specific immunity [101]. Chemokines are pro-inflammatory cytokines released by cells and are used to signal or attract other cells to a site of injury or infection. The name is derived from chemotactic cytokines. Two specific cytokines, tumor necrosis factor alpha and interleukin-1, are further described in sections 1.5.1 and 1.5.2, because of their interactions in vascular tissues and one is used later in experiments to invoke a desired reaction from cultured endothelial cells.

1.5.1 Tumor Necrosis Factor Alpha

Since inflammation is a cellular response to injury, stress or infection, cells will upregulate specific receptors in response to those stresses. The inflammatory response is defined by the recruitment of leukocytes to the affected tissue and a shift in the fluid exchange balance through the arterial wall [102, 103].

Tumor necrosis factor alpha (TNF- α) and interleukin-1 (IL-1) are both mediators of inflammation. The process of inflammation was elucidated by Menkin in 1959 when

he described a mediator he called necrosin as being endogenous in nature. In 1975, the mediator TNF- α was defined by Carswell and Old. It behaved like necrosin, previously described by Menkin [104]. TNF- α is highly conserved among species [105] and its function is concentration dependent. At low concentrations it is a pro-inflammatory cytokine and causes the upregulation of endothelial cell receptors and activation and upregulation of macrophages and leukocytes. At higher concentrations it causes cell apoptosis and has anti-tumorogenic properties. [106]

1.5.2 Interleukin 1

Interleukin 1 (IL-1) was one of the first cytokines described by scientists, like Menkin and Beeson in the 1940s as an endogenous pyrogen because of its ability to induce fever when purified samples were administered to normal animals [107]. The entire interleukin group contains over 30 members and IL-1 is a family of pro-inflammatory molecules containing 11 members, all encoded by separate genes [100]. Both IL-1 alpha (IL-1 α) and beta (IL-1 β), are pro-inflammatory molecules in their mature or active forms. The molecules are encoded by a 7 exon gene on chromosome 2 of the human genome and are produced as precursor peptides. The precursors are proteolytically cleaved to become the mature or active forms.

1.6.0 Cardiovascular Disease

Cardiovascular disease is the number one killer of adults in the United States and according to the American Heart Association, 864,480 Americans died in 2005 from some form of cardiovascular disease. Cancer was responsible for 559,312 deaths and accidents for 117,809 deaths. Coronary heart disease caused one in five deaths in the United States in 2004 [108]. Coronary heart disease is caused by atherosclerosis, a

pathological disease causing narrowing of the coronary arteries due to the buildup of oxidized lipids, macrophages and smooth muscle cells in the vessel wall. This process is characterized by an inflammatory response perpetuated by endothelial dysfunction [109] followed by the accumulation of lipids [110], recruitment of leukocytes [111], and activation of smooth muscle cells [112] which eventually form mature plaques. This pathological process occurs over the course of several decades and can be described in six stages. The first stage has been shown to start in as early as the first decade of human life [113-115]. The start of lesion development occurs in areas of endothelial dysfunction. The endothelial cells become permeable and express adhesion molecules on their surface. In stage I lesions, some of the macrophages develop into isolated foam cells after ingesting oxidized low density lipoproteins. In stage II lesions, the lipids accumulate within the smooth muscle cells, the macrophage foam cells accumulate and both cell types form distinct layers that are seen grossly as fatty streaks. The accumulation of macrophages stimulates an inflammatory response in the tissue causing increased production of cytokines. Stage III lesions contain the same cells and cholesterol esters as seen in stage I and II lesions with the addition of extracellular lipid droplets. This accumulation of extracellular material is the link between early and advanced stages of atherosclerosis. Stages I, II and III can occur during the first three decades of life respectively [116]. Advanced stages of atherosclerosis are described by atheromas, lesions that disrupt the intimal structure. Stage IV lesions contain a lipid core caused by the accumulation of extracellular lipids in a distinct region.

This core disrupts the normal intima, and tissue remodeling is initiated by invasive macrophages and migrating smooth muscle cells. Stage V lesions can develop

into three different forms. Type V(a) have multiple layers or cores separated by thick fibrous tissue. Type V(b) lesions have a calcified lipid core, causing severe changes in the elastic properties of the intima. Type V(c) is used to describe lesions with small or absent lipid cores, but with extensive fibrous tissue. Stage VI lesions are stage V and IV lesions that have further modifications. Type VI(a) lesions have surface disruptions, type VI(b) lesions have either hematoma or hemorrhage associated with the lesion and type VI(c) lesions have thrombotic deposits. These different types of surface modification are sometimes called complicated lesions [117].

2. Construction and Characterization of Modified Vesicle Design

Vesicles for targeted drug delivery can be made from several different types of materials such as natural or synthetic surfactants, polymers, peptides, minerals and metals. Vesicles fabricated from semiconductors and single wall nanotubes have also been used as drug carriers [118]. They are very stable and have long circulation times but are not biodegradable and present possible long-term health risks. Membrane vesicle designs using molecules that self-organize when placed into aqueous solutions and form non-covalent structures provide a design that has been used in nature. This is the design chosen for this study and the construction is described in the following sections.

2.1.0 Amphiphiles

Auto-assembly vesicles and cell membranes are formed from molecules called amphiphiles. These are molecules that have two different domains with opposite behaviors towards aqueous environments. Amphiphiles have one distinct region that attracts water molecules (hydrophilic) while the other region repels water molecules (hydrophobic). This property makes them a surface active agent also known as a surfactant. Amphiphiles can be made from natural and synthetic surfactants as well as peptides and co-block polymers. The molecule properties can be further described by their tendency to dissolve in an aqueous liquid (hydrophilicity) or a fatty liquid (lipophilicity), known as the hydrophilic-lipophilic balance (HLB). The HLB is commonly described on a dimensionless scale where 0 is very lipophilic and 20 is very hydrophilic.

There are two major classes of surfactants, non-ionic and ionic. The ionic surfactants can be cationic (positively charged), anionic (negatively charged) or zwitterionic (both positive and negative domains in the head group) that can be positive or negative depending on the pH of the solvent. The ionic and non-ionic surfactants have hydrophobic tail sections composed of long hydrocarbon chains that are attached to hydrophilic head sections with a large hydrodynamic radius compared to the tail section as shown in figure 2.0. The difference in the hydrodynamic radius of the head and tail section is responsible for the formation of the non-covalent structures made from the aggregating surfactant molecules.

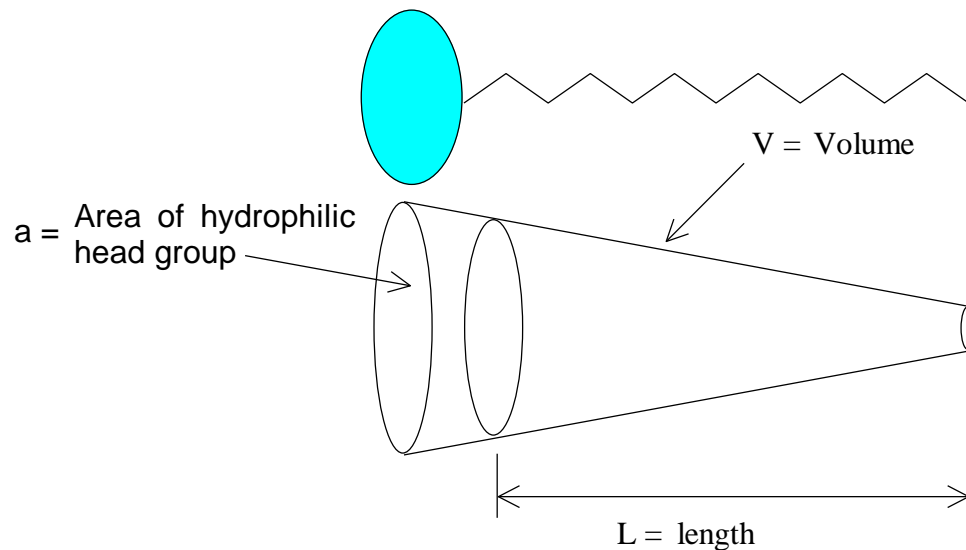


Figure 2.0 Hydrodynamic Shell of a Surfactant Molecule

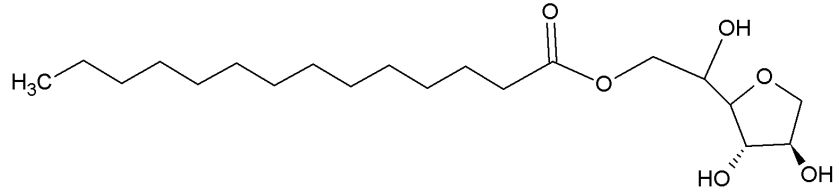
One equation describing this basic behavior of the molecule is the non-dimensional critical packing parameter (CPP).

$$CPP = \frac{v}{a \cdot l} \quad \text{Equation 2.0}$$

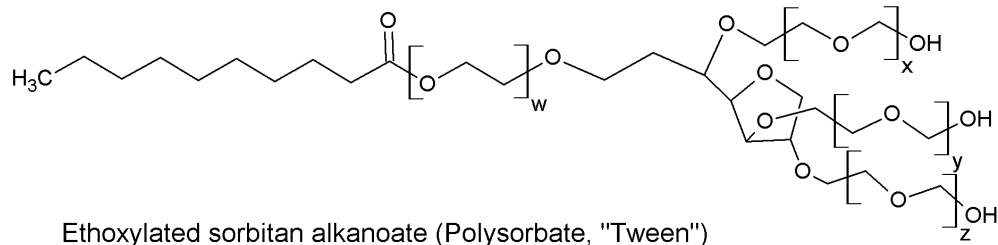
In equation 2.0, “V” is the volume of the molecule, “a” is the effective head group area and l is the hydrophobic tail chain length. Amphiphiles that have a CPP value below 0.5 will form micelle structures. Cylindrical micelles will form when the CPP is in the range of 0.3 to 0.5. When the CPP range is between 0.5 and 1, amphiphiles will form both vesicles and flexible bilayers. Therefore, this is the target range for the surfactants used in this study. When the CPP range is equal to 1, then lamella and planar structures are formed. Inverse micelles are formed when value of the calculated CPP is greater than 1.

2.1.1 Non-Ionic Surfactants

Non-ionic surfactants are synthetic amphiphiles that are commonly used as detergent emulsifiers. The two surfactants used in this study are sorbitan monostearate (Span 60) and polyethylene sorbitan monostearate (Tween 61). Both contain fatty acid tails composed of approximately equal amounts of stearic acid ($\text{CH}_3(\text{CH}_2)_{16}\text{COOH}$) and palmitic acid ($\text{CH}_3(\text{CH}_2)_{14}\text{COOH}$). Three hydroxyl groups attached to the head groups makes the molecules hydrophilic. The Tween 61 molecule has three oligomeric chains of polyoxyethylene used to tether the hydroxyl groups to the head of the molecule as shown in figure 2.1.



Sorbitan Alkanoate (Sorbitan ester, "Span")



Ethoxylated sorbitan alkanoate (Polysorbate, "Tween")

Figure 2.1 Molecules: Span 60 and Tween 61

2.1.2 Cholesterol

Cholesterol is a steroid which exhibits a slight amphiphilic tendency due to the hydroxyl group at the head of the ring structure as shown in figure 2.2. Cholesterol, with an HLB factor of 2.96 is used to stabilize the bilayer membrane by adding rigidity due to the planar configuration of the molecule. Steroid molecules that are closely related to cholesterol, such as β -cholestanol, β -sitosterol and stigmasterol can be used to tailor the leakage and stability of the membrane [119].

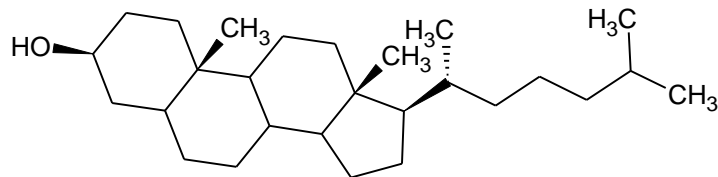


Figure 2.2 Cholesterol

2.2.0 Polyethylene Glycol

Polyethylene glycol (PEG) is a hydrophilic polymer made from repeating units of ethylene oxide and is shown in figure 2.3. The polymer is also named polyethylene oxide (PEO) and polyoxyethylene (POE). PEG is commonly used to refer to polymers with molecular weights below 20,000 Da while polymers with molecular weights greater than 20,000 Da are commonly referred to as PEO. POE is used to describe all weights of the polymer.

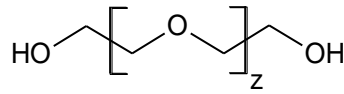


Figure 2.3 Polyethylene Glycol (PEG)

The polymer behavior is based on temperature, solvent, molecular weight and the concentration of the polymer. When the polymer is synthesized, it may have a distribution of molecular weights. Separation techniques are used to sort the polymer chains on a size basis. The polydispersity index (PDI) is a measure of how similar the molecules are to one another in size and weight (equation 2.3). It can be calculated by the ratio in the number average molar mass (equation 2.1) and the weight average molar mass (equation 2.2).

$$\bar{M}_n = (\sum n_i M_i / \sum M_i) \quad \text{Equation 2.1}$$

$$\bar{M}_w = (\sum w_i M_i / \sum w_i) \quad \text{Equation 2.2}$$

$$\text{PDI} = \bar{M}_w / \bar{M}_n \quad \text{Equation 2.3}$$

PEG has been used in a variety of drug delivery applications. Conjugation of PEG to peptides and proteins is used to modify their behavior in the body. Since PEG is highly water soluble, it can be used to modify proteins and drugs that are not very soluble in aqueous solutions [120]. PEG conjugation can be used to control the membrane

permeability of small molecules used as chemotherapeutic agents [121]. It is also used to modify protein and peptide circulation time while maintaining bioavailability and slowing enzymatic degradation [122-125].

PEG can also be conjugated or adsorbed onto the surface of small particles or vesicles. The addition of the polymer to the surface helps to slow the attachment of serum proteins that tag the particles for removal [126]. This approach has been used in liposome production to hide them from phagocytes, creating stealth liposomes [12, 15, 127-135]. Another benefit of PEG conjugation is steric stabilization of the particle by physically separating the vesicle membranes from one another thereby preventing vesicle fusion [136].

The conformation of the grafted PEG chains is dependent on the distance between surface attachment points (D) and chain length of the polymer (R). There are three primary conformations: pancake ($D \gg R$), mushroom ($D > R$) and brush ($D \leq R$) with transition phases between them. For a PEG chain of 2000 Da (PEG 2000), the pancake conformation is typical when the PEG surface concentrations are 1.3 mol%. Mushroom conformation is found when PEG surface concentrations are at 4.5 mol%. At higher PEG concentrations of 9 mol%, the polymer interaction forces the chains to extend into the brush conformation [137]. In liposomes, it has been shown that PEG 2000 with a 5 mol% surface concentration extends blood circulation times compared to liposomes without the PEG chains. For the immuno-niosome vesicle design, a bifunctional PEG 2000 was used.

2.3.0 Molecule Synthesis

Vesicles used as drug carriers can be constructed, loaded and functionalized using a variety of methods and chemistries. Drug-loaded niosomes that can be functionalized

after construction by using a linker molecule activated by adjustment to an alkaline pH, provide a functionalization method that is simple and nondestructive to the encapsulated therapeutic agent. The surfactant is modified to form a functionalized surfactant molecule that can be used to create the niosome vesicles.

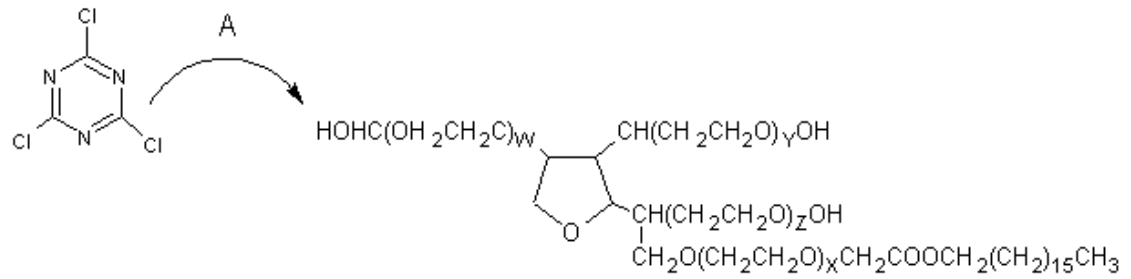
Table 2.0 Immuno-niosome Materials

Material description	Catalog number	Manufacturer
Tween 61	P-3065	Sigma-Aldrich
Span 60	85546	Fluka
Omega-Hydroxyl alpha-amino PEG, MW 2000 Da	HO-PEG2000-NH2	JenKem Technology Co., Ltd.
Cholesterol	362794-5G	Sigma-Aldrich
N,N-diisopropylethylamine, redistilled	387649-100ML	Sigma-Aldrich
Chloroform	AC61028-1000	Acros Organics
Dicetyl phosphate	101546	MP Biomedicals, LLC
Cyanuric chloride	C95501	Sigma-Aldrich

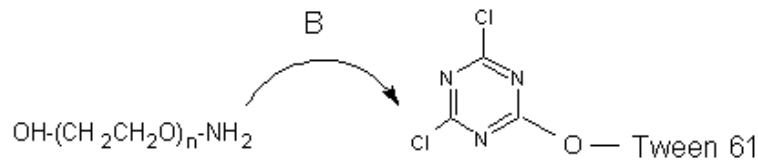
2.3.1 Functionalized Non-Ionic Surfactant

Polyoxyethylene sorbitan monostearate (Tween 61) is a non-ionic surfactant with a fatty acid hydrophobic tail structure composed primarily of stearic acid and a hydrophilic head group with three short polyoxyethylene chains. The linker molecule cyanuric chloride (CC), is covalently attached to the surfactant through nucleophilic substitution to the hydroxyl group on the terminal end of one of the polyoxyethylene chains. Tween 61, dissolved in dry chloroform and CC in a 0.8 molar ratio of [CC:Tween

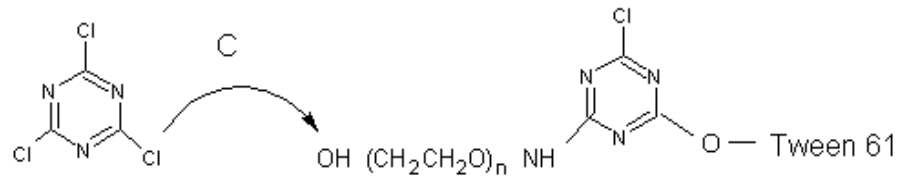
61] in the presence of a 3 fold molar ratio of N,N-diisopropylethylamine (DIPEA) are mixed together. To form the functionalized surfactant Tween-CC, the mixture is placed in a 50 ml round bottom flask attached to a sealed rotary evaporator under a nitrogen atmosphere for 36 hours. Next, an intermediate molecule is created by covalently binding the amine group on the bi-functional PEG molecule to the previously functionalized Tween-CC surfactant in a 0.9 molar ratio [PEG:Tween-CC] in the presence of 2 fold molar ratio of DIPEA. To functionalize this intermediate molecule, CC is covalently bound to the terminal hydroxyl group on the PEG chain in a 0.8 molar ratio [CC:Tween-CC-PEG] in the presence of 2 fold molar DIPEA for 36 hours to form Tween-CC-PEG-CC. The reaction steps are shown in figure 2.4.



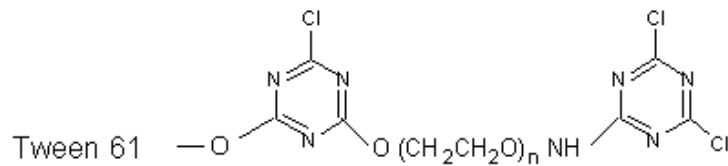
Reaction A
 Cyanuric chloride (CC) + Tween 61 \longrightarrow Tween-CC



Reaction B
 PEG+Tween-CC \longrightarrow Tween-CC-PEG



Reaction C
 CC + Tween-CC-PEG \longrightarrow Tween-CC-PEG-CC



Final product, Tween-CC-PEG-CC

Figure 2.4 PEGylated Surfactant Synthesis

2.3.2 Functionalized Cholesterol

In addition to the functionalized PEGylated molecule described in section 2.3.1, a second functionalized molecule was synthesized to provide options for targeted drug delivery. Cholesterol is a fat soluble molecule that can be incorporated in vesicles and micelles made from non-ionic surfactants. Using functionalized micelles, lipophilic and hydrophobic agents that would normally destabilize a bilayer membrane can be delivered to a specific target. The cyanuric chloride (CC) functionalized cholesterol provides a site for antibody conjugation that is in close proximity to the vesicle surface, thereby enhancing the fusibility of the vesicle with the endothelial cell outer membrane. This occurs when the vesicle is less than 2nm from the cell surface and provides an additional delivery strategy. The synthesis was carried out as previously described. The cholesterol dissolved in dry chloroform was reacted for 36 hours with CC in a 1:0.9 molar ratio in the presence of DIPEA under a nitrogen atmosphere. The CC replaces the hydroxyl head group on the cholesterol molecule forming the molecule cholesterol-CC as shown in figure 2.5.

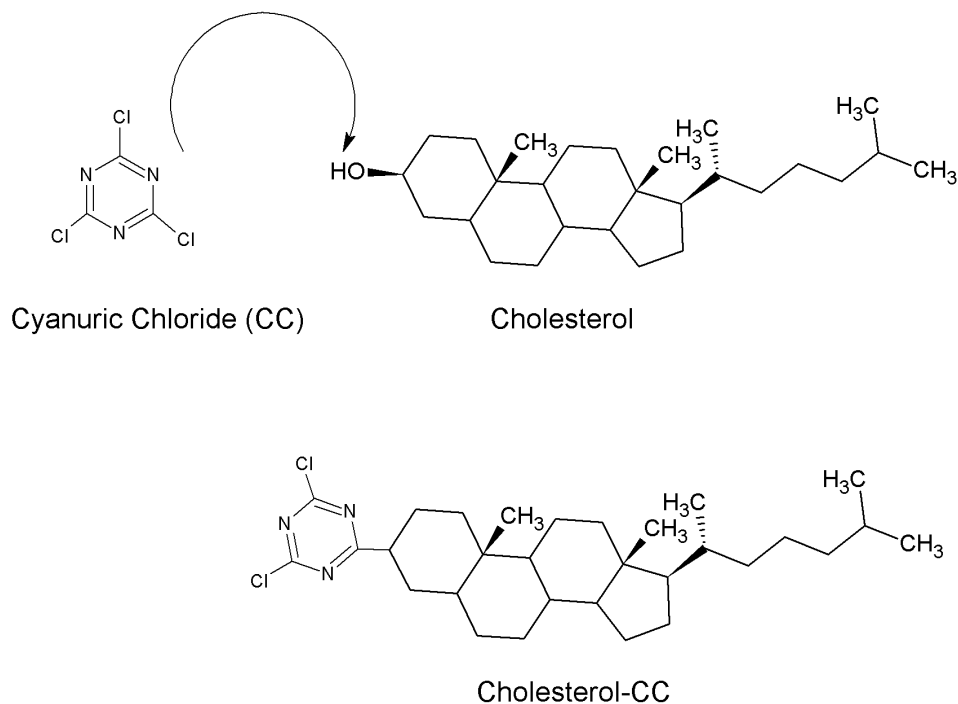


Figure 2.5 Functionalized Cholesterol Synthesis

2.4.0 Vesicle Synthesis

Vesicle formation is a multi-step process driven by the reduction of the amphiphile surfactant molecule energy state that forms ordered, non-covalent structures as described in section 2.1.0. Membrane formation is a process that requires a temperature-dependent phase change and mechanical shear forces. The materials used are a combination of surfactant, functionalized surfactant, cholesterol and an electrostatic agent. The ratios of materials are derived from previous studies where a 1:1:0.01 molar ratio of cholesterol, surfactant and an electrostatic agent respectively, provide a stable membrane structure. Here, dicetyl phosphate (DCP) is used as the electrostatic agent since it provides a slight negative charge which helps the formed vesicles repel one another in solution.

2.4.1 Thin Film Formation and Hydration

The first step in vesicle formation is the production of lamella that are formed from the materials in round bottom glass flasks on a rotary evaporator. Functionalized and non-functionalized non-ionic surfactants, cholesterol and dicetyl phosphate are dissolved in chloroform. The mixture is reduced under a nitrogen atmosphere at low pressures. When the solution is reduced to a thin film, the pressure is reduced to 50 bar for 2 hours and then purged with nitrogen under atmospheric pressure at 4 L/min to remove trace chloroform from the film.

To form vesicles, the thin films are hydrated using an aqueous solution containing a hydrophilic drug or dye. The aqueous solution is placed in a round bottom flask on a sealed rotary evaporator that has been purged with nitrogen. The temperature is raised above the gel crystalline phase using a hot water bath and a shear force is applied by rotation of the flask on a rotary evaporator to separate the lamella into sheets to form a combination of multilayer and bilayer vesicles in solution.

2.4.2 Vesicle Extrusion

To control the vesicle size distribution, a barrel extruder (LIPEX™, Northern Lipids Inc.) and polycarbonate membranes are used. The membranes are commercially available with uniform pore sizes ranging from 1 μm down to 50 nm, allowing control of the desired extruded vesicle size. The extruder is surrounded by a water jacket in order to maintain the extrusion temperature above the gel crystalline phase. The raw solution of multilayer vesicles (MLVs) and bi-layer vesicles (BLVs) is loaded into the extruder and pushed across the polycarbonate membranes using high pressure nitrogen gas. Multiple passes are performed to create uniform vesicle dispersions in the bulk solution.

2.4.3 Size Exclusion Chromatography Introduction

Size exclusion chromatography (SEC) is a method used to separate molecules from a solution based on their size. Other types of SEC include: gel filtration chromatography (GFC)-aqueous system and gel permeation chromatography (GPC) – non-aqueous system, used for polymer separation. Both types of SEC use a non-adsorptive stationary phase to eliminate any reactive process of the sample with the stationary phase. The separation process is driven by two primary phenomena, diffusion and exclusion. This is accomplished by placing the sample in a column with a porous packing material stationary media. The material allows small molecules to diffuse within the stationary packing material while the larger molecules are excluded by size, and flow freely around the packing material. This difference in traveling time or retention time allows for sample separation as shown in figure 2.6.

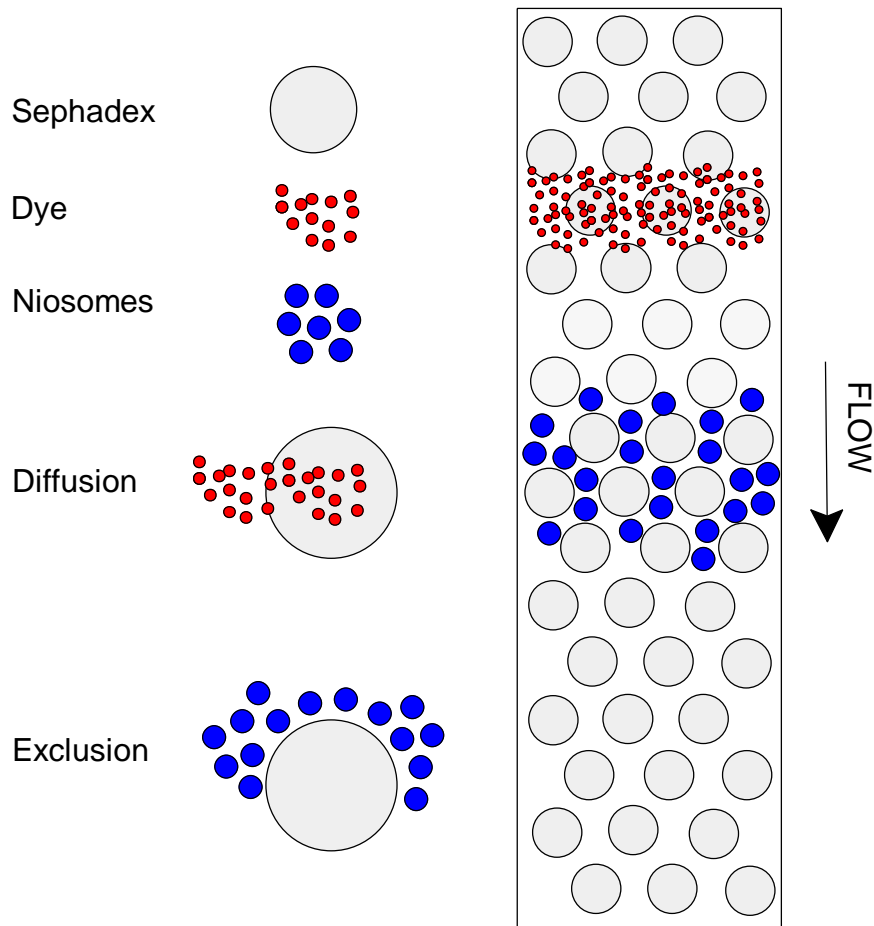


Figure 2.6 Size Exclusion Chromatography

2.4.3.1 SEC Volumetric Theory

The separation process is based on the variation in hydrodynamic sizes of the sample molecules to be processed and their interaction with the packing material. The porosity of the packing material and the packing geometry create the volumetric parameters that are used to describe how the sample elutes from the column.

$$K_{av} = \frac{V_e - V_o}{V_t - V_o} \quad \text{Equation 2.4}$$

This volumetric distribution is described by equation 2.4, where K_{av} is the average volumetric distribution coefficient, V_e is the elution volume, V_t is the total volume, or the sum of the outer (V_o) and the inner volume (V_i) of the packing material, sephadex. V_i

is the inner volume of the packing material and is equal to $V_t - V_o$. $V_e - V_o$ is the retention volume and if the packing material particles do not retain the solute (sample), then the value of $K_{av} = 0$. A graphical depiction is shown in figure 2.7.

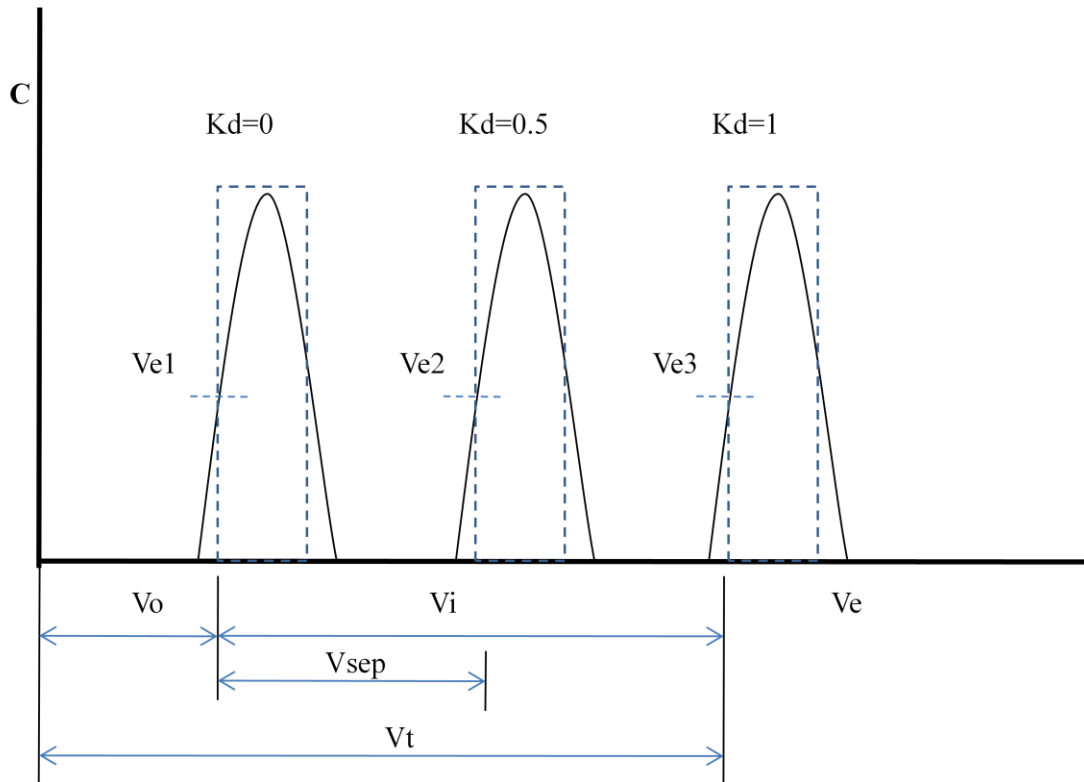


Figure 2.7 Size Exclusion Chromatography Elution Profile

2.4.3.2 SEC Methods

In fluorescent dye loaded niosome production, the formed vesicles must be separated from the free (unencapsulated) dye. The bulk sample containing dye-loaded niosomes and free dye is injected in a column that is packed with small porous spheres made from cross-linked dextran (Sephadex). To prevent the vesicles from collapsing or swelling, the aqueous solvent phase used is phosphate buffered saline solution with the same osmotic strength as the dye solvent. An Akta Prime (GE Healthcare) chromatography system equipped with a pH probe, conductivity probe, pressure sensor,

mercury lamp and UV filter set is used for the separation. The column is a 70 cm model XK 16 and is used for separating large bulk samples up to 2 ml, however we have found that sample sizes of 500 ul avoid fouling in the entrance, causing back mixing of the sample. Figure 2.8 is the elution profile of a 2 ml sample where the peak spread from where the sample clogged the packing material as it entered the column.

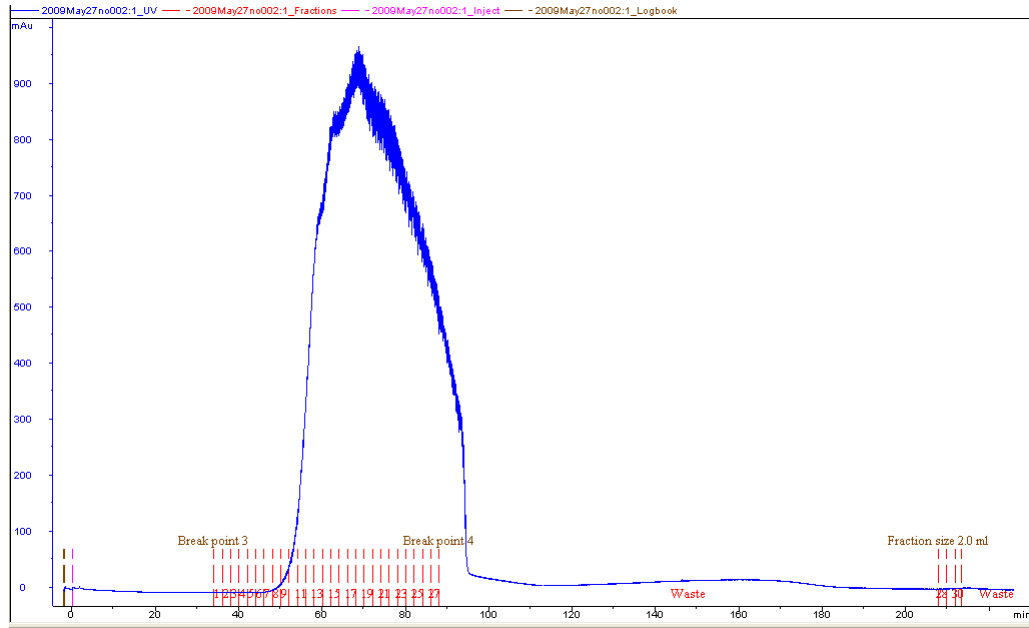


Figure 2.8 Elution Profile from 2 ml Sample Size

Figure 2.9 is the elution profile from a 500 ul sample that was injected into the column. The narrow peak shows that the sample was able to pass through the entrance without fouling the packing material to the point that causes back mixing of the sample.

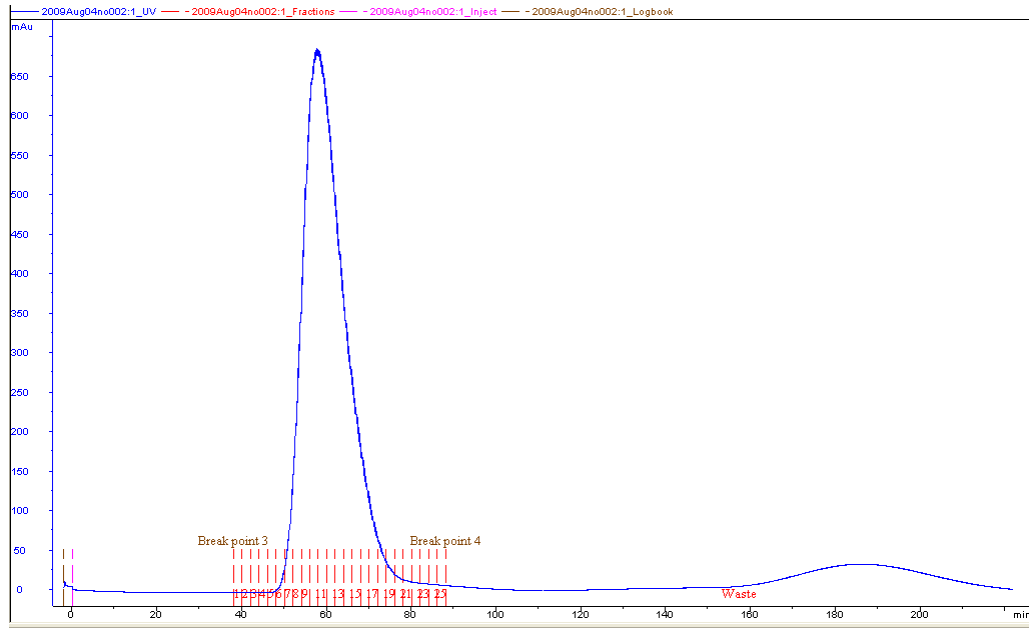


Figure 2.9 Elution Profile from 500 ul Sample Size

2.4.4 Antibody Conjugation

Immuno-niosomes are created when antibodies are conjugated to the exterior surface of the niosomes. This procedure is conducted at room temperature (25°C) on an orbital shaker table for 16 hours. First, the conjugation is initiated by adjusting the pH of the niosome solution to 8.8 as described by Bendas and Hood [16, 17]. At pH 8.8, the chloride groups on the cyanuric chloride molecule are activated and thus a covalent bond is formed via nucleophilic substitution with one of the disulfide groups on the Fc region of the IgG as shown in figure 2.10.

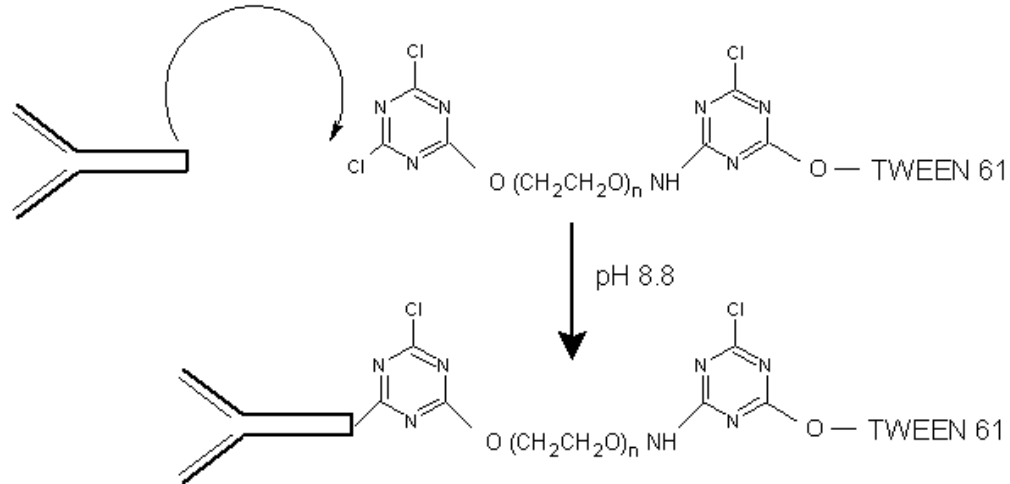


Figure 2.10 Antibody Conjugation

After antibody conjugation, the solution is loaded in a disposable PD-10 chromatography column packed with sephadex G-25. The immuno-niosome fraction is eluted with one column volume of 0.01M phosphate buffered saline. The pH of the sample is verified and adjusted if necessary. The excess unconjugated antibodies can be recovered by subsequent column elution.

2.5.0 Vesicle Metrology

To determine vesicle size stability and dispersion properties, a variety of methods were used to gather data on the niosomes after synthesis. The methods include chromatography, microscopy, flow cytometry and dynamic light scattering techniques.

2.5.1 Thin Layer Chromatography Introduction

Thin layer chromatography (TLC) provides an economical method of sample analysis without the need for expensive equipment and materials typically used in high performance liquid chromatography (HPLC). Although HPLC is more sensitive and can detect trace concentrations it is recommended as a follow-up procedure to TLC. TLC is also recommended for development and optimization of the solvent system used for the

separation. The flat plates allow for visual inspection of the separation. Samples that have components that interfere with the separation or are at concentrations below the limit of detection will need to be preprocessed by separation or concentration respectively prior to using TLC. Separation can be completed using a simple solvent partitioning procedure (Folch method, [138]), ion exchange columns [139] or solid phase extraction columns [140].

The TLC separation process is based on a mobile phase composed of a combination of solvents that carry the sample up the plate by convective forces and a stationary phase acting as the adsorbent and attracting the sample to the matrix by hydrogen bonds and dipole interactions. The solvent system contains polar and nonpolar solvents creating an organic/inorganic partition on the plate. The sample is separated into its components as the mobile phase moves up the plate.

2.5.1.1 Thin Layer Chromatography Methods

Table 2.1 TLC Materials

Item	Description	Manufacturer
TLC Plates	20 x 20, Silica Gel 60Å , 250um Fluorescent Indicator.	Whatman® Catalog No: 4861-820
TLC Tank	Glass 25 cm x 25 cm Tank	Fisher
Micro-Pipettes	1 Lambda (1 ul)	Drummond # 1-000-0010
Micro-Pipettes	5 Lambda (5 ul)	Drummond # 1-000-0050
Atorvastatin	Atorvastatin Calcium	Pfizer
Chloroform	Solvent	Fisher

Table 2.1 (Continued)

Item	Description	Manufacturer
Diethyl Ether	Solvent	Fisher
Hexane	Solvent	Fisher
Acetic Acid	Solvent	Fisher
Methanol	Solvent	Fisher
UV Lamp	254nm Ultraviolet hand held lamp	Cole Parmer
Camera	35mm SLR digital , EOS 20D	Cannon

For the TLC separation, 20x20 cm glass plates coated with a thin layer of silica (stationary phase) impregnated with a fluorescent indicator were used. When the TLC plate is exposed to ultraviolet light, the separated components block the fluorescent signal as indicated by a dark spot on the plate. If the component of interest does not fluoresce or absorb, a stain can be applied to the plate which will react with or stain the separated component so it can be imaged.

Atorvastatin calcium was encapsulated in a previously designed immuno-niosome. TLC analysis was used to determine the actual concentration of atorvastatin calcium within the immuno-niosomes. Some of the samples were processed prior to TLC separation to concentrate and separate components. Standards were applied directly to the plate using disposable glass capillary tubes (microcap). Two solvent systems were chosen. The first separation was completed in chloroform (a proton donor), methanol (polar) and 4% acetic acid in a [45:55:4] volumetric ratio. The second development was completed using hexane (as the diluent), diethyl ether (proton acceptor), and acetic acid in a [80:20:1.5] volumetric ratio. The methanol and chloroform form a partition on the

plate based on their polarity. The hexane and ether are used to separate lipids and cholesterol. The acetic acid is used as a solvent modifier to reduce tailing of the sample during separation when lipids are present.

2.5.1.2 Thin Layer Chromatography Results

The plates are analyzed using an open software routine in MATLAB, that determines the spot density from an image (shown in Figure 2.11) taken with a 35mm SLR digital camera [141]. The plate is illuminated by a mounted 254nm lamp. The focal distance of the camera, position of the lamp and position of the sample spot are held constant.

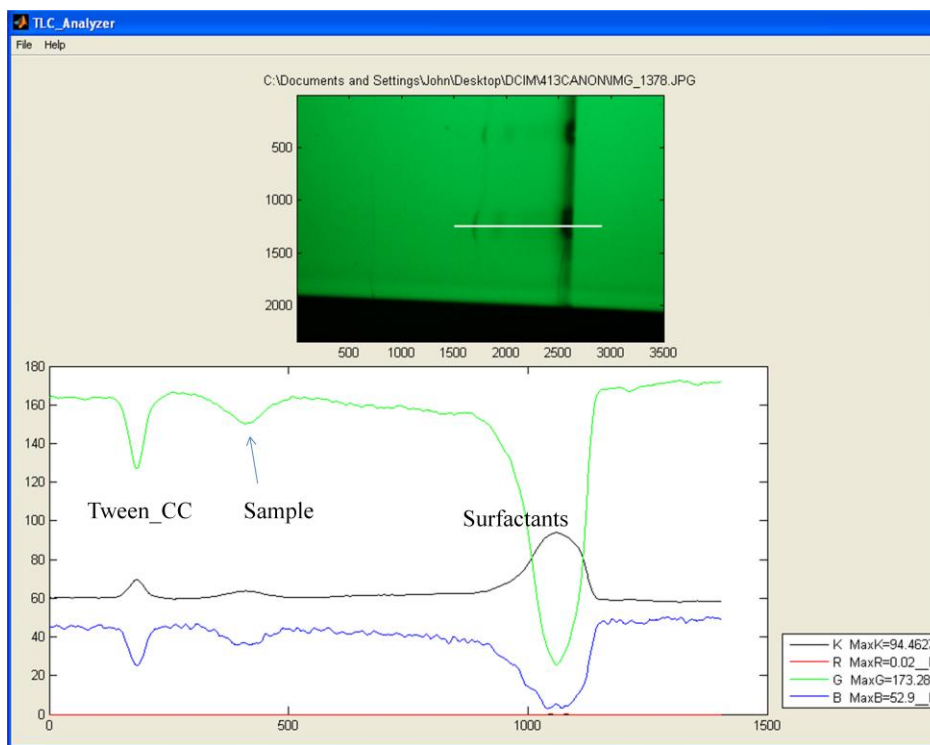


Figure 2.11 TLC Image Analysis

The calibration curve in Figure 2.12 was generated using known concentrations of pure atorvastatin dissolved in methanol. The standards were directly spotted onto the TLC plate and then developed. The linearity of the standards ($R^2=0.9898$) shows the sample

follows the Beer-Lambert law [142]. Standards and unknowns are included on each TLC plate to allow for comparison between plates. To determine the actual encapsulation of atorvastatin used to treat apolipoprotein E knockout mice, immuno-niosome samples were dehydrated on a vacuum concentrator and reconstituted using methanol. The atorvastatin dissolves freely in methanol while cholesterol and Span 60 (niosome components) do not. Samples were rehydrated in 1/10th the volume of the original sample in order to concentrate the drug. Additionally, standards were separated on the same plate to provide a concentration reference. It was determined that the concentration of atorvastatin encapsulated in the immuno-niosomes was 1.68E-05 mg/ml, well below the expected concentration of 0.15 mg/ml.

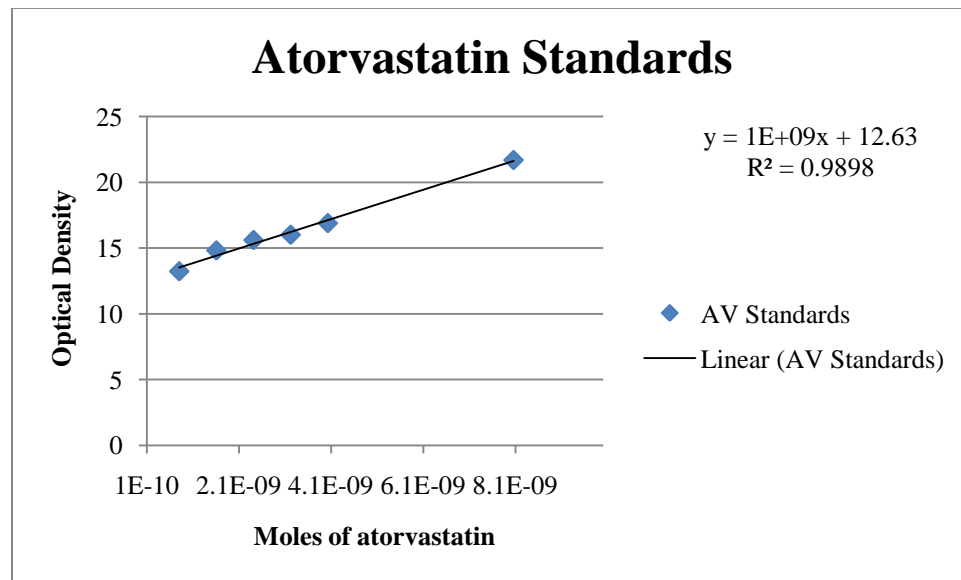


Figure 2.12 Atorvastatin Standards

2.5.2 Fluorescent Microscopy

Fluorescent microscopy is used to confirm specific binding of the immuno-niosomes to cell surface receptors. The antibody conjugation to the immuno-niosomes is also imaged using this technique. Materials may exhibit fluorescent behavior when they

have been excited by a beam of light. Fluorescence was first described by Stokes when he noticed that some minerals emitted visible light when an invisible source light was used to illuminate them [143]. This process can be described in three steps using a simple Jablonski diagram (Figure 2.13).

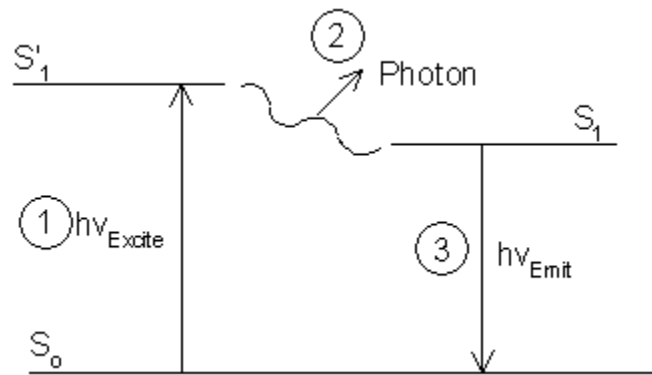


Figure 2.13 Jablonski Diagram

First, the energy state of the molecule is increased by the absorption of light from a source. The second step is the release of a photon from the molecule after it has been excited by an external source. The third step is the energy level drop to the normal state after the release of a photon. This energy difference between the two states is called the “Stokes shift” and was described by Alexander Jablonski in 1935 [144]. Fluorescence microscopy takes advantage of the ability to separate a specific spectrum of light that is emitted from a molecule by using optical filters. To confirm antibody conjugation to the functionalized surfactant, large vesicles ($>1\mu\text{m}$) were produced with 5% functionalized PEG2000 to create the PEGylated immuno-niosomes. Immuno-niosomes conjugated with fluorescein isothiocyanate (FITC) labeled antibodies are shown by the arrow in figure 2.14 (400X magnification).

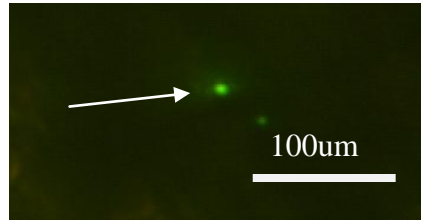


Figure 2.14 PEGylated FITC Conjugated Immuno-niosomes

Another type of functionalized molecule was synthesized to provide alternative conjugation strategies that are described in section 5.3.0. This was accomplished using cholesterol and functionalizing the molecule with the cyanuric chloride linker chemistry. Confirmation of the functionalized cholesterol was accomplished by imaging large vesicles ($>1\mu\text{m}$) that were conjugated with fluorescently tagged antibodies. Figure 2.15 is a black and white image taken of the fluorescent tagged immuno niosomes made with 10% functionalized cholesterol (200x magnification, bright spots indicate fluorescent tagged immuno-niosomes).

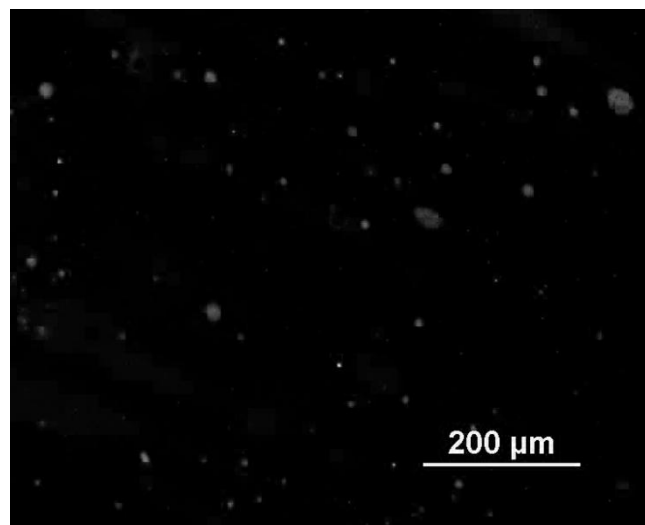


Figure 2.15 FITC Conjugated Immuno-niosomes Using Functionalized Cholesterol

2.5.3 Flow Cytometry

Flow cytometry is a technique used to examine cells and microscopic particles in suspension. For the experiments shown below, an LSR II flow cytometer (Becton Dickinson) was used. Cells or particles are either tagged with a fluorescent labeled antibody or a fluorescent dye can be encapsulated in the particles. The particles are suspended and move in a flowing stream through a laser path. Median fluorescent intensity and forward and side scatter from the dye and particle is detected using a photomultiplier tube. Forward scatter data is used to indicate cell volume and side scatter data is used to examine the complexity of internal structures of the cell or particle. Flow cytometry is commonly used to count fluorescently labeled cells in a mixed population. In this study it was used to confirm antibody conjugation and provide a map of the population distribution of the vesicles, to confirm data collected using dynamic light scattering instrumentation. Immuno-niosome samples were conjugated with Fluorescein isothiocyanate (FITC) labeled goat anti rat IgG antibodies. Figures 2.16 and 2.17 and tables 2.2 and 2.3 show forward and side scatter data along with median fluorescence intensity for the two populations from a sample of 5% PEGylated immuno-niosomes that were hydrated with phosphate buffered saline and conjugated with FITC labeled IgG. Figure 2.18 is dynamic light scattering data for the same sample illustrating the two different size vesicle populations. Previously the immuno-niosomes size was controlled using extrusion techniques and size exclusion chromatography. By combining these size and purification techniques 99.7% of the population was the same size.

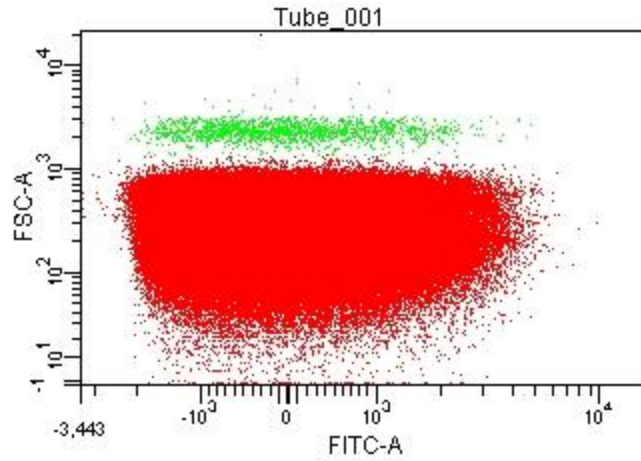


Figure 2.16 5% PEG Sample Forward Scatter Distribution

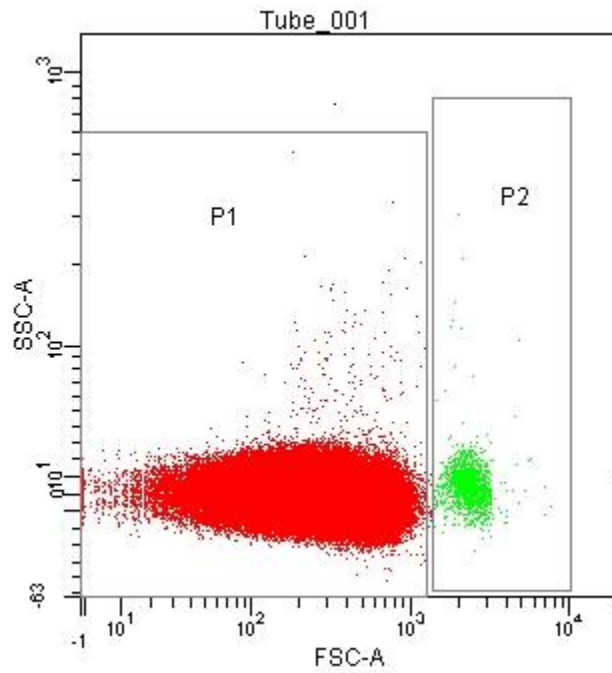


Figure 2.17 5% PEG Sample Particle Size Distribution

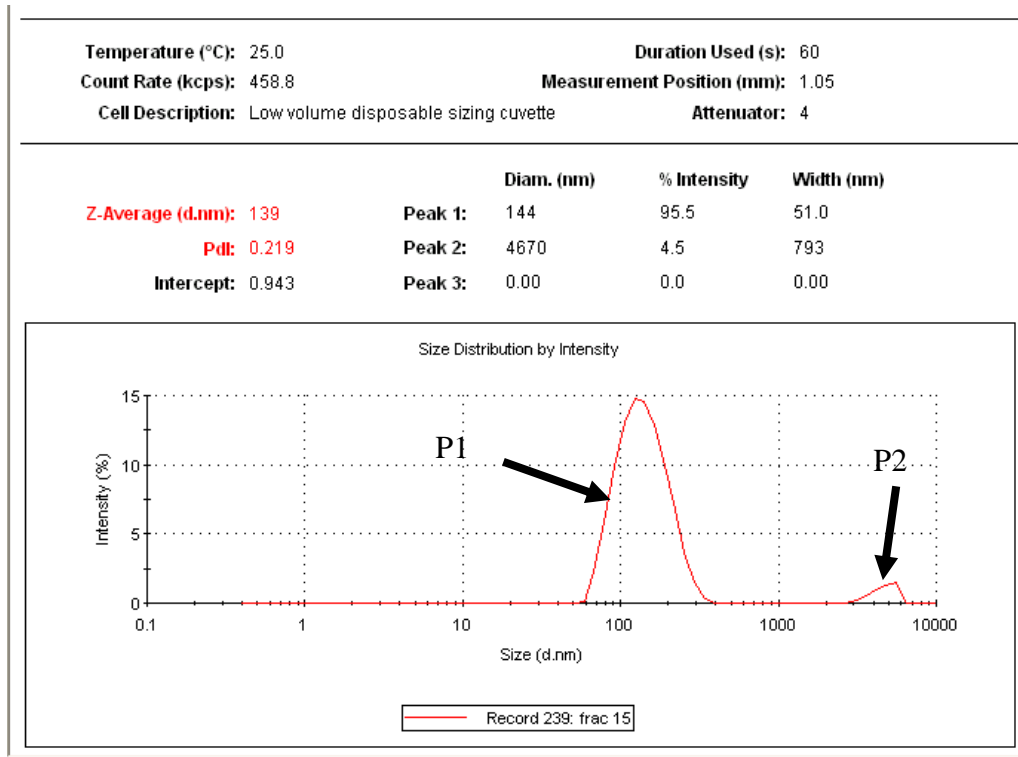


Figure 2.18 5% PEG Sample Dynamic Light Scattering Data

Table 2.2 5% PEG Sample Event Population

Tube: Tube_001			
Population	#Events	%Parent	%Total
All Events	411,588		100.0
P2	1,424	0.3	0.3
P1	410,162	99.7	99.7

Table 2.3 5% PEG Sample Median Distribution

Tube Name: Tube_001			
Population	%Parent	FITC-A Median	FITC-A Mean
P2	0.3	-74	12
P1	99.7	-88	-4

Fluorescent dye loaded niosomes were prepared using 10% functionalized cholesterol. To maintain large vesicle sizes, the niosomes were not extruded. However they were vortexed to create large vesicles and then separated from the free dye using

size exclusion chromatography. The different sized fractions were mixed together. Forward scatter data illustrating the three different population sizes is shown in figure 2.19 and table 2.4. The three different population sizes are also shown using dynamic light scattering as shown in figure 2.20.

Table 2.4 10% Functionalized Cholesterol Median Population

Tube Name: Tube_004							
Population	FSC-A Mean	FSC-H Mean	FSC-W Mean	SSC-A Mean	SSC-H Mean	SSC-W Mean	FITC-A Mean
All Events	296	291	67,668	274	282	15,970	20
P1	806	902	58,249	3,688	3,019	29,881	42
P2	272	269	67,723	103	141	15,617	19
P3	10,874	9,061	77,753	74,350	62,226	79,962	696

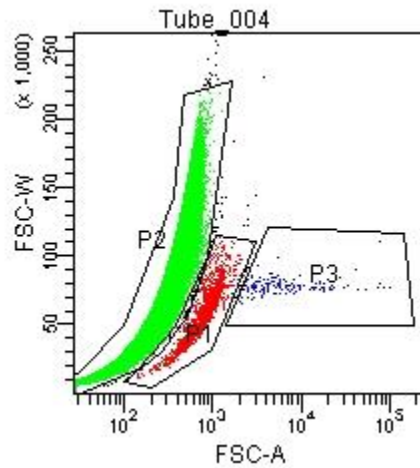


Figure 2.19 10% Functionalized Cholesterol Forward Scatter Distribution

	Diam. (nm)	% Intensity	Width (nm)
Z-Average (d.nm): 377	Peak 1: 215	48.8	58.3
Pdl: 0.644	Peak 2: 1500	45.0	684
Intercept: 0.973	Peak 3: 4660	6.2	742

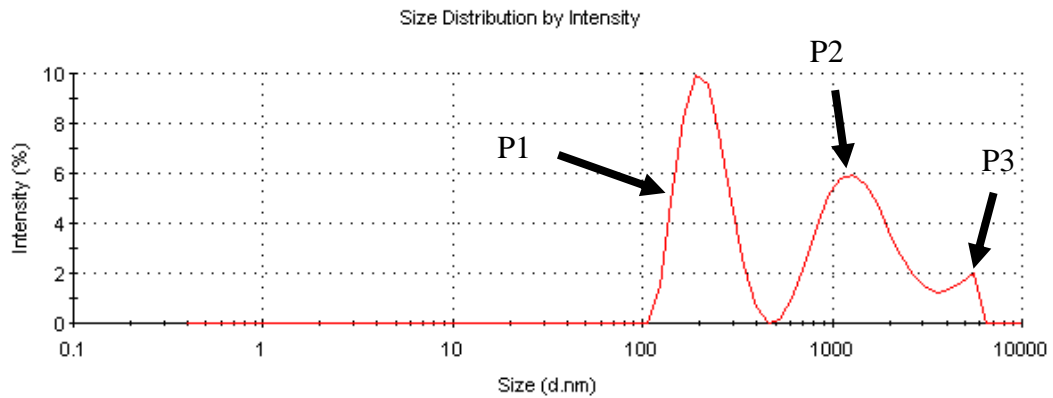


Figure 2.20 10% Functionalized Cholesterol Sample Dynamic Light Scattering Data

2.5.4 Transmission Electron Microscopy

Transmission electron microscopy (TEM) is used to provide sample images with high resolution and magnification that cannot be achieved with light microscopy. This is accomplished in a device that shoots a focused beam of electrons through the sample. The signal can be detected using an electronic camera or the resulting beam can be viewed on a phosphorus screen. A beam of high energy electrons emanate from an electron gun that is passed through a very thin section of material to produce images. The electron beam must be under vacuum to prevent unwanted molecular interactions.

Table 2.5 Transmission Electron Microscopy Materials

Item	Description	Manufacture
2% glutaraldehyde	Fixative made from 50% stock	Fisher
2% Osmium Tetroxide	Fixative and contrast stain	EMS

Table 2.5 (continued)

2% Uranyl Acetate	Stain	EMS
Acetone	Solvent	Fisher
Ethanol	Anhydrous agent	Fisher
Propylene Oxide	Solvent	EMS
Embed 812	Resin	EMS
Araldite 502	Resin	EMS
Dodecenyl Succinic Anhydride	Anhydride	EMS
2,4,6-tridimethylamino methyl phenol (DMP-30)	Accelerator	EMS
Lead Nitrate	Stain	EMS
Sodium Citrate	Stain	EMS
1N Sodium Hydroxide	Reagent	Fisher
20nm Gold Particles	Electron dense marker	EMS
5nm Iron Oxide particle	Magnetic particle	Oceannanotech
Copper Grids	Sample holder TEM	EMS
Formvar Coated Grids	Sample holder TEM	EMS

A transmission electron micrograph of the solution containing 5% PEGylated surfactants hydrated with 0.01M phosphate buffered saline is shown in figure 2.21 The solution was stained with uranyl acetate, placed on a formvar coated carbon grid and imaged. The arrows indicate multi-layer membranes from the vesicles in the bulk solution.

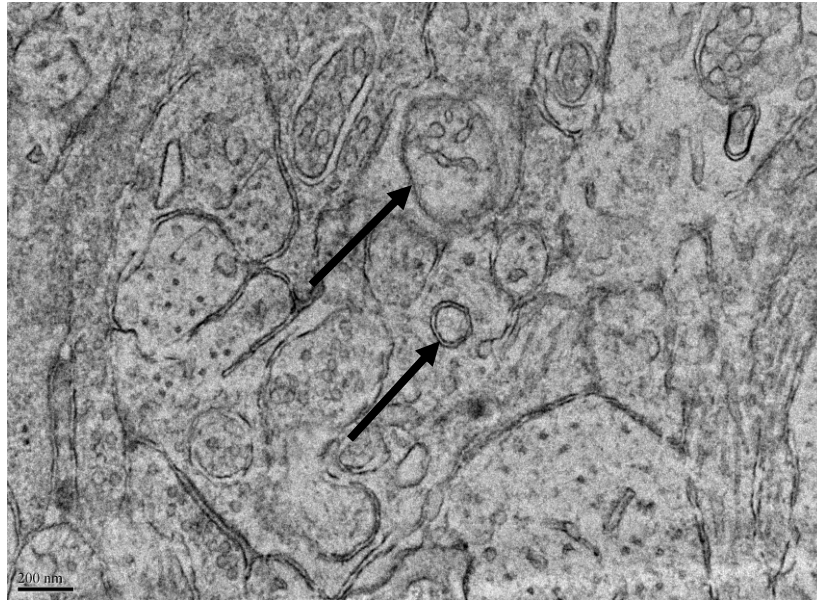


Figure 2.21 TEM of Bulk Solution

A transmission electron micrograph of niosomes prepared with 5% PEGylated surfactant and hydrated with 0.01M phosphate buffered saline is shown in figure 2. The vesicles were treated with osmium tetroxide to stabilize the vesicle membrane through chemical fixation. The vesicle suspension was placed on a formvar coated carbon grid, dried and imaged.

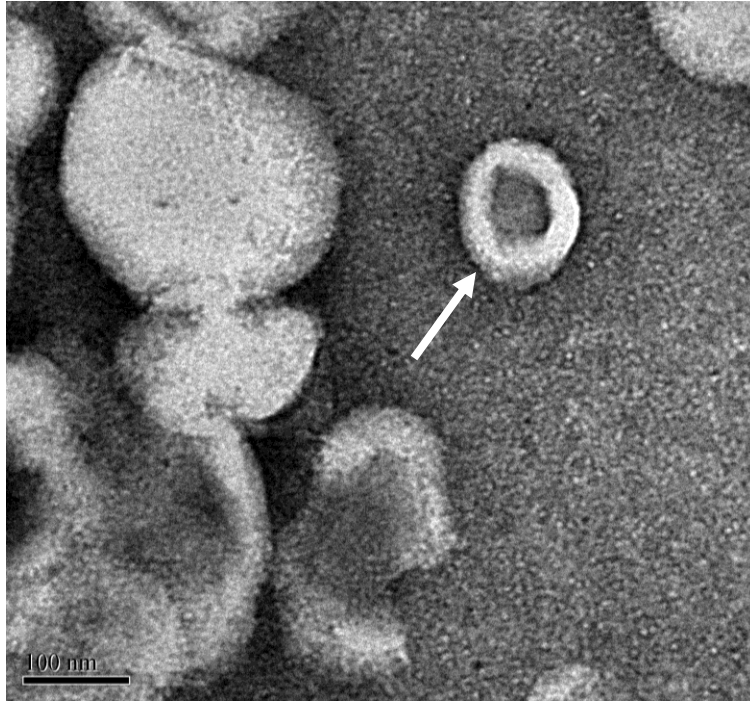


Figure 2.22 TEM of Extruded 5% PEGylated Niosomes

A transmission electron micrograph of 5% PEGylated surfactant niosomes containing 5nm paramagnetic FeO particles in 0.01M phosphate buffered saline is shown in figure 2.23. The vesicle suspension was placed on a formvar coated carbon grid, dried and imaged.



Figure 2.23 TEM of 5% PEGylated FeO-Loaded Niosomes

2.5.5 Dynamic Light Scattering

Dynamic light scattering (DLS) is also known as photon correlation spectroscopy (PCS) or quasi-elastic light scattering (QLS). DLS uses the physics of small particle behavior to correlate data from light scattered by the particles in solution [145, 146]. The sample is placed into a cuvette and a monochromatic light source such as a laser is passed through the sample (figure 2.24). The scattered light that has collided with the particles in the sample is collected and the data is analyzed.

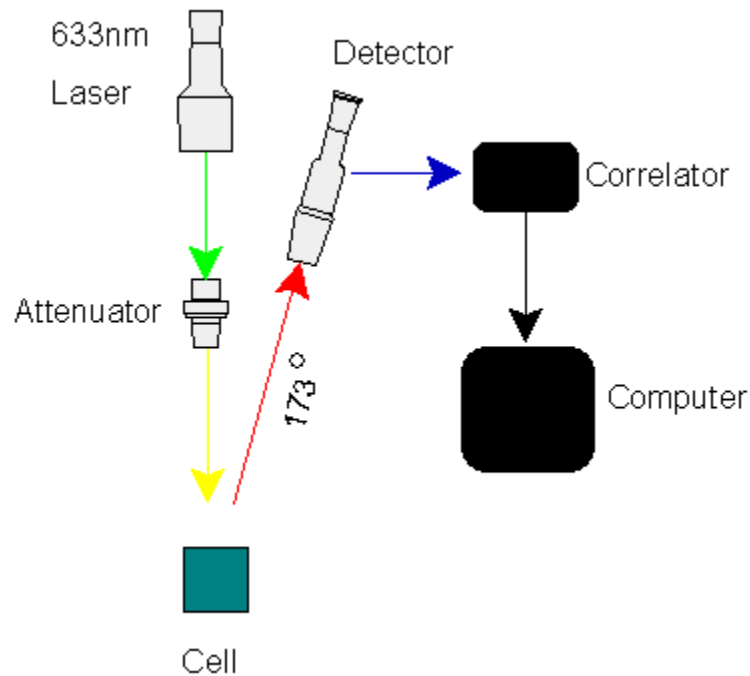


Figure 2.24 Dynamic Light Scattering

The theory of dynamic light scattering is based on Brownian motion caused by thermal energy causing random motion of a particle in solution. For spherical particles the relationship of the radius and the diffusion coefficient (equation 2.5) is given by the Stokes Einstein equation [147], where the diffusion coefficient (D) is equal to the mobility of the particle (μ_p) multiplied by Boltzmann's (k_B) constant and the absolute

temperature (T). The mobility (equation 2.6) of a particle is the ratio of the particle's terminal drift velocity (V_p) to an applied force (F). The Boltzmann's constant (equation 2.7) relates the energy of the microscopic particle to the energy level of the macroscopic surroundings. It is the gas constant (R) divided by Avogadro's number (N_A). Applying Stokes law for frictional force (F_d) (equation 2.8), the drag coefficient γ is formed (equation 2.9) with R being the particle radius and μ being the viscosity of the fluid. Using Stokes law, the Einstein equation becomes a relationship of the apparent diffusion coefficient and the radius of the particle (equation 2.10) that can be rearranged to yield the apparent radius of a particle when the diffusion coefficient is known (equation 2.11) [148].

$$D = \mu_p k_B T \quad \text{Equation 2.5}$$

$$\mu_p = V_p / F \quad \text{Equation 2.6}$$

$$k_B = R / N_A = 1.38E-23 \text{ [JK}^{-1}\text{]} \quad \text{Equation 2.7}$$

$$F_d = 6\pi R V \mu \quad \text{Equation 2.8}$$

$$\gamma = 6\pi R \mu \quad \text{Equation 2.9}$$

$$D = (k_B T) / (6\pi R \mu) \text{ [m}^2\text{s}^{-1}\text{]} \quad \text{Equation 2.10}$$

$$R_{App} = (k_B T) / (6\pi \mu D_{App}) \quad \text{Equation 2.11}$$

In dynamic light scattering data analysis, the light scattered from the sample is used to determine the time it takes for the particle to move from its original starting position. The correlation function is used to relate the change in time and the difference of the current position of the particle compared to its original position. At low concentrations, the correlation function can relate the size of the particle to the temperature and the viscosity of the fluid. A graph of the correlation function for a

niosome sample is shown in figure 2.25. On the left side near time =0, the correlation of the position of the particle to its original position is equal to one, meaning the starting position of the particle is directly related to its current position. As time increases, this relationship is eventually lost and there is no correlation of the current position of the particle to where it originated. The rate of decay is used to calculate the radius of the particles.

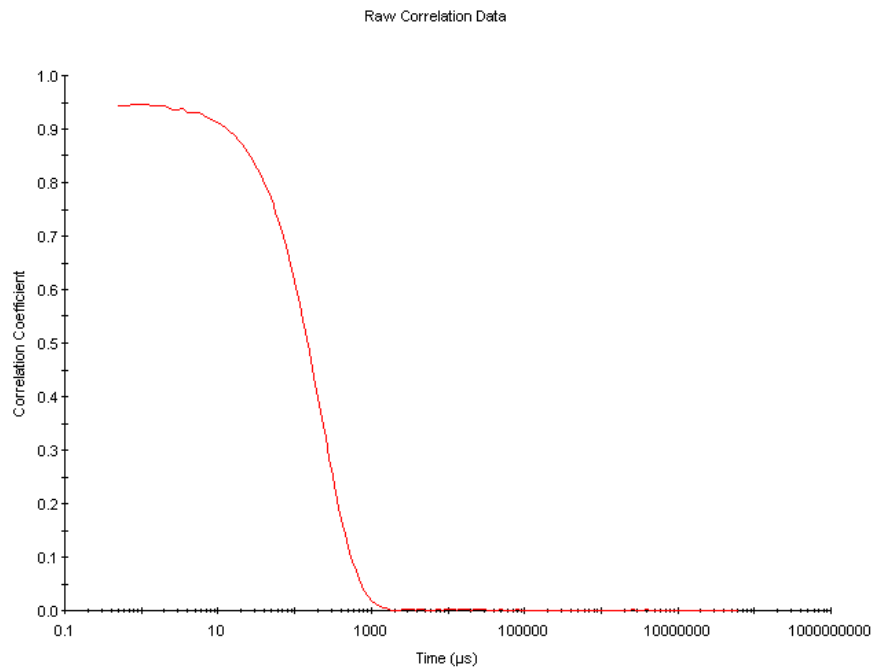


Figure 2.25 Niosome Sample Correlation Data

Niosomes containing Span 60 and 10% Tween or Span 60 and 5% PEG, were placed in sealed cuvettes and measured every 7 days over a 90 day period. Care was taken not to disturb the samples during the time course and particle sedimentation was noted in the non-PEGylated niosome samples. The results from these data suggest the PEG had a positive effect in maintaining vesicle suspension and size dispersion, shown in figure 2.26

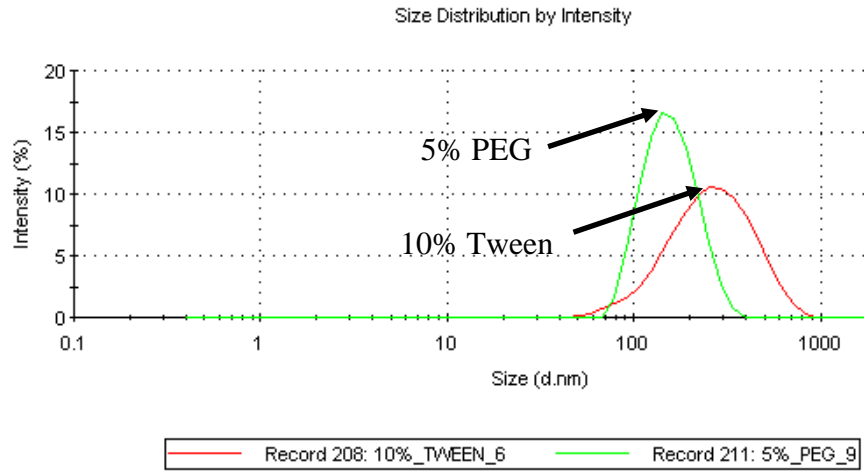


Figure 2.26 Data from Stability Comparison Study on Day90

3. Evaluation of Receptor-Conjugated Vesicles

Binding studies were conducted to investigate immuno-niosome interactions with endothelial cells. Several methods were used to gather data to ensure the results were not biased by the detection technique. Most of the techniques were based on an encapsulated fluorescent dye to detect the cell bound immuno-niosomes. Gold particles were encapsulated for transmission electron microscopy experiments.

3.1.0 Cell Culture

Primary bovine aortic endothelial cells (BAEC) and endothelial basal media (EBM-2) were purchased from Lonza. The cells were plated at an average density of 6.7×10^5 cells/cm² and grown in T-25 culture flasks (Costar) using EBM-2 supplemented with 10% heat inactivated calf serum and 100 units/ml penicillin and 100 ug/ml streptomycin in a humidified 5% CO₂/95% air incubator at 37°C. When the cells reached 85% confluency, aliquots were frozen back in a 50:50 (V:V) mixture of supplemented EBM-2 and DMSO supplemented cryopreservative (Profreeze, Cambrex Bio Science).

Endothelial cells used in binding experiments were allowed to proliferate in tissue culture flasks to a cell viability of 98% prior to high density plating and were used from passage 2 to passage 5. The cells were rinsed three times with 0.01M phosphate buffered saline solution (PBS) and then were detached from the flask bottom using 4% trypsin/EDTA in 0.01M PBS for 2 minutes. The cells were collected and resuspended in serum-supplemented EBM-2 to neutralize the trypsin. The suspension was centrifuged at 900 Gs to form a cell pellet. The cell pellet was resuspended in fresh supplemented EBM-

2 and plated onto growing surfaces of choice, i.e. flasks, glass slides, glass cover slips or 96 and 24 multi-well plates. The glass slides and cover slips were cleaned with 100% ethanol (ETOH) and dried prior to steam sterilization. For some experiments, the glass surfaces were treated with sterile 1M NaOH for 30 minutes and rinsed with 0.1M PBS three times to improve cell adhesion.

3.2.0 Fixed Cell Binding

Fixed endothelial cells under static conditions were used to determine the binding efficiency of the PEGylated immuno-niosomes (INs) to endothelial cells. For receptor specific binding, the cells were treated with the cytokine, tumor necrosis factor alpha (TNF- α), to invoke an inflammatory response in the endothelial cells for expression of the targeted cell surface receptors. This was accomplished by treating the cells with 20 ng/ml TNF- α in supplemented EBM-2 for 24 hours before the experiment. After incubation with TNF- α , the cells were chemically fixed to preserve the receptors to prevent internalization or turnover of the expressed receptors over long time courses. The cells were fixed with a solution made from 2% glutaraldehyde in 0.01M PBS to maintain the osmotic balance in the sample. The fixation causes cross linking between protein molecules. Glutaraldehyde was used for the fixation because it is a larger molecule than formaldehyde and is able to bridge greater distances. For some experiments the commercial preservative Histochoice was used since it has less auto-fluorescence signal than glutaraldehyde. After fixation, the cells were rinsed three times with 0.01M PBS. Some PBS was left on the cells after the last rinse to maintain sample moisture. It was removed just prior to immuno-niosome sample application.

The niosome concentration is indicated by the total surfactant content of the sample. Black plastic 96 well culture plates with clear bottoms were used for the experiments using fluorescent dye to reduce signal cross talk between wells. BAEC were plated and grown as previously described in section 3.1.0. The cells were treated with TNF- α for 24 hours, fixed and the treated with a 2% solution of normal goat serum in 0.01M PBS to block nonspecific binding. The cells were then incubated with fluorescein-loaded immuno-niosomes that were conjugated with CD44, clone KM201. The PEGylated immuno-niosomes were compared to the previous immuno-niosome design to determine the effect of the PEG tether used for antibody conjugation. The endothelial cells were incubated for 5, 10, 15, 30, 60 and 120 minutes with 1.5, 3, and 6 mM of 10% Tween immuno-niosomes or 5% PEGylated immuno-niosomes at 37°C. Following incubation, each cell well was rinsed three times with 0.01M PBS to remove unbound immuno-niosomes. The plate was imaged on a Typhoon 9410 flat bed fluorescent scanner (GE Healthcare) using the 488nm laser to excite the fluorescent dye. Data was collected at 528nm with a setting of 600volts on the photomultiplier tube, a pixel size of 100 microns and a focal plane of 3mm to account for the distance from the bottom of the plate to the imaging surface. The cell density was determined by treating the cells with a solution of 20ng/ml propidium iodide and using excitation/emission of 535/620nm on the Typhoon. The raw data was analyzed with Quantity One software. For each well, the fluorescent volume was calculated by taking 5 mm regions of interest at 5 different locations. The error bars in figures 3.0 and 3.1, indicate the standard deviation for the measurement. The results from the vesicle comparison study showed an increase in the binding performance of the 5% PEGylated INs over the previous 10% Tween IN design.

This was most evident with the higher vesicle concentration and longer incubation times. The results of the vesicle comparison study are shown in figures 3.0 and 3.1, and the data is summarized (percent difference in binding) in table 3.0.

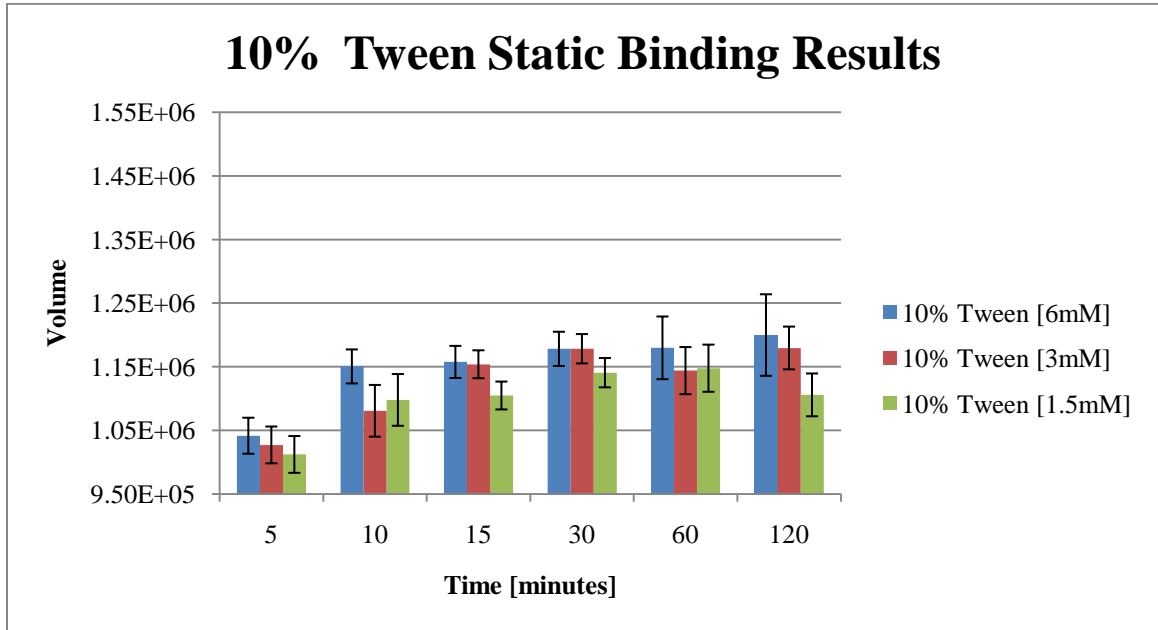


Figure 3.0 Fixed Cell Binding: 10% Tween Fluorescein-loaded IN (CD44, KM201)

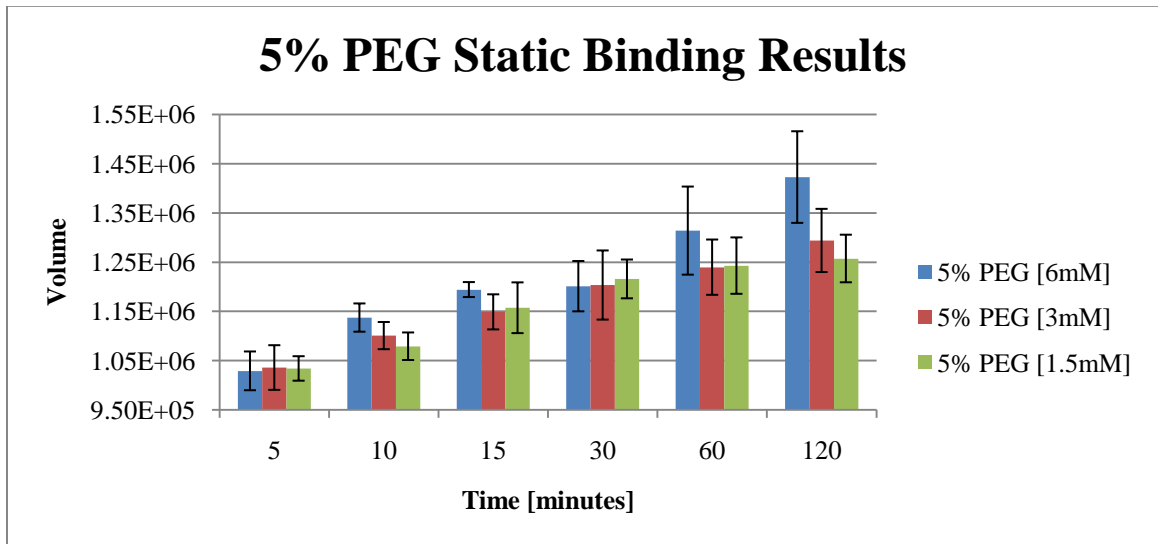


Figure 3.1 Fixed Cell Binding: 5% PEG Fluorescein-loaded IN (CD44, KM201)

Table 3.0 Static Binding Results

Time [minutes]	6mM % Diff.	3mM % Diff.	1.5mM % Diff.
5	1.21	0.84	2.12
10	1.16	1.82	1.73
15	3.11	0.44	4.63
30	1.93	2.10	6.37
60	10.76	8.03	7.96
120	17.00	9.25	12.82

3.3.0 Live Cell Binding

We sought to determine how the immuno-niosomes interacted with live cells and to confirm BAEC uptake of the immuno-niosomes using CD44 as the target receptor. A study comparing the CD44 receptor to other receptors was conducted using carboxyrhodamine 110 fluorescent dye loaded immuno-niosomes conjugated with CD44, ICAM-1 or VCAM-1 antibodies. Confocal microscopy was used to confirm uptake using the CD44 receptor and to examine binding patterns between ICAM-1 and CD44 INs binding to the BAEC.

3.3.1 Multiwell Plate Experiments

Two different experiments were conducted using live cells grown in multiwell plates to provide IN and active cell surface receptor binding data. For both experiments the cells were grown and plated as previously described in section 3.1.0. In the first experiment, cells were plated in black plastic 96 well tissue culture plates with clear

bottoms and grown until they were 85% confluent. This experiment was designed to determine if antibodies that target different receptors have similar nonspecific binding properties. To determine nonspecific binding, the cells were not treated with cytokines prior to incubation with the immuno-niosomes. The immuno-niosomes were conjugated with ICAM-1, VCAM-1 or the CD44 antibody. A control vesicle was not conjugated with antibodies. A 3mM immuno-niosome solution in Dulbecco's Modified Eagle Medium (DMEM) was used for the experiment. Cells were incubated with immuno-niosomes or control vesicles for 0.5, 1.0, 2.0 and 4.0 hours in a humidified 5% CO₂/95% air incubator at 37°C.

Each cell well was rinsed three times with 0.01M phosphate buffered saline (PBS) to remove unbound vesicles. The plate was imaged on a Typhoon 9410 flat bed fluorescent scanner (GE Healthcare) using the 488nm laser to excite the fluorescent dye. Data was collected at 528nm with a setting of 600volts on the photomultiplier tube, a pixel size of 100 microns and a focal plane of 3mm. The cell density was determined by treating the cells with a solution of 20ng/ml propidium iodide and imaging using an excitation/emission of 535/620nm on the Typhoon. The results of the experiment indicate that the nonspecific binding is antigen independent as shown in figure 3.2

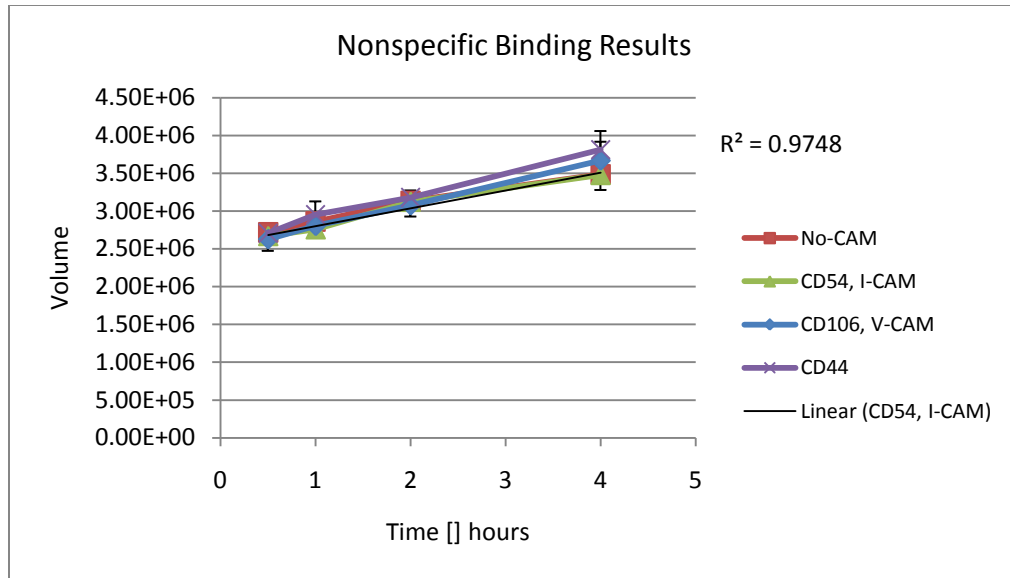


Figure 3.2 Nonspecific Binding Results

The second experiment was designed to compare the binding performance of the different receptor-targeted immuno-niosomes to live cells. The cells were plated in black plastic 24 well tissue culture plates with clear bottoms and grown until they were 85% confluent. Control cells were not treated while the other cells were treated with 20ng/ml TNF- α for 24 hours. Then all the cells were treated with a 2% solution of normal goat serum in 0.01M PBS to reduce nonspecific binding prior to incubation with the immuno-niosomes. The immuno-niosomes were conjugated with ICAM-1, VCAM-1 or the CD44 antibody. A control vesicle was not conjugated with antibodies. A 1.5mM immuno-niosome solution in DMEM was used in the experiment. Cells and antibody conjugated immuno-niosomes or control vesicles were incubated for 1, 2 and 4 hours in a humidified 5% CO₂/95% air incubator at 37°C. Each cell well was rinsed three times with 0.01M phosphate buffered saline (PBS) to remove unbound vesicles. The plate was imaged on a Typhoon 9410 flat bed fluorescent scanner (GE Healthcare) using the 488nm laser to excite the fluorescent dye. Data was collected as previously described. The cell density

was determined by treating the cells with a solution of 20ng/ml propidium iodide and imaging using an excitation/emission of 535/620nm on the Typhoon. The results of the experiment indicate that by four hours post-immuno-niosome binding, the three antigens have similar binding to the endothelial cells as shown in figure 3.3.

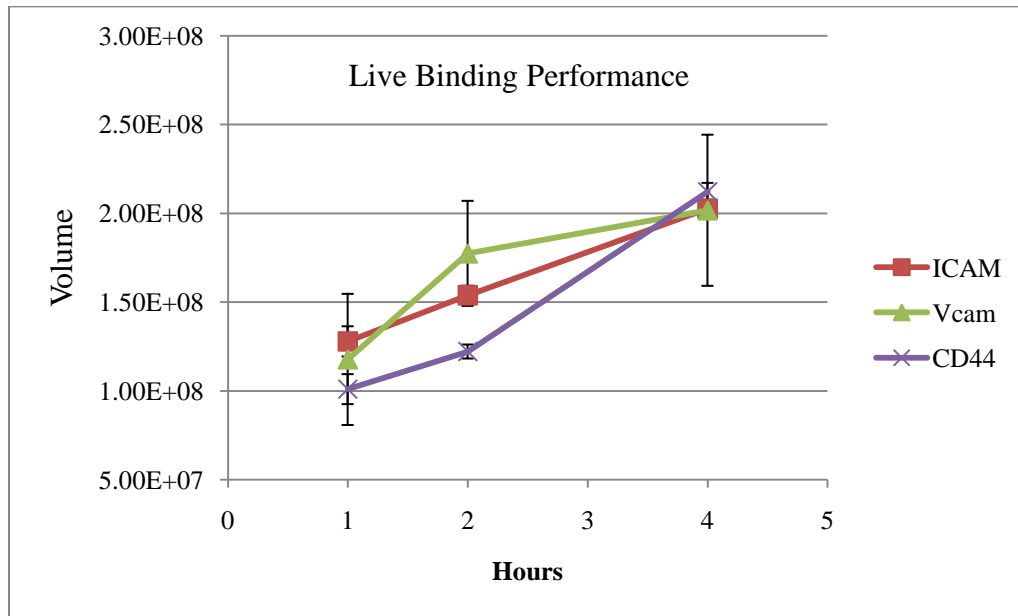


Figure 3.3 Live Binding Performances

3.3.2 Confocal Laser Scanning Microscopy

Confocal microscopy was used to determine binding characteristics of the immuno-niosomes (INs) to activated bovine aortic endothelial cells (BAECs). Confocal microscopy uses multiple focal planes, called the z-stack to reconstruct images. Each plane is scanned with a focused beam of laser light. This is accomplished one line at a time over the surface from one end of the image to the other. The software that reconstructs the images uses a setting called maximum projection. This setting uses the maximum average intensity from each plane to reconstruct the compiled image. This method is an improvement over standard fluorescent microscopy since data from the out-of-focus plane is not used, providing better image contrast and resolution.

Two types of experiments were conducted using confocal microscopy. The cells were grown as previously described in section 3.1.0 and plated in 8 well glass tissue culture chamber slides (Lab Tek II, Fisher Scientific). In the first experiment, the cells were activated using an injury model. The injury was created by scratching the cells in each well in an “x” pattern with a 200ul pipet tip, 24 hours prior to incubation with the INs. The INs were loaded with 1mM carboxyrhodamine 110 dye since it is more photo stable than fluorescein-based dyes. The INs were conjugated with either ICAM-1 or CD44 antibodies and incubated with the injured cells for one hour. The cells were rinsed three times with 0.01M phosphate buffered saline (PBS) solution before fixation with Histochoice fixative to preserve the cells and bound vesicles. The slides were cover-slipped with a number 1.5 glass cover and mounting media containing 4',6-diamidino-2-phenylindole (DAPI) stain to identify the cell nucleus. DAPI is a stain that when bound to double stranded DNA fluoresces approximately 20 times greater than DAPI alone. An image of the cells and ICAM-1 INs from the injury model is shown in figure 3.4, with arrows pointing at the injury border. The fluorescent intensity of across the injury (ROI 1) is shown in figure 3.5.

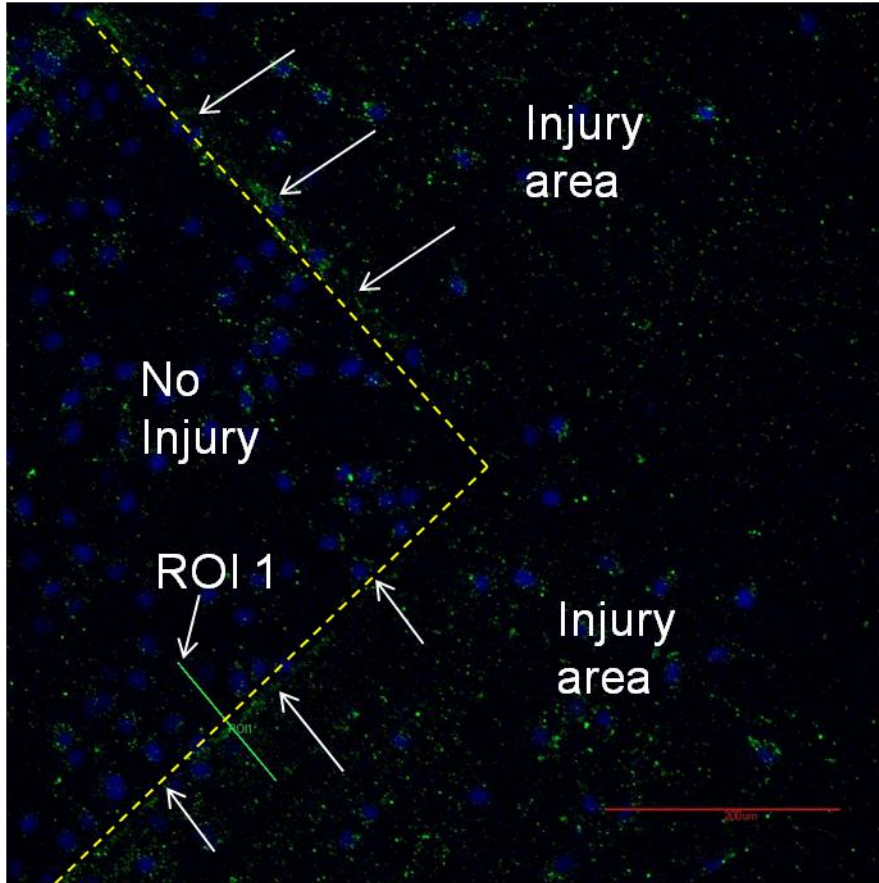
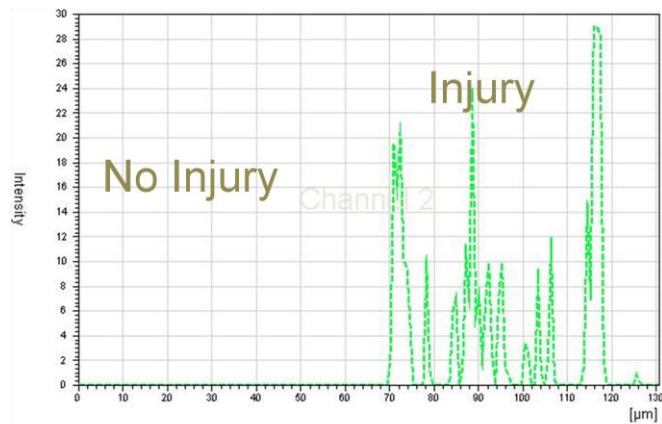


Figure3.4 One Hour Scratch Injury ICAM (200X Magnification)



ROI 1 fluorescent intensity

Figure 3.5 Graph of Fluorescent Intensity from Region of Interest 1

The injury model was used to compare the binding of ICAM-1 and CD44 antibodies against the receptors expressed by the injured endothelial cells. Figure 3.6 is an image of

how the regions of interest were located; the results are shown in table 3.1 (fluorescence \pm standard deviation).

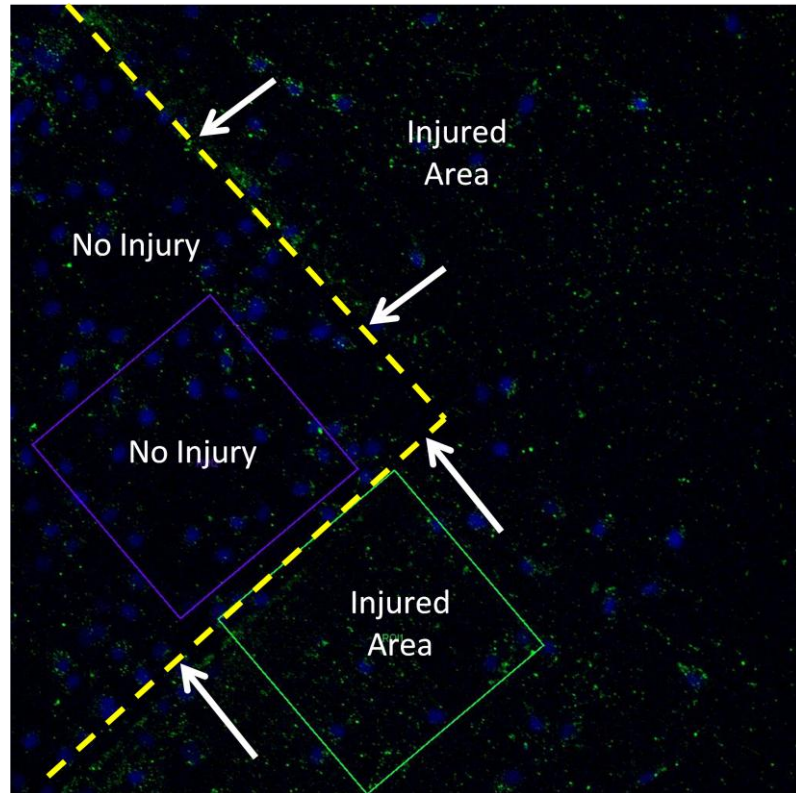


Figure 3.6 Injury Model Region of Interest (200X Magnification)

Table 3.1 Injury Binding Results

Pixel Density	CD44	ICAM-1
Injured ROI	1052828(+/-993.21)	383184(+/- 325.96)
Non Injured ROI	633041(+/-543.01)	179019(+/- 168.65)
Difference	419787	204165

Uptake of the antibody conjugated immuno-niosomes into the activated endothelial cells was confirmed in the second set of experiments using confocal microscopy techniques. The INs were loaded with 1mM Carboxyrhodamine 110

fluorescent dye, extruded across 200nm polycarbonate membranes and purified using size exclusion chromatography. The dye loaded niosomes had an average size of 168nm based on dynamic light scattering data. The INs were conjugated with CD44, ICAM-1 or VCAM-1 antibodies. The cells were grown as previously described in section 3.1.0 and plated in 8 well glass tissue culture chamber slides and grown until they were 85% confluent. The cells were treated with 20 ng/ml TNF- α for 24 hours before being treated with a 2% solution of normal goat serum in 0.01M PBS for one hour to reduce nonspecific binding prior to incubation with the immuno-niosomes. The cells were incubated with a 3mM solution of immuno-niosomes in Dulbecco's modified eagle medium (DMEM) for 1, 2, 3 and 4 hours. The cells were rinsed three times with 0.01M PBS before fixation with Histochoice fixative to preserve the cells and bound vesicles. A 5 ug/ml solution of wheat germ agglutinin conjugated to Alexa Fluor 633 (WGA Alexa Fluor 633, Invitrogen) in 0.01M PBS was used to stain the cell membrane. The slides were cover-slipped with a number 1.5 glass cover-slip and mounting media containing 4',6-diamidino-2-phenylindole (DAPI) nucleic acid stain to identify the cell nucleus. In figures 3.7 through 3.13, the carboxyrhodamine 110 fluorescent dye is shown in green. Figures tagged with an (A) indicate TNF- α activated endothelial cells and figures tagged with a (B) indicate control endothelial cells that were not treated with TNF- α . Internalized dye within the cell is indicated by the arrow in figure 3.7(A). Endothelial cells with no injury or TNF- α treatment served as the control as shown in figure 3.7(B).

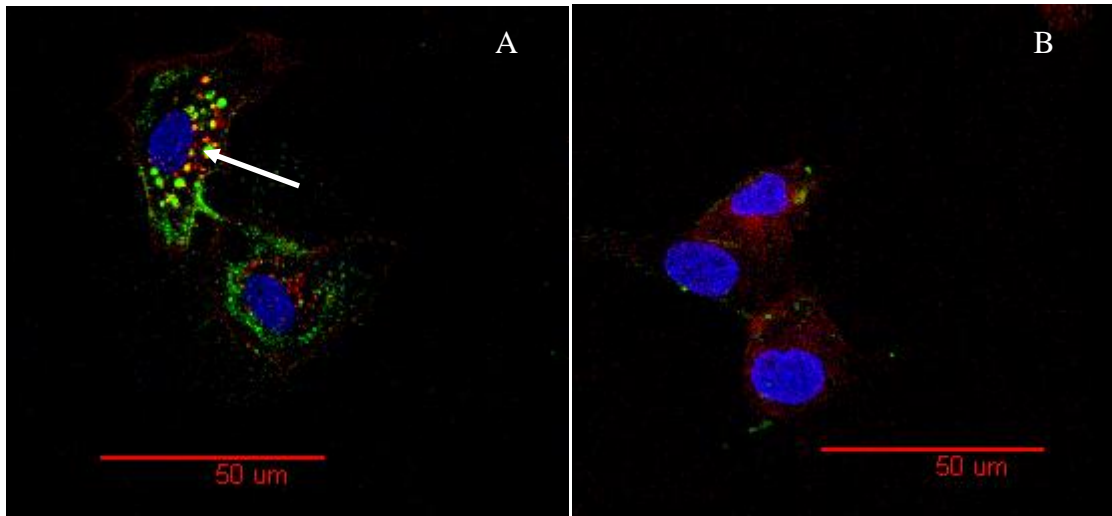


Figure 3.7 (A) 4 Hour PEGylated CD44 Immuno-niosomes, (B) Control, 4 Hour PEGylated CD44 Immuno-niosomes, (630X Magnification)

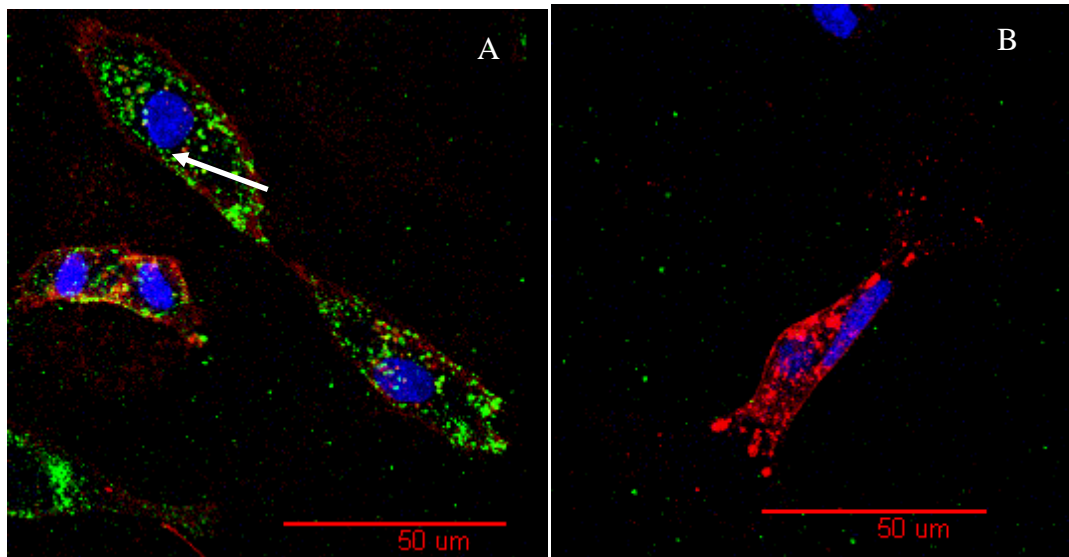


Figure 3.8 (A) 3 Hour PEGylated CD44 Immuno-niosomes, (B) Control, 3 Hour PEGylated CD44 Immuno-niosomes, (630X Magnification)

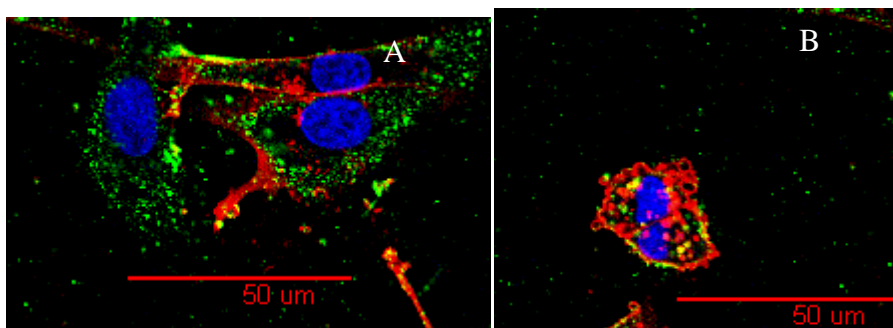


Figure 3.9 (A) 2 Hour PEGylated CD44 Immuno-niosomes, (B) Control, 2 Hour PEGylated CD44 Immuno-niosomes, (630X Magnification)

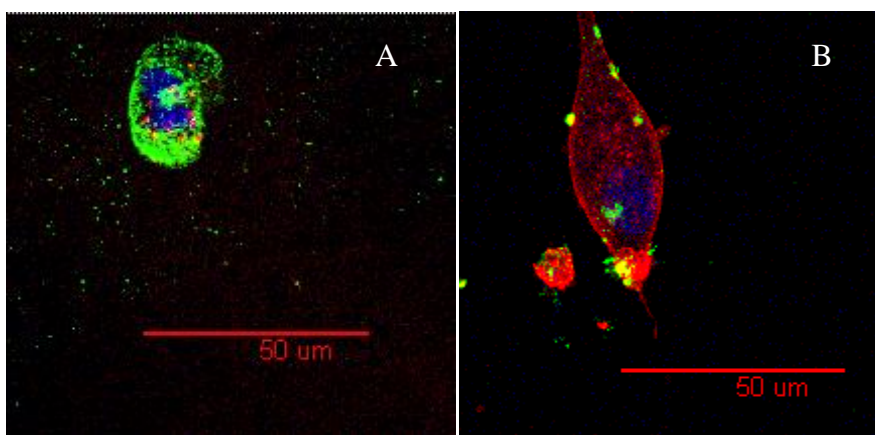


Figure 3.10 (A) 1 Hour PEGylated CD44 Immuno-niosomes, (B) Control, 1 Hour PEGylated CD44 Immuno-niosomes, (630X Magnification)

Figures 3.8 (A and B) shows endothelial cells that were incubated for 3 hours with PEGylated CD44 conjugated immuno-niosomes. The arrows point at immuno-niosomes that have formed clusters on lipid rafts on the cellular membrane as they are being internalized. Figures 3.9 (A and B) show endothelial cells that were incubated for 2 hours with PEGylated CD44 conjugated immuno-niosomes. The clusters of immuno-niosomes have formed, but they are not as distinct as the clusters in the 3 and 4 hour incubations. This suggests that the endocytotic pathway involves lipid rafts and clustering of cell surface receptors. Figures 3.10 (A and B) show endothelial cells that were

incubated for 1 hour with PEGylated CD44 conjugated immuno-niosomes. The immuno-niosomes are bound to the cell surface but have not formed clusters as seen with longer incubation times. Internalization is confirmed by the Z-stack images shown in figure 3.11 (A-D) showing the internalized dye in the 1-4 hour treated samples (A) from figures 3.7-3.10.

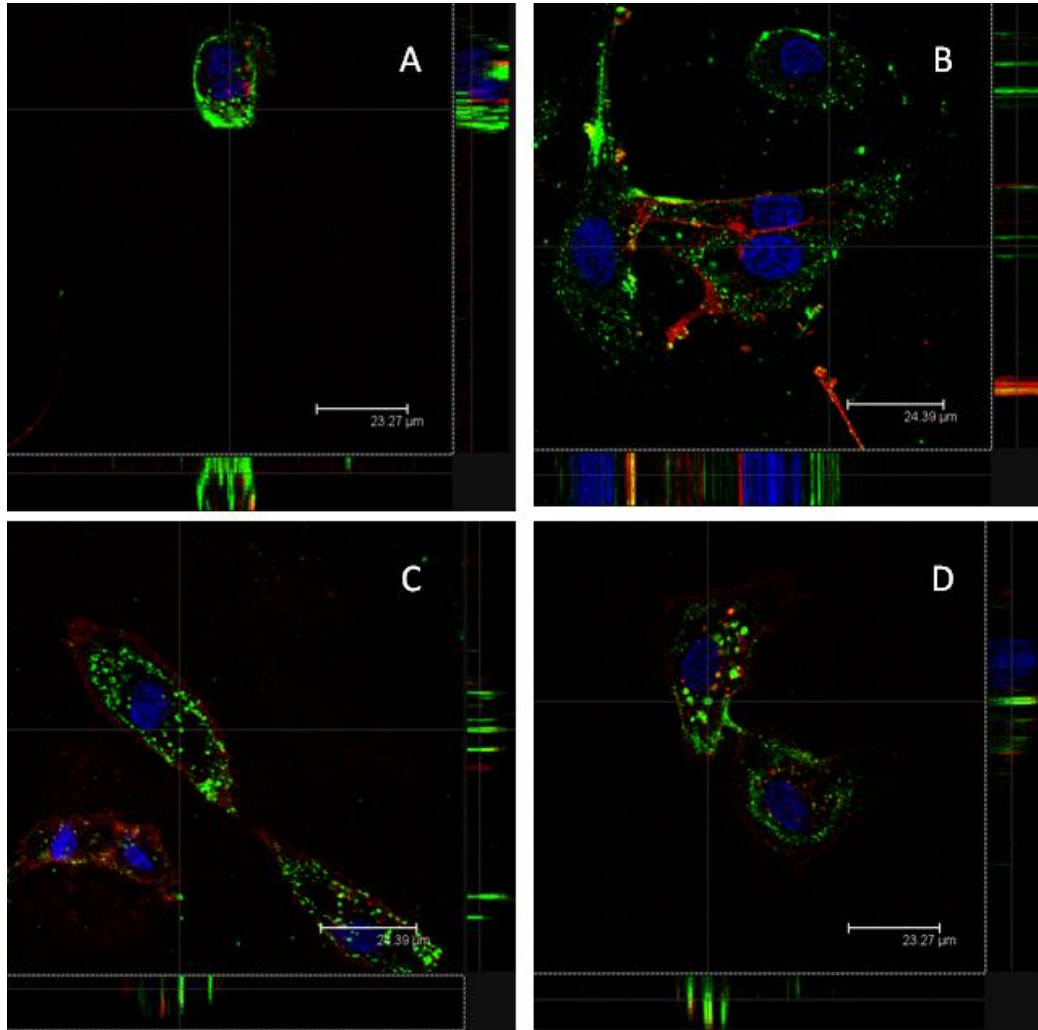


Figure 3.11 (A-D) Z-stack of the 1-4 Hour PEGylated CD44 Immuno-niosomes, (630X Magnification)

To compare immuno-niosome binding to endothelial cells using a different antigen. PEGylated niosomes were conjugated with VCAM-1. Endothelial cells incubated for four hours with PEGylated VCAM-1 conjugated immuno-niosomes are shown in figures 3.12 (A and B). The arrows point at immuno-niosomes that have formed clusters on lipid rafts on the cell membrane, similar to PEGylated immuno-niosomes that were conjugated with CD44.

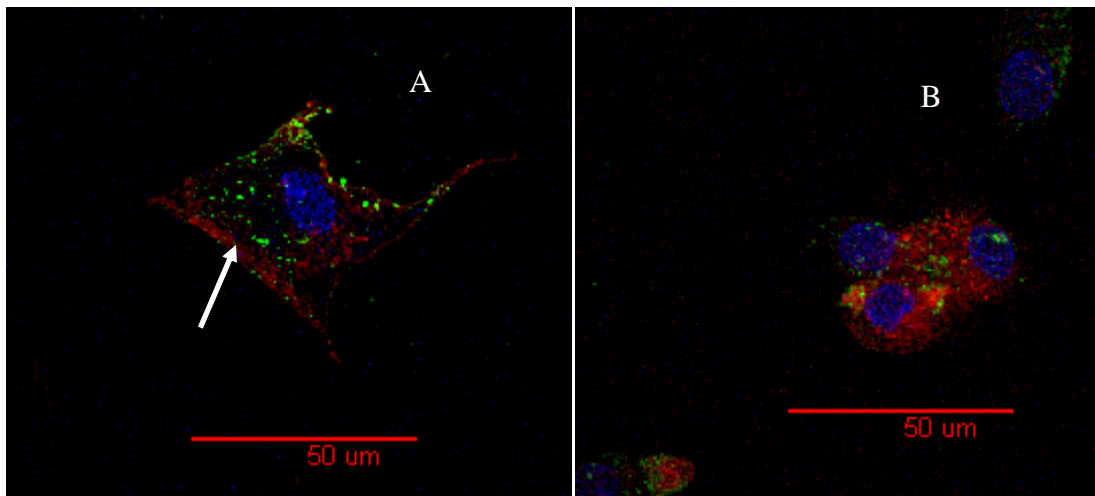


Figure 3.12 (A) 4 Hour PEGylated VCAM-1 Immuno-niosomes, (B) Control, 4 Hour PEGylated VCAM-1 Immuno-niosomes, (630X Magnification)

Confocal microscopy was also used to image immuno-niosomes made from functionalized cholesterol. The steroid was functionalized with cyanuric chloride as previously described in section 2.3.2 and immuno-niosomes were made with 10% functionalized cholesterol loaded with 1mM carboxyrhodamine 110 and conjugated with ICAM-1 antibodies. The cells were grown and plated in 8 well glass tissue culture chamber slides. They were treated with 20 ng/ml TNF- α followed by 2% goat serum prior to incubation with immuno-niosomes as previously described. Figure 3.13 (A) and (B) are images of endothelial cells incubated for 4 hours with immuno-niosomes made

with 10% functionalized cholesterol. The vesicles appear to have formed dense clusters on the endothelial cell surface.

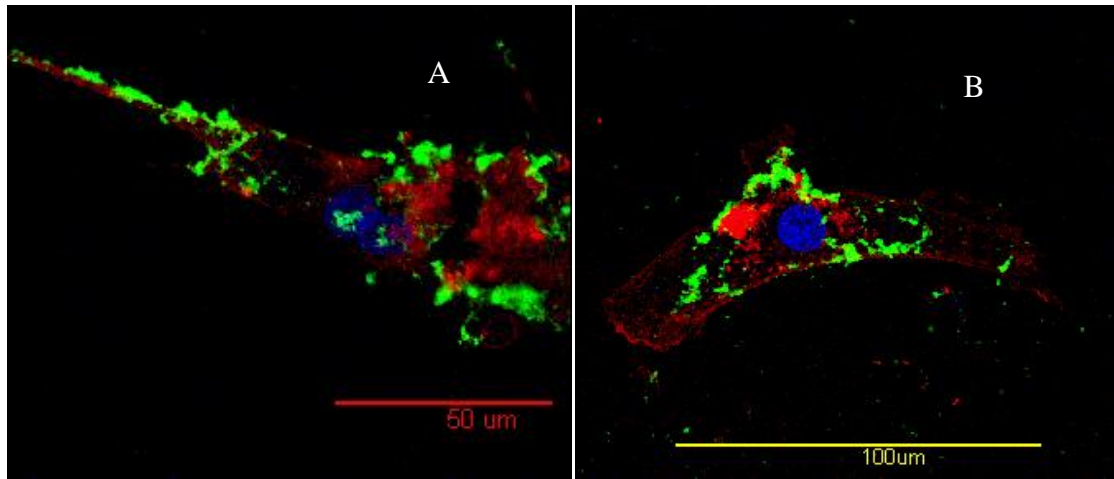


Figure 3.13 (A) 4 Hour ICAM Cholesterol Immuno-niosomes, (B) Control, 4 Hour ICAM Cholesterol Immuno-niosomes (630X Magnification)

3.3.3 Transmission Electron Microscopy

Transmission electron microscopy (TEM) was used to image immuno-niosomes loaded with albumin coated 20nm gold nanoparticles. Gold is an electron dense material that provides a strong signal when viewed with TEM. The immuno-niosomes were conjugated with antibodies that target the CD44 cell surface receptor. Endothelial cells were grown in T-25 culture flasks as previously described in section 3.1.0. The cells were treated with 20 ng/ml TNF- α in supplemented EBM-2 for 24 hours. The cells were fixed with 2% glutaraldehyde in 0.01M phosphate buffered saline (PBS) for 15 minutes. The cells were washed three times with 0.01M PBS to remove excess glutaraldehyde. The cells were treated with 2% osmium tetroxide (OsO₄, a heavy metal compound that is used as a fixative and a stain) for 30 minutes and rinsed with deionized water three times to remove excess osmium and salts. The cells were removed from the flasks using a cell scraper and were recovered by centrifugation at 900g to form a cell pellet. Since epoxide

resins are not miscible with water, the samples must be dehydrated. To protect the cells during this process, the dehydration is done slowly and great care is taken to ensure the samples do not dry completely between steps by ensuring the sample is always covered in solution. Samples are dehydrated for 2 minutes each step in 20% (v/v), 30%, 50%, 70%, 90% ethanol at 4°C followed by 100% ethanol at room temperature and 100% ethanol at 4°C. Prepared resin (Appendix A, note 1) is diluted with solvent in a 1:1 (v/v) ratio. The cell pellets are immersed in this solution for one hour and agitated to ensure adequate infiltration of the cells. The cells are spun at 900g for 5 minutes to form a pellet and the excess resin is removed and replaced with pure resin at room temperature for one hour. This step is repeated one additional time. To embed the samples, the cell pellets are then placed in labeled casting trays with pure resin and heated to 60°C for 24-48 hours to polymerize the resin.

Thick sections of the embedded cells are cut and stained with semithin stain and viewed using light microscopy to inspect the samples. Then thin sections, 50-70um, are cut from the embedded samples and floated on prepared mesh grids (Appendix A, note 2) and placed sample side up for drying in petri dishes lined with filter paper. Uranyl acetate (UA) staining of the thin sections is performed by prepping a disposable 4-well petri dish with a section of dental wax and adding a drop of prepared UA stain (Appendix A, note 3) corresponding to each grid to be stained. Grids with samples are placed sample side down on the UA stain for 10 minutes. The samples are washed with deionized water in a series of three beakers. The grids are agitated by moving the sample vertically in each beaker. The washed grids are placed on the filter paper and dried before lead staining. Lead staining is performed on dry grids as follows. The petri dish is prepared as

previously described. Sodium hydroxide (NaOH) pellets (to remove CO₂) are placed in the chamber with the dental wax. Prepared lead citrate stain is added (Appendix A, note 4). The grids are floated sample side down on the drops of lead stain for 1-3 minutes. The grids are washed as before in a series of three beakers filled with deionized water and allowed to dry sample side up on filter paper. A transmission electron micrograph taken at 30kv of gold loaded, internalized PEGylated CD44 conjugated immuno-niosome is shown in figure 3.14. The arrow points to gold particles that have been internalized inside the endothelial cell. The arrow in figure 3.15 points to a gold loaded PEGylated CD44 conjugated immuno-niosome bound to the cell membrane. Because gold is not metabolized, sections of tissue samples from the liver and spleen (from in vivo experiments) would provide information on how the immuno-niosomes interact with the organs.

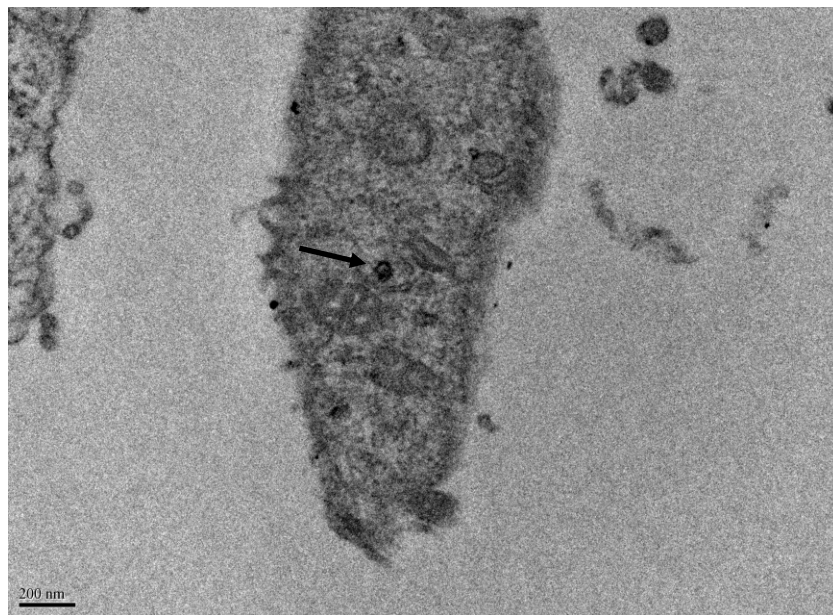


Figure 3.14 Gold Loaded, Internalized Immuno-niosomes

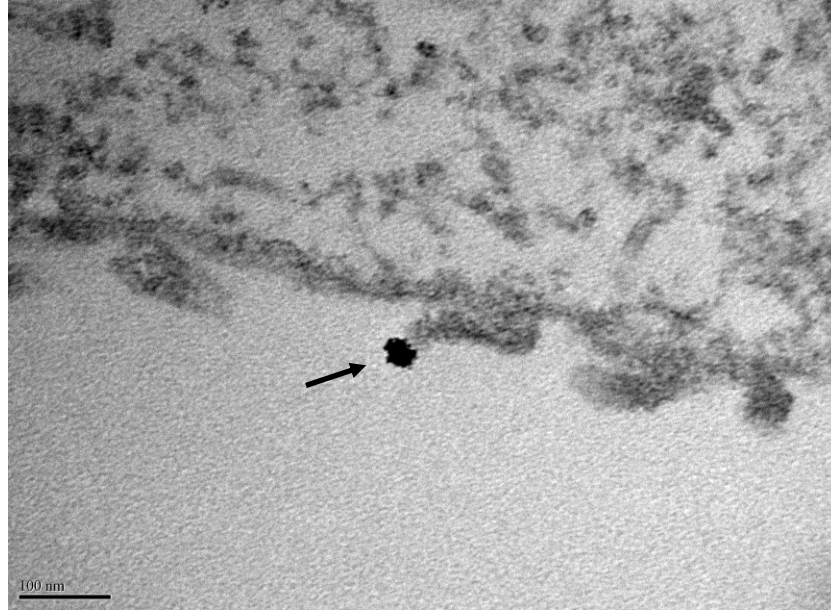


Figure 3.15 Gold Loaded Immuno-niosome Bound to Cell Membrane

3.4.0 pH Sensitive Dye Study

When the endothelial cell internalizes the targeted delivery vesicle by the process of endocytosis, the process can be tracked by using a fluorescent agent that shifts spectrum with changing pH conditions. A family of pH sensitive dyes, seminaphthorhodafluor-carboxylic acid (SNARF), can be used to track such environmental pH changes. [149-156, 157]. It was hypothesized that encapsulation of the pH sensitive dye could be used to track the different steps associated with vesicle internalization [158-161]. It is well understood that cellular internalization pathways utilize vacuoles that employ a pH change. This intracellular change creates a condition that causes conformational changes in proteins, thus enabling the sorting and recycling of cellular receptors to the cell surface. Endocytosis is a multistep process that can involve multiple transport vacuoles such as early endosomes, late endosomes and lysosomes [162]. This process can be monitored by using an indicator to determine the time course of the pH shift in the micro environment. Carboxy SNARF-4 was selected for the study

based on reports of SNARF-1 interacting with the liposome membrane [163]. Samples of SNARF-4 dye were placed in a steady state spectrofluorometer (ISS PC1) to gather spectral data from the dye at different pH values. The stock solution of dye was diluted to a $1\mu\text{M}$ concentration in 0.01M phosphate buffered saline solution and the pH was adjusted using 1N hydrochloric acid. The samples were excited at 488nm and the spectra of the $1\mu\text{M}$ SNARF-4 dye, with a pH ranging from 5.45 to 7.2 were recorded as shown in figure 3.16.

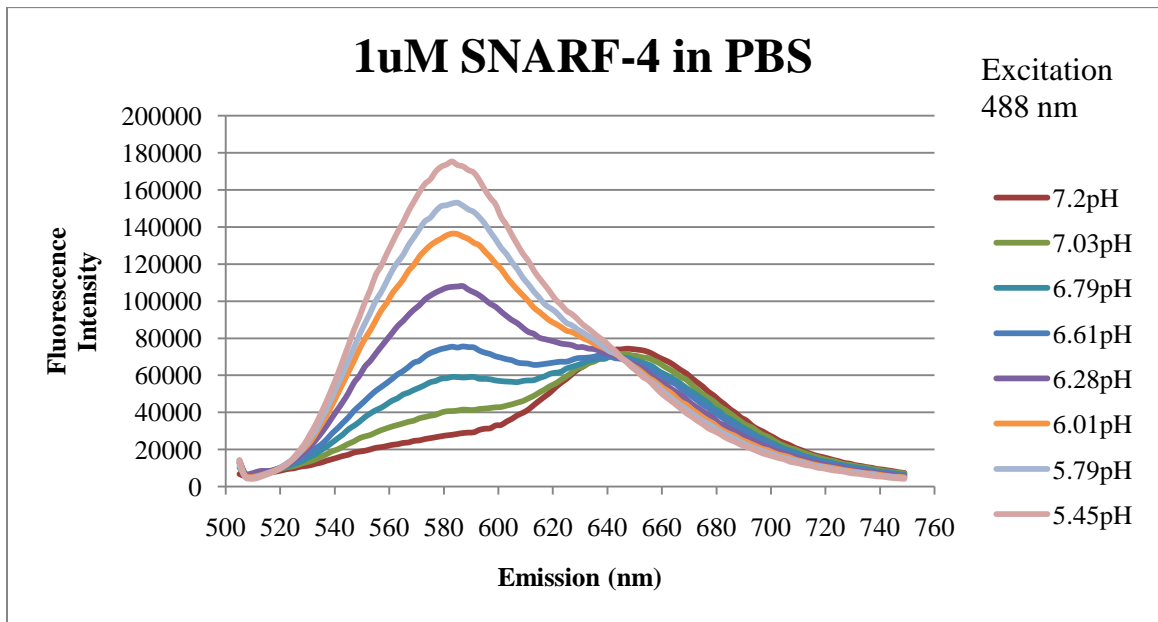


Figure 3.16 Fluorescence Spectra of $1\mu\text{M}$ SNARF-4 in PBS, pH 5.45 to 7.2

There was a strong pH dependent shift in the SNARF-4 dye spectra. It shifted from 650 nm at a pH of 7.2 to 580 nm at pH 5.4. This data suggested the dye could indicate the intracellular pH changes in the different cellular compartments. Therefore $1\mu\text{M}$ SNARF-4 dye was encapsulated in niosomes made from Span 60, cholesterol and dicetyl phosphate. The samples were then placed into the spectrofluorometer and the spectra at various emission wavelengths were recorded. When the SNARF-4 loaded niosomes at a pH of 7.2 were excited at 488nm, the spectrum showed a peak at 520 nm

(figure 3.16). This result was unexpected, therefore the experiment was repeated using new samples of niosomes loaded with SNARF-4 dye. The results of the two experiments confirmed the spectra of the SNARF-4 loaded niosomes had a peak at 520 nm when excited at 488 nm at a pH of 7.2, as shown in figure 3.17.

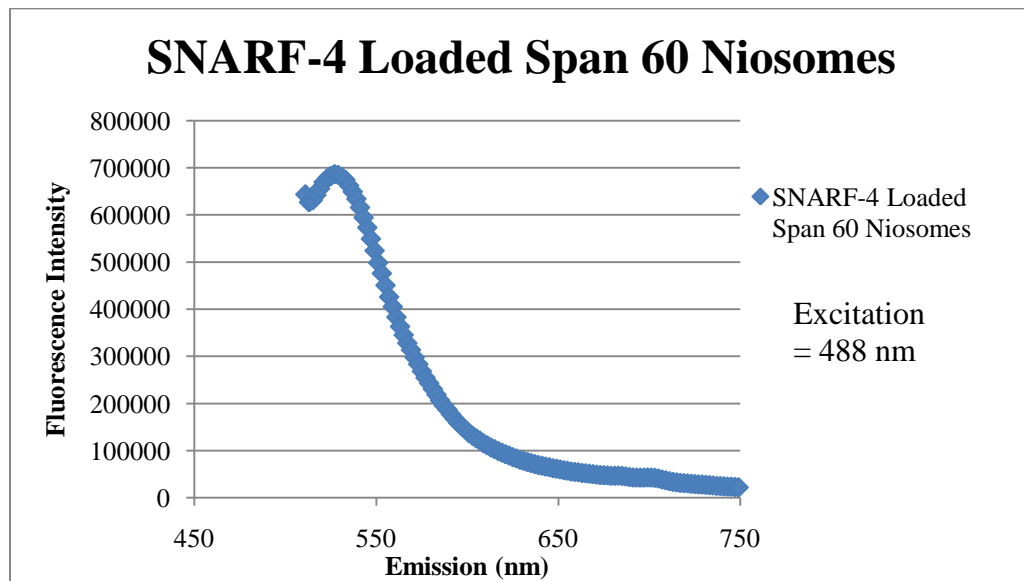


Figure 3.17 Spectrum of SNARF-4 Loaded Span 60 Niosomes at pH 7.2

The spectra of the individual components of the niosomes were recorded to determine the source of the 520 nm emission peak. Cholesterol was found to fluoresce with a strong signal when placed in 0.01M phosphate buffered saline solution, the same concentration was to make niosomes at a pH of 7.2 (figure 3.18). The ring structure of cholesterol shown in figure 2.2 is thought to be the source of the signal.

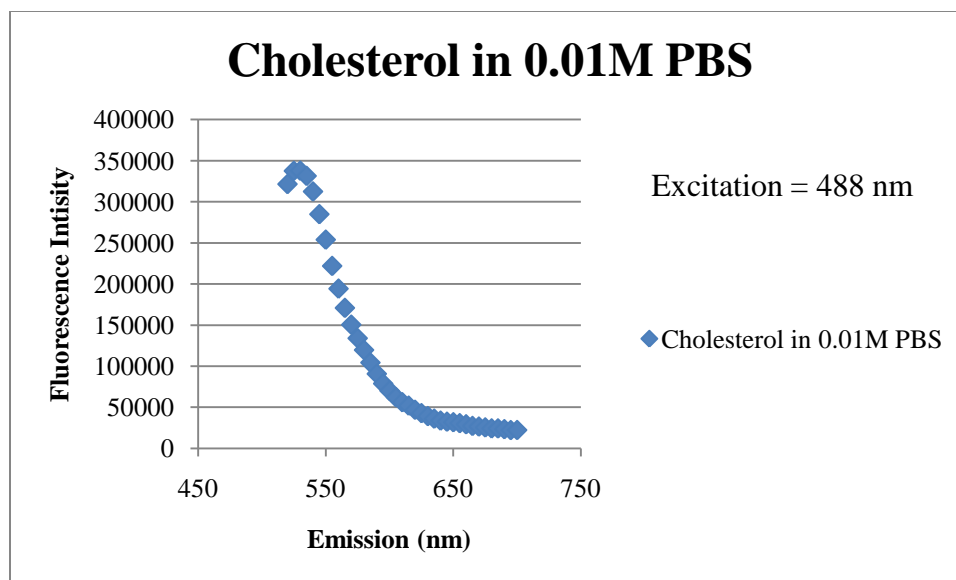


Figure 3.18 Spectrum of Cholesterol

3.5.0 Vesicle Binding in Flow

In preparation for in vivo studies, the confirmation of the ability of PEGylated CD44 conjugated immuno-niosomes to bind to endothelial cells in flow was confirmed using a parallel plate flow chamber (CytoDyne, La Jolla, CA.). The chamber was attached to a syringe pump as shown in figure 3.19.

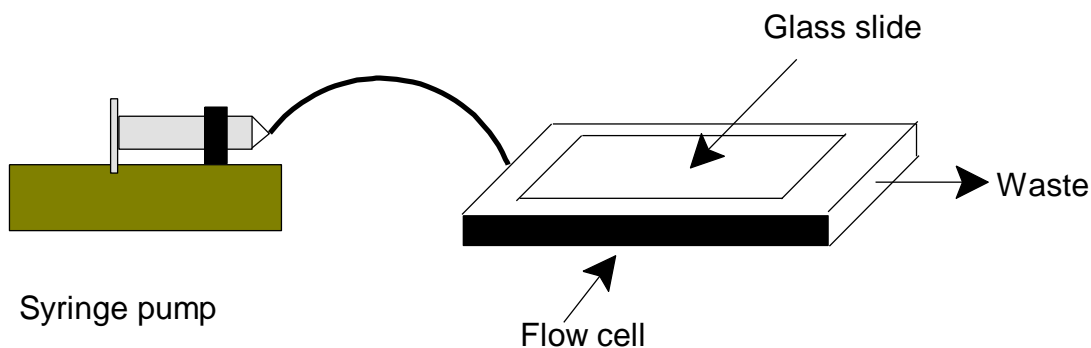


Figure 3.19 Flow Cell

Endothelial cells were cultured as previously described in section 3.1.0. Cells were plated at a density of 2×10^3 total cells on 75 mm x 38 mm glass slides that were steam sterilized

and treated with 1M sodium hydroxide. The cells were grown to 80% confluency before treatment with 20 ng/ml TNF- α for 24 hours. The cells were fixed with a solution made from 2% glutaraldehyde in 0.01M phosphate buffered saline (PBS) and rinsed to remove excess glutaraldehyde. A 60 ml syringe was loaded with 0.01M PBS and the system was primed with 10 ml PBS to remove any air. The slide was placed on the flooded chamber then vacuum was applied to hold the slide in place. Before starting the pump, a 2ml bolus injection of a 3mM solution of PEGylated CD44 conjugated immuno-niosomes loaded with 5mM 5(6)carboxyfluorescein was injected upstream of the chamber. Then the pump was started and 50 ml of PBS was eluted at a flow rate (Q) of 14 ml/min through the chamber. Using equation 3.0, the calculated endothelial cell shear stress (τ) was 10.4 dynes/cm², using a viscosity (μ) of 9×10^{-3} dyn/s*cm², channel height (h) of 2.2×10^{-2} cm and a channel width (b) of 2.5 cm[164].

$$\tau = (6Q\mu) / (bh^2) \quad \text{Equation 3.0}$$

Fluorescence microscopy was used to verify immuno-niosome binding in flow to endothelial cells placed in the parallel plate flow chamber. The samples were post stained with 4',6-diamidino-2-phenylindole, dihydrochloride (DAPI) to determine the location of the cell nucleus. The arrows in figure 3.20 point at bound vesicles on the endothelial cells.

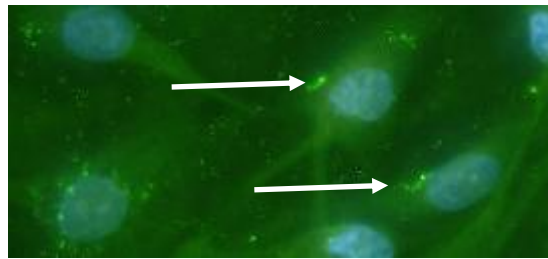


Figure 3.20 PEGylated CD44 Conjugated Immuno-niosomes Bound to Endothelial Cells Under Flow Conditions (400x Magnification)

4. Enhancement of the Modified Vesicle Designs for Targeted Delivery in Vivo

To determine the bio-distribution of the immuno-niosomes in vivo it is necessary to use a fluorescent dye where there is minimal imaging interference from living tissues, e.g. hemoglobin, collagen, cholesterol and water. A near infrared dye with a maximum emission spectrum of 800 nm was used (IRDye 800CW carboxylate, LiCor Biosciences).

4.1.0 Multi Well Plate Imaging

Free and encapsulated IRDye 800CW was imaged using an in vivo imaging system (Xenogen IVIS Spectrum, Caliper Life Sciences). Both epi and trans-illumination methods were used to measure fluorescence intensity at excitation/emission 745/800 nm. Figure 4.0 shows a 96 well plate with two concentrations of IRDye 800CW (A1-3) 1nmol, (B1-3) 4 nmol and (C1-3) 0.01M phosphate buffered saline solution (PBS). The minimum IRDye 800CW concentration detectable using epi-illumination with a 5 second exposure time was 1 nmol.

1 nmol Dye

4 nmol Dye

PBS

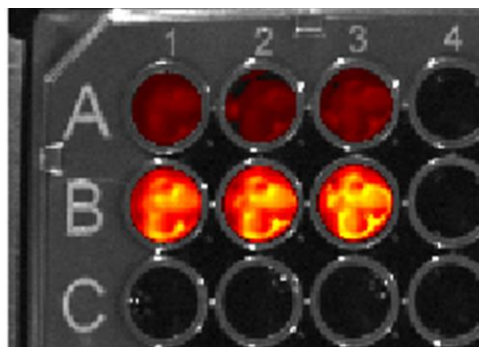


Figure 4.0 IRDye 800CW Bulk Solutions

In the next experiment, 0.01M PBS was encapsulated in 5% PEG and 10% Tween niosomes (figure 4.1 A1-3 and B1-3 respectively). IRDye 800CW was encapsulated in

5% PEG niosomes in 1 nmol (Lane D1-3) and 4 nmol (Lane C1-3) concentrations. Three different volumes of the samples, 100 ul (column 3), 200 ul (column 2) and 300 ul (column 1) were imaged using epi-illumination (5 second exposure, F2 aperture, small binning) and the image is shown in figure 4.2. It was determined that the PBS loaded niosomes did not have a signal that would interfere with the dye, and that 4 nmol IRDye 800CW loaded niosomes were required for imaging at these settings.

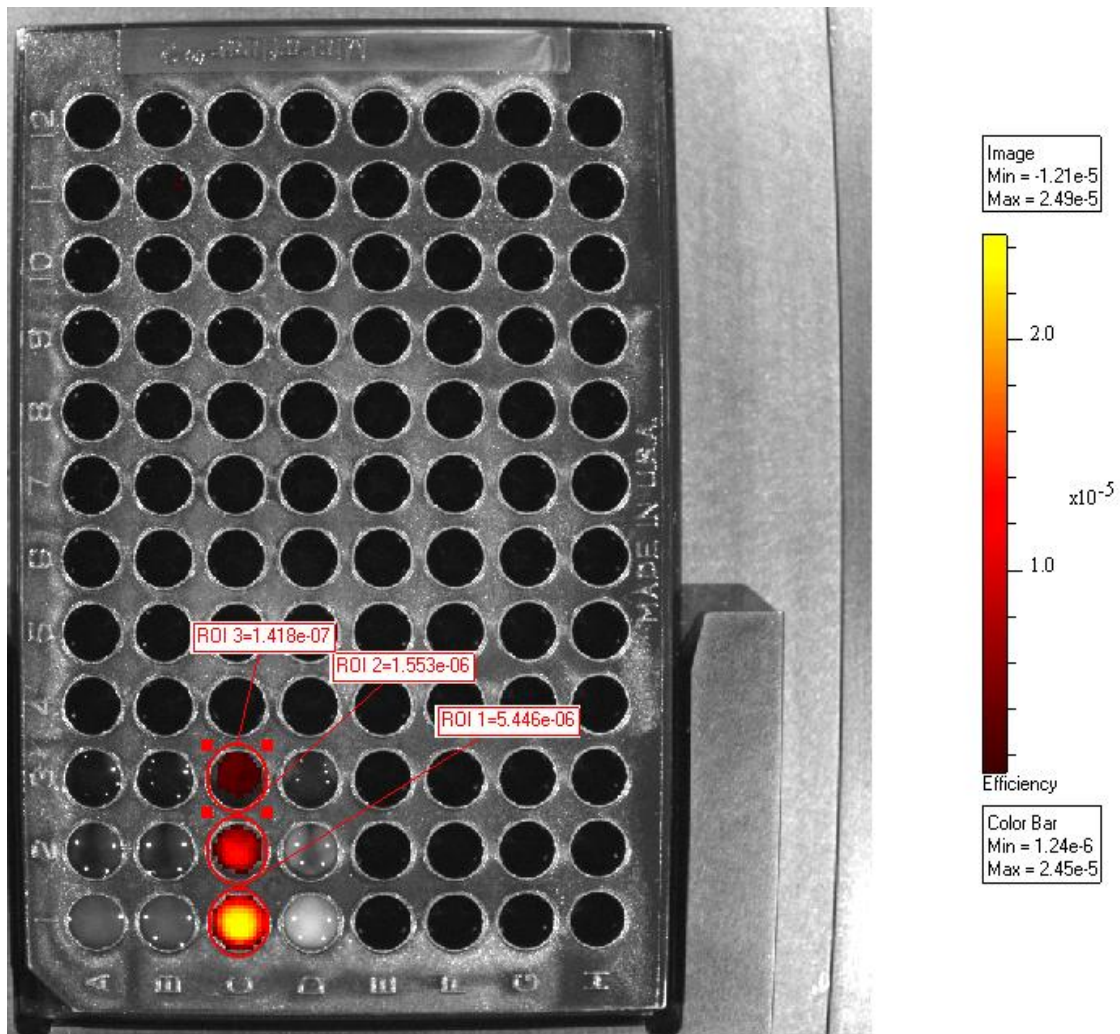


Figure 4.1 IRDye 800CW Reference Samples

Based on these results, niosomes were loaded with 4 nmol IRDye 800CW, extruded across 200 nm polycarbonate films and purified using size exclusion chromatography

(SEC) as described in Section 2.4.3. Three volumes of 4 nmol IRDye 800CW loaded niosomes, 300, 200, 100 ul (Row A, B, C respectively in Figure 4.2) were imaged to confirm previous results. The results shown in Figure 4.2 show that the method is repeatable and that extruded, SEC purified niosomes loaded with 4 nmol IRDye800CW can be imaged using epi-illumination on the Xenogen IVIS Spectrum.

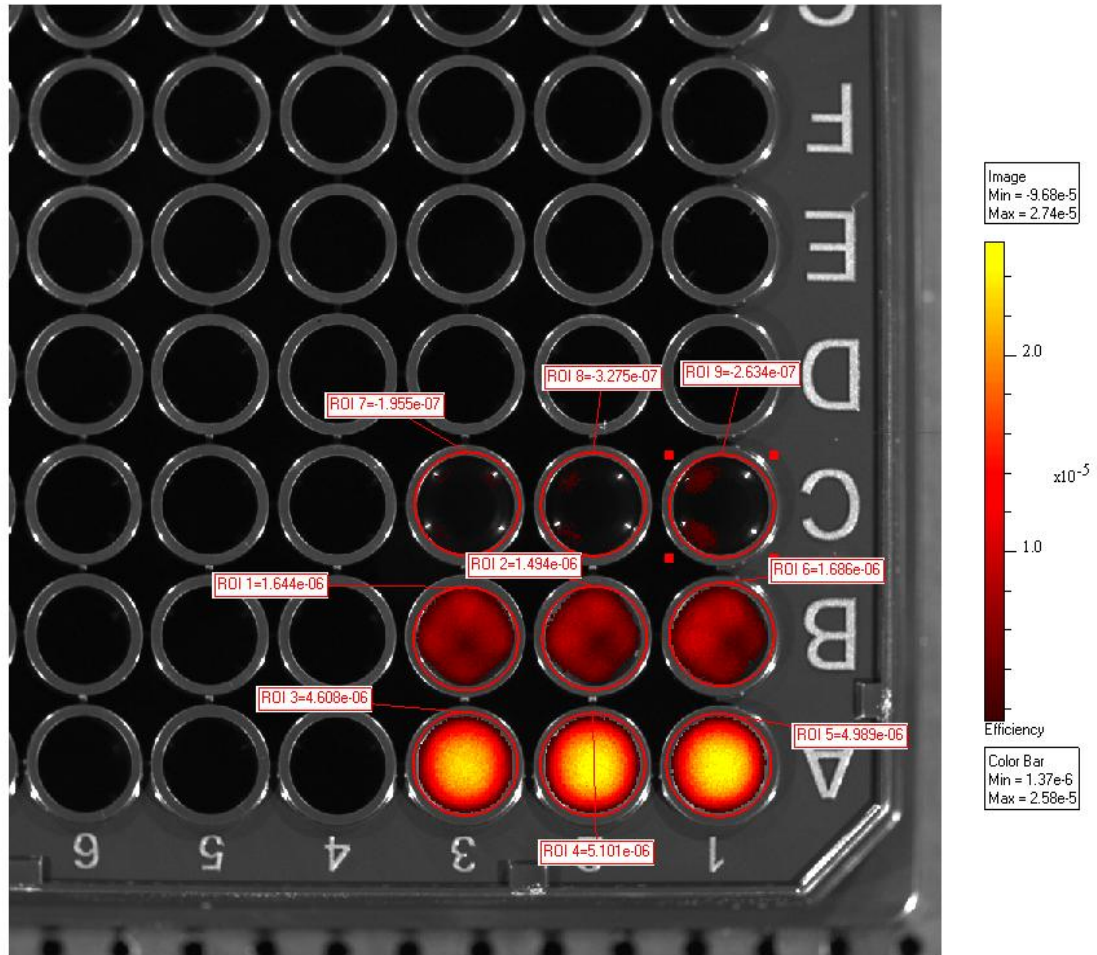


Figure 4.2 4nmol IRDye 800CW Loaded 5% PEGylated Niosomes

4.2.0 Phantom Mouse Imaging

To determine preliminary concentrations of fluorescent dye and immunoniosomes for in vivo studies, a synthetic mouse called the phantom mouse was used to image samples of niosomes loaded with the IRDye800CW fluorescent dye. IVIS

Spectrum generated epi-illumination images of pipettes loaded with free and encapsulated 4, 8, and 12 fmol IR800CW dye (1,2 and 3ul of 4 nM dye) as shown in figure 4.3.

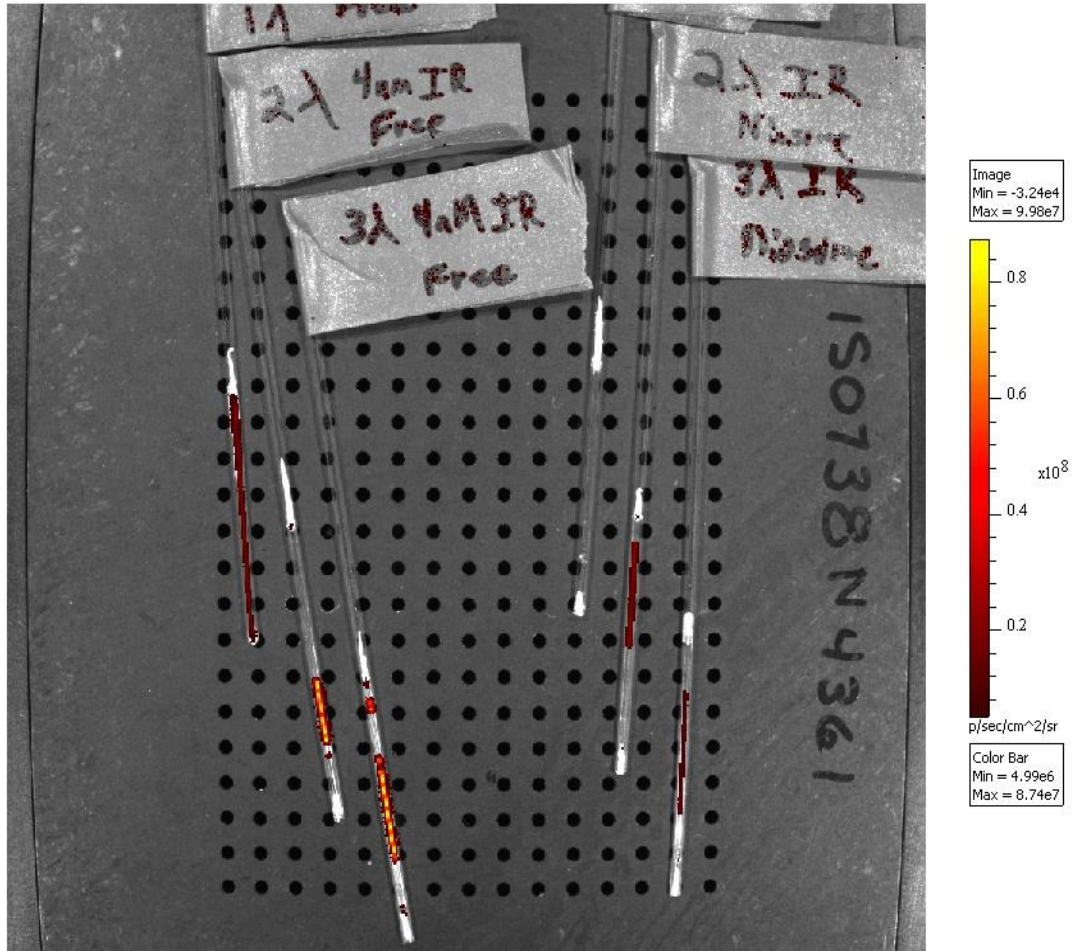


Figure 4.3 IRDye 800CW Pipette Standards for Phantom Mouse

Image #: JAE20090613102930
Sat ,Jun 13, 2009 10:29:46
Level=High, Em=800 , Ex=745, Epi-illumination
Bin:(HR)4, FOV:13, f1, 1s
Camera: ISO738N4361, Spectral Instruments TE

User: John Elliott
Group: belly up-phantom mouse; 1sec; fstop1
Experiment: field of view C
Comment1: 3ul of 4nM niosome IR800cw
Comment2: source b phantom; trans; high lamp

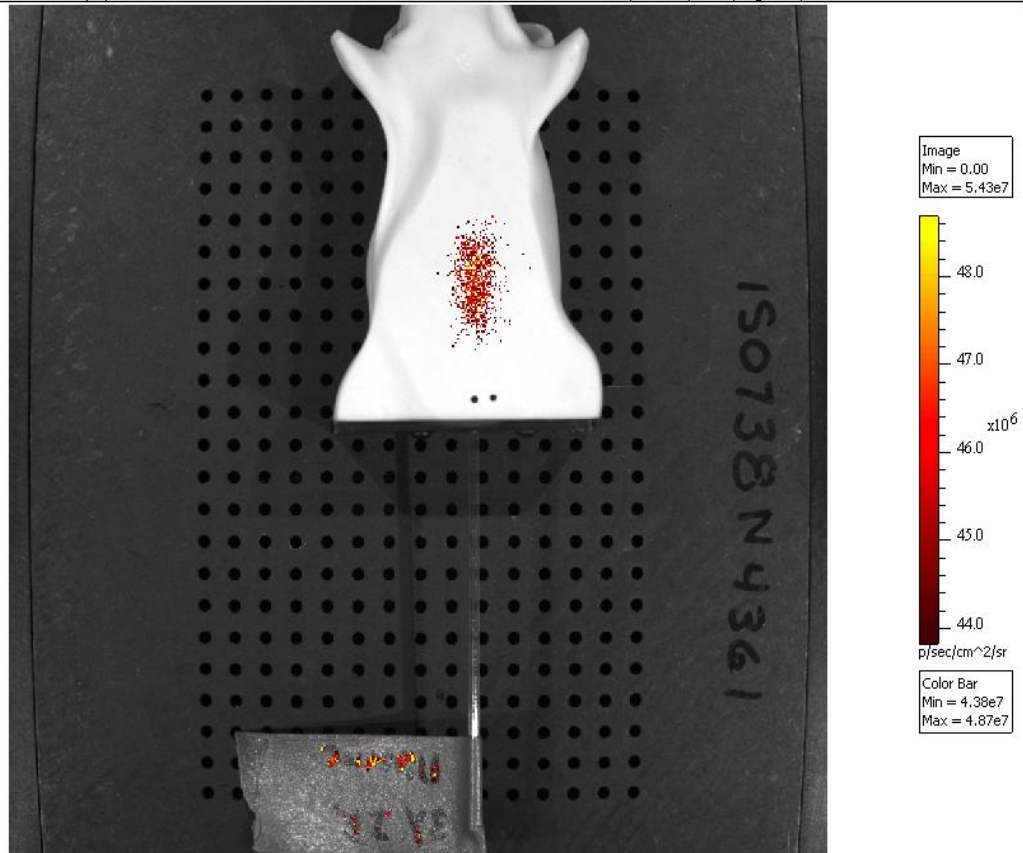


Figure 4.4 Minimum Detection Limits with Epi-illumination

To determine the limit of detection for the IRDye800CW loaded niosomes, the phantom mouse was imaged in the ventral position with a 12 fmol IRDye 800CW loaded niosome sample for 1 second with F1 aperture, high lamp, binning set at level 4 with epi-illumination as shown in Figure 4.4. For comparison the phantom mouse was placed in the dorsal position and the same sample was imaged using trans-illumination, shown in figure 4.5. The sample emitted a signal of $2.6E9$ photons/sec/cm² when imaged for 5 seconds F2 aperture, high lamp, binning at level 4. Results indicate the niosome and dye concentrations are adequate for pilot in vivo imaging studies.

Image #: JAE20090613102039
Sat, Jun 13, 2009 10:21:01
Level=High, Em=800, Ex=745, Trans-illumination
Bin:(HR)4, FOV:13, f2, 5s
Camera: ISO738N4361, Spectral Instruments TE

User: John Elliott
Group: phantom mouse; 5sec; fstop2
Experiment: field of view C
Comment1: 3ul of 4nM free IR800cw
Comment2: source b phantom; trans; high lamp

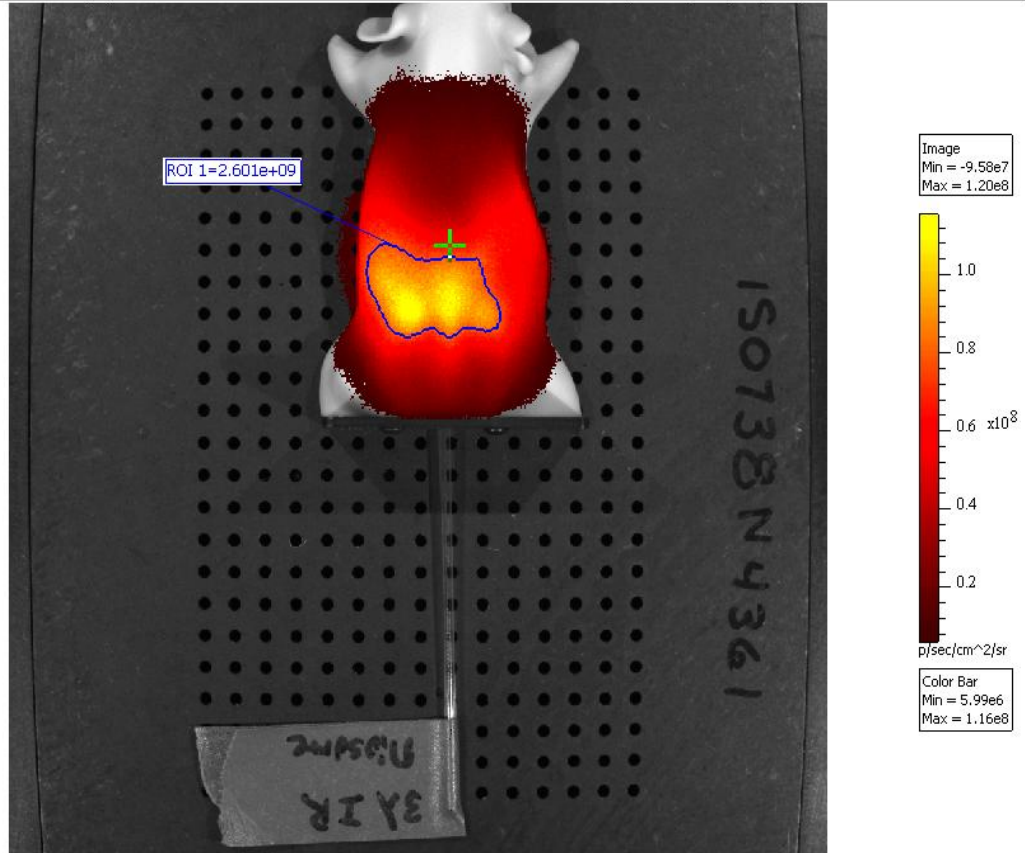


Figure 4.5 Phantom Mouse Imaged Under Trans-illumination

5. Discussion and Future Direction

5.1.0 Vesicle Design and Manufacturing

Many vesicle designs have been developed to transport therapeutic agents to specific sites in the body. While no one design provides a solution for every application, techniques using bilayer membranes to entrap therapeutic agents have proven successful. Polymers provide vesicle stability, but the harsh conditions used for the polymerization process can be detrimental to the agent being entrapped. Amphiphiles made from peptides are easily metabolized in the body making them biocompatible. However, because the molecules can be broken down so easily, the vesicle life span is low, and spontaneous release of the entrapped drug can cause toxic dosage levels. In the niosome production, the use of synthetic non-ionic surfactants provides an economical and physiological advantage compared to traditional phospholipids used in liposome production. Because phospholipids have the tendency to oxidize over time, great care must be taken to ensure the product remains safe for use. Synthetic surfactants also have an advantage because surfactants derived from natural sources require extra processing to ensure there are no pathological contaminants.

The 200 nm size chosen for the niosome design provides an internal volume that can contain a substantial dosage of the therapeutic agent, yet is small enough to evade opsonization (coating of the vesicles by plasma proteins) and recognition by the reticuloendothelial system. The 200 nm size is large enough to eliminate the non-specific uptake of the vesicles through the process of cellular pinocytosis. The 200 nm size also

allows the vesicle to remain in suspension for an extended period of time. The addition of polyethylene glycol to the niosome (PEGylation) provides a mechanical boundary between vesicles. This steric stabilization further enhances the stability of the niosome suspension. The PEG chains also reduce the attachment of plasma proteins to the niosome membrane surface. This is a very important feature that has been shown by other groups to increase the circulation time of the vesicle in vivo.

Targeting specific endothelial cell surface receptors allows for intravenous delivery of the vesicles. This route delivers all of the vesicles to the blood where they will encounter the endothelial cells lining the vessel walls. CD44, an inflammatory receptor expressed by activated endothelial cells after cytokine exposure or physical injury, is the targeted receptor. The CD44 receptor is also present on many cancer cells and provides a method of delivering a therapeutic vesicle directly to the tumor. In addition to targeting CD44, ICAM-1 and VCAM-1, other inflammatory receptors expressed by endothelial cells were targeted, and binding of PEGylated immuno-niosomes (IN) with the three different receptors types was compared. We investigated nonspecific binding and the ability of the PEGylated immuno-niosomes to bind fixed and live endothelial cells. We showed by confocal microscopy that PEGylated immuno-niosomes can be internalized by the endothelial cell when they bind to the CD44 receptor (figure 3.11). This suggests that the targeting scheme is capable of delivering therapeutics to specific cells.

Two methods were used to stimulate the upregulation of inflammatory cell surface receptors. One method was the exposure of the cell to the pro-inflammatory cytokine, tumor necrosis factor alpha (TNF- α). This is a well described process that has been used in vitro to mimic the natural process of inflammation. An injury model was

used to investigate the capacity of the PEGylated immuno-niosomes to target cells that have experienced physical trauma.

The concentration of atorvastatin encapsulated in immuno-niosomes was determined using thin layer chromatography (TLC). It was found that two solvent systems were required to separate all the immuno-niosome components from the atorvastatin. The atorvastatin-loaded immuno-niosomes were pre-processed prior to TLC separation to remove the surfactant and to concentrate the sample. Using known atorvastatin concentrations, a standard curve was created. We determined that this TLC separation method gave us the ability to accurately determine concentration as indicated by the linear correlation coefficient (R^2) of 0.9898 between the known and unknown atorvastatin concentrations.

In the previous immuno-niosome design developed in our lab by Hood et al., cyanuric chloride was used to link the Tween 61 and CD44 antibody used to target the niosome to the endothelial cells. In the work reported here, polyethylene glycol with cyanuric chloride linking chemistry was added to this previous design, creating the PEGylated immuno-niosome (figure 1.0). The linker chemistry was used to attach and functionalize the PEG to the head group of the Tween 61 surfactant. The size and amount of PEG used was based on previous liposome designs [12-15] and the results from the fixed cell binding experiments (figures 3.0 and 3.1) which showed improved binding of PEGylated CD44-IN as compared with CD44-IN to the activated endothelial cells. The current PEGylated INs contain PEG surfactant on both the interior and exterior of the vesicle. The immuno-niosome design can be further modified by incubating niosomes

with PEGylated micelles to create PEGylated immuno-niosomes with the PEG only on the immuno-niosome outer surface.

Therapeutic agent or dye entrapment occurs during the thin film hydration process. This process time was extended from one to four hours, keeping other conditions constant, to provide a bulk solution that was more homogenous than previously obtained. Use of a more homogenous bulk solution lessened the previously seen fouling of the polycarbonate membranes used for vesicle extrusion. With a bulk solution hydration time of one hour, the membranes in the extruder needed to be replaced after four passes. When the hydration time of the bulk solution was extended to two hours, eight-ten passes through the extruder could be accomplished before the membranes fouled. When the hydration time of the bulk solution was extended to four hours, the number of passes before the membranes fouled approached 20. The high number of passes translates to better size control of the vesicles and lower numbers of vesicles becoming entrapped in the extruder membranes (less waste).

After bulk solution extrusion, the encapsulated and free therapeutic agent or dye was separated using size exclusion chromatography. This type of separation results in some sample loss and sample dilution. Under theoretical conditions, separation of vesicles based on size is based on the assumption that there are no entrance or exit effects from the column. However, empirically we showed that when the sample was loaded on the column, the interaction of the bulk solution and the entrance region caused back mixing (figure 2.8). The sample volume loaded on the column was reduced from 2 ml to 500 μ l (figure 2.9). The reduction in sample volume loaded resulted in symmetric elution profiles where the vesicle size correlated with the elution fraction. To determine PEG

incorporation efficiency in the niosomes, the bulk solution was spiked with free PEG. The spiked sample was loaded and eluted through the column. The resulting elution profile showed an extra peak that was not present in samples that were not spiked with free PEG. These results indicated that the PEG modified surfactant was incorporated in the PEGylated niosome (results not shown).

A difference in PEGylated niosome versus niosome size distribution was determined using dynamic light scattering. The addition of PEG to a vesicle can alter the niosome solution viscosity and change its light absorbance properties which will affect data collected using dynamic light scattering. To minimize the effects of the PEG on the PEGylated niosome size distribution measurements, the samples were diluted with 0.01 M phosphate buffered saline, to maintain osmolarity and prevent PEGylated niosome rupture. The large dilution of the PEGylated niosome sample caused the sample viscosity to approach pure solvent (phosphate buffered saline). The size distribution changed by only 4 nm, indicating that the PEG did not affect PEGylated niosome size distribution and that the original measurements were valid. The PEGylated niosome size distribution was also measured using transmission electron microscopy (figures 2.17 and 2.18) and flow cytometry (figures 2.11 and 2.12, tables 2.0 and 2.1). The PEGylated niosome size distribution supports the original measurements using dynamic light scattering (figure 2.13).

5.2.0 Experimental Conclusions

The binding efficiency of the PEGylated and non-PEGylated immuno-niosomes to tumor necrosis factor alpha (TNF- α)-activated endothelial cells was compared. The endothelial cells were plated in black/clear bottom multiwell culture plates. 5,6-

Carboxyfluorescein was encapsulated in the PEGylated CD44-IN and CD44-IN to visualize binding to the endothelial cells. To prevent the endothelial cell surface receptors from being internalized or recycled over the two hour experimental time course, the cells were fixed prior to incubation with the PEGylated CD44-IN or CD44-IN. Binding of the PEGylated CD44-IN to activated endothelial cells was increased 17% over binding of the CD44-IN to activated endothelial cells (figures 3.0, 3.1, table 3.0). These data demonstrate that PEGylation of the immuno-niosomes improves specific binding to activated endothelial cells.

Next, experiments were conducted to determine the non-specific binding of the PEGylated immuno-niosomes to live endothelial cells. Fluorescent dye was encapsulated in the PEGylated CD44-IN, VCAM-1-IN and ICAM-1-IN to visualize binding. Non-specific binding of the PEGylated CD44-IN, VCAM-1-IN and ICAM-1-IN to unactivated endothelial cells was measured. It was determined that non-specific binding was linear over the four hour time course (Figure 3.2). These data demonstrate that non-specific binding of the PEGylated IN to the unactivated endothelial cells was not antibody dependent.

Next, experiments were conducted to determine the interaction of the PEGylated immuno-niosomes with live endothelial cells. Fluorescent dye was encapsulated in the PEGylated CD44-IN, VCAM-1-IN and ICAM-1-IN to visualize binding. The endothelial cells were activated with TNF- α for 24 hours prior to incubation with the PEGylated IN to induce an inflammatory response. Specific binding of the PEGylated CD44-IN, VCAM-1-IN and ICAM-1-IN to the activated endothelial cells was measured. It was determined that all three PEGylated IN had similar binding to the activated endothelial

cells over the four hour time course (Figure 3.3). These data suggest that the use of antibodies on the PEGylated IN that target CD44 is as effective as those that target VCAM-1 or ICAM-1.

Next, experiments were conducted to confirm uptake of the PEGylated immuno-niosomes by activated endothelial cells. Fluorescent dye was encapsulated in the PEGylated CD44-IN, VCAM-1-IN and ICAM-1-IN to visualize binding and uptake to activated endothelial cells using a confocal microscopy. The images captured provided confirmation that the immuno-niosome payload was internalized by the endothelial cells (Figures 3.7-3.13). This was a major accomplishment that had not been seen before using the vesicle design and antibody combination.

Next, experiments were conducted to determine the interaction of the PEGylated immuno-niosomes with physically injured endothelial cells using confocal microscopy. The cells were injured 24 hours prior to incubation with 5,6-carboxyrhodamine loaded immuno-niosomes that were conjugated with CD44 or ICAM antibodies. The results indicated the immuno-niosomes can target endothelial cells that have sustained trauma from a physical injury (Figures 3.4, 3.5 and 3.6, Table 3.1). This is another important finding and the results suggest that injuries sustained from battlefield wounds can be targeted by therapeutic immuno-niosomes. This also means that the immuno-niosome could deliver therapeutic agents to venous grafts after coronary surgery.

5.3.0 Future Directions

Experiments designed to determine the performance of the PEGylated immuno-niosomes in vivo have been approved and funded through the Signature Interdisciplinary Program In Cardiovascular Research (SIPCVR), a pilot grant program funded by USF

Health. The proposed experiments will assist us in determining the bio-distribution of the CD44, ICAM or VCAM conjugated immuno-niosomes in apolipoprotein E knockout (apoE -/-) mice and wild type control mice (C57BL/6). The data will also give insight to the pharmacokinetics (described in section 1.1.1) of the PEGylated immuno-niosomes in vivo. The experimental design is to target sites of vascular inflammation caused by atherosclerosis in the apo-E -/- mice. The mice will be injected with fluorescent dye loaded immuno-niosomes, fluorescent dye loaded niosomes without antibodies or free dye. Near infrared fluorescent dye, IRDye 800cw will be used so the animals can be imaged live using the Xenogen IVIS Spectrum (described in section 4.2.0). The organs will be imaged whole and then sectioned to give greater detail of the interactions and binding of the immuno-niosomes with organs and cells.

The next experiments will be based on the information gained from, the pilot study. To improve endothelial cell binding in large arteries, modification to the immuno-niosome design will be made using the functionalized cholesterol (described in section 2.3.2) and a biotinylated PEG to conjugate both antibodies and selectins, respectively. These modifications will provide a design that will allow the immuno-niosome to attach with low affinity to the vessel wall via selectin binding and then roll to a site of inflammation where the antibody can bind with high affinity, mimicking leukocyte binding.

References

1. Bangham, A.D., M.M. Standish, and N. Miller, *Cation Permeability of Phospholipid Model Membranes - Effect of Narcotics*. *Nature*, 1965. 208(5017): p. 1295-1297.
2. Bangham, A.D., M.M. Standish, and J.C. Watkins, *Diffusion of Univalent Ions across Lamellae of Swollen Phospholipids*. *Journal of Molecular Biology*, 1965. 13(1): p. 238-252.
3. Bangham, A.D., M.M. Standish, and Weissman.G, *Action of Steroids and Streptolysin S on Permeability of Phospholipid Structures to Cations*. *Journal of Molecular Biology*, 1965. 13(1): p. 253-259.
4. Gregoriadis, G., *Engineering liposomes for drug delivery: progress and problems*. *Trends Biotechnol*, 1995. 13(12): p. 527-37.
5. Azmin, M.N., et al., *The Effect of Non-Ionic Surfactant Vesicle (Niosome) Entrapment on the Absorption and Distribution of Methotrexate in Mice*. *Journal of Pharmacy and Pharmacology*, 1985. 37(4): p. 237-242.
6. Baillie, A.J., et al., *The Preparation and Properties of Niosomes Non-Ionic Surfactant Vesicles*. *Journal of Pharmacy and Pharmacology*, 1985. 37(12): p. 863-868.
7. Kim, R.S. and F.S. LaBella, *Comparison of analytical methods for monitoring autoxidation profiles of authentic lipids*. *J Lipid Res*, 1987. 28(9): p. 1110-7.
8. Schwaber, J., *Immunoglobulin Production by a Human-Mouse Somatic-Cell Hybrid*. *Experimental Cell Research*, 1975. 93(2): p. 343-354.
9. Abuchowski, A., et al., *Alteration of Immunological Properties of Bovine Serum-Albumin by Covalent Attachment of Polyethylene-Glycol*. *Journal of Biological Chemistry*, 1977. 252(11): p. 3578-3581.
10. Bekersky, I., et al., *Pharmacokinetics, excretion, and mass balance of liposomal amphotericin B (AmBisome) and amphotericin B deoxycholate in humans*. *Antimicrobial Agents and Chemotherapy*, 2002. 46(3): p. 828-833.
11. Boswell, G.W., et al., *Toxicological profile and pharmacokinetics of a unilamellar liposomal vesicle formulation of amphotericin B in rats*. *Antimicrobial Agents and Chemotherapy*, 1998. 42(2): p. 263-268.

12. Allen, T.M. and C. Hansen, *Pharmacokinetics of Stealth Versus Conventional Liposomes - Effect of Dose*. *Biochimica Et Biophysica Acta*, 1991. 1068(2): p. 133-141.
13. Allen, T.M., et al., *Liposomes Containing Synthetic Lipid Derivatives of Poly(Ethylene Glycol) Show Prolonged Circulation Half-Lives In vivo*. *Biochimica Et Biophysica Acta*, 1991. 1066(1): p. 29-36.
14. Agrawal, A.K. and T.M. Allen, *Attachment of Antibodies to Pegylated Liposomes by the Biotin-Avidin Method*. *Faseb Journal*, 1992. 6(1): p. A493-A493.
15. Allen, T.M., et al., *Stealth Liposomes - an Improved Sustained-Release System for I-Beta-D-Arabinofuranosylcytosine*. *Cancer Research*, 1992. 52(9): p. 2431-2439.
16. Bendas, G., et al., *Targetability of novel immunoliposomes prepared by a new antibody conjugation technique*. *International Journal of Pharmaceutics*, 1999. 181(1): p. 79-93.
17. Hood, E., et al., *Immuno-targeting of nonionic surfactant vesicles to inflammation*. *International Journal of Pharmaceutics*, 2007. 339(1-2): p. 222-230.
18. Cuff, C.A., et al., *The adhesion receptor CD44 promotes atherosclerosis by mediating inflammatory cell recruitment and vascular cell activation*. *J. Clin. Invest.*, 2001. 108(7): p. 1031-1040.
19. Libby, P., P.M. Ridker, and A. Maseri, *Inflammation and atherosclerosis*. *Circulation*, 2002. 105(9): p. 1135-1143.
20. Muro, S., et al., *Intracellular uptake and trafficking of immunoconjugates targeted to endothelial surface adhesion molecules*. *Molecular Biology of the Cell*, 2001. 12: p. 91A-91A.
21. Prokop, A. and J.M. Davidson, *Nanovehicular intracellular delivery systems*. *Journal of Pharmaceutical Sciences*, 2008. 97(9): p. 3518-3590.
22. Muro, S., et al., *Control of endothelial targeting and intracellular delivery of therapeutic enzymes by modulating the size and shape of ICAM-1-targeted carriers*. *Molecular Therapy*, 2008. 16(8): p. 1450-1458.
23. Deosarkar, S.P., et al., *Polymeric particles conjugated with a ligand to VCAM-1 exhibit selective, avid, and focal adhesion to sites of atherosclerosis*. *Biotechnology and Bioengineering*, 2008. 101(2): p. 400-407.

24. Koopman, G., et al., *CD44 isoforms, including the CD44 V3 variant, are expressed on endothelium, suggesting a role for CD44 in the immobilization of growth factors and the regulation of the local immune response*. Biochemical And Biophysical Research Communications, 1998. 245(1): p. 172-176.
25. Ross, J.S., et al., *Expression of the CD44 cell adhesion molecule in urinary bladder transitional cell carcinoma*. Modern Pathology, 1996. 9(8): p. 854-860.
26. Vincent, T. and N. Mechti, *IL-6 regulates CD44 cell surface expression on human myeloma cells*. Leukemia, 2004. 18(5): p. 967-975.
27. Mayer, S., et al., *Increased soluble CD44 concentrations are associated with larger tumor size and lymph node metastasis in breast cancer patients*. Journal of Cancer Research and Clinical Oncology, 2008. 134(11): p. 1229-1235.
28. Palapattu, G.S., et al., *Selective Expression of CD44, a Putative Prostate Cancer Stem Cell Marker, in Neuroendocrine Tumor Cells of Human Prostate Cancer*. Prostate, 2009. 69(7): p. 787-798.
29. Matsuzawa, S., et al., *Quantification of Antibodies by the Volume Distribution Analysis of Latex-Particles*. Proceedings of the Japan Academy Series B-Physical and Biological Sciences, 1980. 56(5): p. 284-289.
30. Hu, L.J., J.L.S. Au, and M.G. Wientjes, *Computational modeling to predict effect of treatment schedule on drug delivery to prostate in humans*. Clinical Cancer Research, 2007. 13(4): p. 1278-1287.
31. Macheras, P., *A fractal approach to heterogeneous drug distribution: Calcium pharmacokinetics*. Pharmaceutical Research, 1996. 13(5): p. 663-670.
32. Fuite, J., R. Marsh, and J. Tuszynski, *Fractal pharmacokinetics of the drug mibefradil in the liver*. Physical Review E, 2002. 66(2): p. 021904-021915.
33. dela Paz, N.G. and P.A. D'Amore, *Arterial versus venous endothelial cells*. Cell and Tissue Research, 2009. 335(1): p. 5-16.
34. Ishii, Y., et al., *Endothelial cell lineages of the heart*. Cell and Tissue Research, 2009. 335(1): p. 67-73.
35. Jurisic, G. and M. Detmar, *Lymphatic endothelium in health and disease*. Cell and Tissue Research, 2009. 335(1): p. 97-108.
36. Tarbell, J.M., *Mass transport in arteries and the localization of atherosclerosis*. Annual Review of Biomedical Engineering, 2003. 5: p. 79-118.

37. Bruce Alberts, D.B., Alexander Johnson, Julian Lewis, Martin Raff, Keith Roberts and Peter Walter, *Essential Cell Biology: An Introduction to the Molecular Biology of the Cell*. 1998, 717 Fith Avenue, New York, NY 10022: Garland Publishing, Inc. 630.
38. Hawkes, C.A. and J. McLaurin, *Selective targeting of perivascular macrophages for clearance of beta-amyloid in cerebral amyloid angiopathy*. Proceedings of the National Academy of Sciences of the United States of America, 2009. 106(4): p. 1261-1266.
39. Stan, R.V., *Endocytosis pathways in endothelium: how many?* American Journal of Physiology-Lung Cellular and Molecular Physiology, 2006. 290(5): p. L806-L808.
40. Conner, S.D. and S.L. Schmid, *Regulated portals of entry into the cell*. Nature, 2003. 422(6927): p. 37-44.
41. Echarri, A., O. Muriel, and M.A. Del Pozo, *Intracellular trafficking of raft/caveolae domains: Insights from integrin signaling*. Seminars in Cell & Developmental Biology, 2007. 18(5): p. 627-637.
42. Tiruppathi, C., et al., *Gp60 activation mediates albumin transcytosis in endothelial cells by tyrosine kinase-dependent pathway*. Journal of Biological Chemistry, 1997. 272(41): p. 25968-25975.
43. Schleimer, R.P. and B.S. Bochner, *The role of adhesion molecules in allergic inflammation and their suitability as targets of antiallergic therapy*. Clinical and Experimental Allergy, 1998. 28: p. 15-23.
44. Lesley, J., et al., *CD44 in inflammation and metastasis*. Glycoconjugate Journal, 1997. 14(5): p. 611-622.
45. Brennan, F.R., et al., *CD44 expression by leucocytes in rheumatoid arthritis and modulation by specific antibody: Implications for lymphocyte adhesion to endothelial cells and synoviocytes in vitro*. Scandinavian Journal of Immunology, 1997. 45(2): p. 213-220.
46. Cuff, C.A., et al., *The adhesion receptor CD44 promotes atherosclerosis by mediating inflammatory cell recruitment and vascular cell activation*. Journal of Clinical Investigation, 2001. 108(7): p. 1031-1040.
47. Koch, A.E., et al., *Immunolocalization of Endothelial and Leukocyte Adhesion Molecules in Human Rheumatoid and Osteoarthritic Synovial Tissues*. Laboratory Investigation, 1991. 64(3): p. 313-320.

48. Banks, R.E., et al., *Circulating Intercellular-Adhesion Molecule-1 (Icam-1), E-Selectin and Vascular Cell-Adhesion Molecule-1 (Vcam-1) in Human Malignancies*. British Journal of Cancer, 1993. 68(1): p. 122-124.
49. Libby, P., et al., *Cytokines regulate vascular functions related to stability of the atherosclerotic plaque*. Journal of Cardiovascular Pharmacology, 1995. 25: p. S9-S12.
50. Newman, P.J., *The biology of PECAM-1*. Journal of Clinical Investigation, 1997. 99(1): p. 3-7.
51. Muller, W.A., et al., *Pecam-1 Is Required for Transendothelial Migration of Leukocytes*. Journal of Experimental Medicine, 1993. 178(2): p. 449-460.
52. Bahra, P., et al., *Each step during transendothelial migration of flowing neutrophils is regulated by the stimulatory concentration of tumour necrosis factor-alpha*. Cell Adhesion and Communication, 1998. 6(6): p. 491-501.
53. Lawrence, M.B. and T.A. Springer, *Neutrophils Roll on E-Selectin*. Journal of Immunology, 1993. 151(11): p. 6338-6346.
54. Patel, K.D., M.U. Nollert, and R.P. McEver, *P-selectin must extend a sufficient length from the plasma membrane to mediate rolling of neutrophils*. Journal of Cell Biology, 1995. 131(6): p. 1893-1902.
55. Crockett-Torabi, E., *Selectins and mechanisms of signal transduction*. Journal of Leukocyte Biology, 1998. 63(1): p. 1-14.
56. Dwir, O., et al., *Membranal cholesterol is not required for L-selectin adhesiveness in primary lymphocytes but controls a chemokine-induced destabilization of L-selectin rolling adhesions*. Journal of Immunology, 2007. 179(2): p. 1030-1038.
57. Finger, E.B., et al., *Adhesion through L-selectin requires a threshold hydrodynamic shear*. Nature, 1996. 379(6562): p. 266-269.
58. Li, X., et al., *Regulation of L-selectin-mediated rolling through receptor dimerization*. Journal of Experimental Medicine, 1998. 188(7): p. 1385-1390.
59. DelMaschio, A., et al., *Polymorphonuclear leukocyte adhesion triggers the disorganization of endothelial cell-to-cell adherens junctions*. Journal of Cell Biology, 1996. 135(2): p. 497-510.
60. Orlova, V.V., et al., *Junctional adhesion molecule-C regulates vascular endothelial permeability by modulating VE-cadherin-mediated cell-cell contacts*. Journal of Experimental Medicine, 2006. 203(12): p. 2703-2714.

61. Resink, T.J., et al., *Cadherins in cardiovascular disease*. Swiss Medical Weekly, 2009. 139(9-10): p. 122-134.
62. Ivanov, D., et al., *Expression of cell adhesion molecule T-cadherin in the human vasculature*. Histochemistry and Cell Biology, 2001. 115(3): p. 231-242.
63. Wyder, L., et al., *Increased expression of H/T-cadherin in tumor-penetrating blood vessels*. Cancer Research, 2000. 60(17): p. 4682-4688.
64. Kuphal, S., et al., *H-Cadherin expression reduces invasion of malignant melanoma*. Pigment Cell & Melanoma Research, 2009. 22(3): p. 296-306.
65. Jin, Z., et al., *Promoter hypermethylation of CDH13 is a common, early event in human esophageal adenocarcinogenesis and correlates with clinical risk factors*. International Journal of Cancer, 2008. 123(10): p. 2331-2336.
66. Qian, Z.R., et al., *Tumor-specific downregulation and methylation of the CDH13 (H-cadherin) and CDH1 (E-cadherin) genes correlate with aggressiveness of human pituitary adenomas*. Modern Pathology, 2007. 20(12): p. 1269-1277.
67. Lee, S.W., *H-cadherin, a novel cadherin with growth inhibitory functions and diminished expression in human breast cancer*. Nature Medicine, 1996. 2(7): p. 776-782.
68. Barclay, A.N., *Membrane proteins with immunoglobulin-like domains - a master superfamily of interaction molecules*. Seminars in Immunology, 2003. 15(4): p. 215-223.
69. Porter, R.R., *Hydrolysis of Rabbit Gamma-Globulin and Antibodies with Crystalline Papain*. Biochemical Journal, 1959. 73: p. 119-126.
70. Stoliar, O.A., et al., *Secretory Iga against Enterotoxins in Breast-Milk*. Lancet, 1976. 1(7972): p. 1258-1261.
71. Mestecky, J. and M.W. Russell, *Passive and active protection against disorders of the gut*. Veterinary Quarterly, 1998. 20: p. S83-S87.
72. Goroff, D.K., et al., *Determinants of B-Cell Activating Ability of Monoclonal Anti-Igd Antibodies*. Federation Proceedings, 1985. 44(4): p. 1296-1296.
73. Nissim, A., M.H. Jouvin, and Z. Eshhar, *Mapping of the High-Affinity Fc-Epsilon Receptor-Binding Site to the 3rd Constant Region Domain of Ige*. Embo Journal, 1991. 10(1): p. 101-107.
74. Yazdanbakhsh, M., P.G. Kremsner, and R. van Ree, *Immunology - Allergy, parasites, and the hygiene hypothesis*. Science, 2002. 296(5567): p. 490-494.

75. Shakib, F., et al., *The Detection of Autoantibodies to Ige in Plasma of Individuals Infected with Hookworm (Necator-Americanus) and the Demonstration of a Predominant IgG1 Anti-Ige Autoantibody Response*. Parasite Immunology, 1993. 15(1): p. 47-53.
76. M.R.G. O'Gorman, A.D.D., *Handbook of Human Immunology*. Second ed. 2008, 6000 Broken Sound Parkway NW, Suite 300, Boca Raton, FL 33487-2742: CRC Press, Taylor and Francis Group.
77. Boes, M., *Role of natural and immune IgM antibodies in immune responses*. Molecular Immunology, 2000. 37(18): p. 1141-1149.
78. Oxelius, V.A., *Serum IgG and IgG Subclass Contents in Different Gm Phenotypes*. Scandinavian Journal of Immunology, 1993. 37(2): p. 149-153.
79. Schwaber, J. and E.P. Cohen, *Human x mouse somatic cell hybrid clone secreting immunoglobulins of both parental types*. Nature, 1973. 244(5416): p. 444-7.
80. Kohler, G. and C. Milstein, *Continuous cultures of fused cells secreting antibody of predefined specificity*. Nature, 1975. 256(5517): p. 495-7.
81. Borland, G., J.A. Ross, and K. Guy, *Forms and functions of CD44*. Immunology, 1998. 93(2): p. 139-148.
82. Thorne, R.F., J.W. Legg, and C.M. Isacke, *The role of the CD44 transmembrane and cytoplasmic domains in co-ordinating adhesive and signalling events*. Journal of Cell Science, 2004. 117(3): p. 373-380.
83. Bajorath, J., *Molecular organization, structural features, and ligand binding characteristics of CD44, a highly variable cell surface glycoprotein with multiple functions*. Proteins-Structure Function and Genetics, 2000. 39(2): p. 103-111.
84. Knudson, W., G. Chow, and C.B. Knudson, *CD44-mediated uptake and degradation of hyaluronan*. Matrix Biology, 2002. 21(1): p. 15-23.
85. Kugelman, L.C., et al., *The Core Protein of Epican, a Heparan-Sulfate Proteoglycan on Keratinocytes, Is an Alternative Form of Cd44 (Journal Investigative Dermatol, Vol 99, Pg 384, 1992)*. Journal of Investigative Dermatology, 1992. 99(6): p. 886-891.
86. Matsumoto, K., et al., *CD44 and CD69 represent different types of cell-surface activation markers for human eosinophils*. American Journal of Respiratory Cell and Molecular Biology, 1998. 18(6): p. 860-866.

87. Bella, J., et al., *The structure of the two amino-terminal domains of human ICAM-1 suggests how it functions as a rhinovirus receptor and as an LFA-1 integrin ligand*. Proceedings of the National Academy of Sciences of the United States of America, 1998. 95(8): p. 4140-4145.
88. Defougerolles, A.R., X. Qin, and T.A. Springer, *Characterization of the Function of Intercellular-Adhesion Molecule (Icam)-3 and Comparison with Icam-1 and Icam-2 in Immune-Responses*. Journal of Experimental Medicine, 1994. 179(2): p. 619-629.
89. Rothlein, R., et al., *A Human Intercellular-Adhesion Molecule (Icam-1) Distinct from Lfa-1*. Journal of Immunology, 1986. 137(4): p. 1270-1274.
90. Staunton, D.E., M.L. Dustin, and T.A. Springer, *Functional Cloning of Icam-2, a Cell-Adhesion Ligand for Lfa-1 Homologous to Icam-1*. Nature, 1989. 339(6219): p. 61-64.
91. Defougerolles, A.R. and T.A. Springer, *Intercellular-Adhesion Molecule-3, a 3rd Adhesion Counter-Receptor for Lymphocyte Function Associated Molecule-1 on Resting Lymphocytes*. Journal of Experimental Medicine, 1992. 175(1): p. 185-190.
92. Kirchhausen, T., D.E. Staunton, and T.A. Springer, *Location of the Domains of Icam-1 by Immunolabeling and Single-Molecule Electron-Microscopy*. Journal of Leukocyte Biology, 1993. 53(3): p. 342-346.
93. Carlos, T.M., et al., *Vascular Cell-Adhesion Molecule-1 Mediates Lymphocyte Adherence to Cytokine-Activated Cultured Human Endothelial-Cells*. Blood, 1990. 76(5): p. 965-970.
94. Osborn, L., C. Vassallo, and C.D. Benjamin, *Activated Endothelium Binds Lymphocytes through a Novel Binding-Site in the Alternately Spliced Domain of Vascular Cell-Adhesion Molecule-1*. Journal of Experimental Medicine, 1992. 176(1): p. 99-107.
95. Chan, B.M.C., et al., *Adhesion to Vascular Cell-Adhesion Molecule-1 and Fibronectin - Comparison of Alpha-4-Beta-1 (Vla-4) and Alpha-4-Beta-7 on the Human B-Cell Line Jy*. Journal of Biological Chemistry, 1992. 267(12): p. 8366-8370.
96. May, M.J., et al., *Vcam-1 Is a Cs1 Peptide-Inhibitable Adhesion Molecule Expressed by Lymph-Node High Endothelium*. Journal of Cell Science, 1993. 106: p. 109-119.

97. Nakashima, Y., et al., *Upregulation of VCAM-1 and ICAM-1 at atherosclerosis-prone sites on the endothelium in the ApoE-deficient mouse*. *Arteriosclerosis Thrombosis and Vascular Biology*, 1998. 18(5): p. 842-851.
98. Hanyu, M., et al., *VCAM-1 expression precedes macrophage infiltration into subendothelium of vein grafts interposed into carotid arteries in hypercholesterolemic rabbits - a potential role in vein graft atherosclerosis*. *Atherosclerosis*, 2001. 158(2): p. 313-319.
99. Dinarello, C.A., *Interleukin-1*. *Reviews of Infectious Diseases*, 1984. 6(1): p. 51-95.
100. Dinarello, C.A., *Historical insights into cytokines*. *European Journal of Immunology*, 2007. 37: p. S34-S45.
101. Bigazzi, P., et al., *Production of Lymphokine-Like Factors (Cytokines) by Simian Virus-40-Infected and Simian Virus-40-Transformed Cells*. *American Journal of Pathology*, 1975. 80(1): p. 69-77.
102. Menkin, V., *Inflammation*. *Journal of Dental Research*, 1949. 28(3): p. 334-334.
103. Menkin, V., *Biology of Inflammation*. *Science*, 1956. 123(3196): p. 527-534.
104. Carswell, E.A., et al., *Endotoxin-Induced Serum Factor That Causes Necrosis of Tumors*. *Proceedings of the National Academy of Sciences of the United States of America*, 1975. 72(9): p. 3666-3670.
105. Old, L.J., *Tumor Necrosis Factor (Tnf)*. *Science*, 1985. 230(4726): p. 630-632.
106. Natoli, G., et al., *Apoptotic, non-apoptotic, and anti-apoptotic pathways of tumor necrosis factor signalling*. *Biochemical Pharmacology*, 1998. 56(8): p. 915-920.
107. Bennett, I.L., Jr., *A study of the relationship between the fevers caused by bacterial pyrogens and by the intravenous injection of the sterile exudates of acute inflammation*. *J Exp Med*, 1948. 88(3): p. 279-84.
108. Rosamond, W., et al., *Heart disease and stroke statistics - 2008 update - A report from the American Heart Association Statistics Committee and Stroke Statistics Subcommittee*. *Circulation*, 2008. 117(4): p. E25-E146.
109. Selwyn, A.P., et al., *Cell dysfunction in atherosclerosis and the ischemic manifestations of coronary artery disease*. *American Journal of Cardiology*, 1997. 79(5A): p. 17-23.

110. Libby, P., M. Aikawa, and U. Schonbeck, *Cholesterol and atherosclerosis*. *Biochimica Et Biophysica Acta-Molecular and Cell Biology of Lipids*, 2000. 1529(1-3): p. 299-309.
111. Jonasson, L., et al., *Regional Accumulations of T-Cells, Macrophages, and Smooth-Muscle Cells in the Human Atherosclerotic Plaque*. *Arteriosclerosis*, 1986. 6(2): p. 131-138.
112. Kranzhofer, R., et al., *Angiotensin induces inflammatory activation of human vascular smooth muscle cells*. *Arteriosclerosis Thrombosis and Vascular Biology*, 1999. 19(7): p. 1623-1629.
113. McGill, H.C., et al., *Origin of atherosclerosis in childhood and adolescence*. *American Journal of Clinical Nutrition*, 2000. 72(5): p. 1307s-1315s.
114. McGill, H.C., et al., *Effects of nonlipid risk factors on atherosclerosis in youth with a favorable lipoprotein profile*. *Circulation*, 2001. 103(11): p. 1546-1550.
115. Imakita, M., et al., *Second nation-wide study of atherosclerosis in infants, children and young adults in Japan*. *Atherosclerosis*, 2001. 155(2): p. 487-497.
116. Sary, H.C., et al., *A Definition of Initial, Fatty Streak, and Intermediate Lesions of Atherosclerosis - a Report from the Committee on Vascular-Lesions of the Council on Arteriosclerosis, American-Heart-Association*. *Arteriosclerosis and Thrombosis*, 1994. 14(5): p. 840-856.
117. Sary, H.C., et al., *A Definition of Advanced Types of Atherosclerotic Lesions and a Histological Classification of Atherosclerosis - a Report from the Committee on Vascular-Lesions of the Council on Arteriosclerosis, American-Heart-Association*. *Circulation*, 1995. 92(5): p. 1355-1374.
118. West, J.L. and N.J. Halas, *Engineered nanomaterials for biophotonics applications: improving sensing, imaging, and therapeutics*. *Annu Rev Biomed Eng*, 2003. 5: p. 285-92.
119. Yamauchi, H., et al., *Molecular-Interactions between Lipid and Some Steroids in a Monolayer and a Bilayer*. *Langmuir*, 1993. 9(1): p. 300-304.
120. Longo, M.A. and D. Combes, *Influence of surface hydrophilic/hydrophobic balance on enzyme properties*. *Journal of Biotechnology*, 1997. 58(1): p. 21-32.
121. Yoshioka, Y., et al., *Optimal site-specific PEGylation of mutant TNF-alpha improves its antitumor potency*. *Biochemical and Biophysical Research Communications*, 2004. 315(4): p. 808-814.

122. Greenwald, R.B., et al., *A new aliphatic amino prodrug system for the delivery of small molecules and proteins utilizing novel PEG derivatives*. Journal of Medicinal Chemistry, 2004. 47(3): p. 726-734.
123. Foser, S., et al., *Improved biological and transcriptional activity of monopegylated interferon-alpha-2a isomers*. Pharmacogenomics Journal, 2003. 3(6): p. 312-319.
124. Bailon, P., W.J. Fung, and J.E. Porter, *Strategies for the preparation and characterization of polyethylene glycol (PEG) conjugated pharmaceutical proteins*. Abstracts of Papers of the American Chemical Society, 1997. 213: p. 183-POLY.
125. Conover, C.D., et al., *The impact of polyethylene glycol conjugation on bovine hemoglobin's circulatory half-life and renal effects in a rabbit top-loaded transfusion model*. Artificial Organs, 1997. 21(8): p. 907-915.
126. Szleifer, I., *Polymers and proteins: Interactions at interfaces*. Current Opinion in Solid State & Materials Science, 1997. 2(3): p. 337-344.
127. Allen, T.M., C.B. Hansen, and D.E.L. Demenezes, *Pharmacokinetics of Long-Circulating Liposomes*. Advanced Drug Delivery Reviews, 1995. 16(2-3): p. 267-284.
128. Allen, T.M., C.B. Hansen, and L.S.S. Guo, *Subcutaneous Administration of Liposomes - a Comparison with the Intravenous and Intraperitoneal Routes of Injection*. Biochimica Et Biophysica Acta, 1993. 1150(1): p. 9-16.
129. Allen, T.M. and E.H. Moase, *Therapeutic opportunities for targeted liposomal drug delivery*. Advanced Drug Delivery Reviews, 1996. 21(2): p. 117-133.
130. Allen, T.M., et al., *Adventures in targeting*. Journal of Liposome Research, 2002. 12(1-2): p. 5-12.
131. Torchilin, V.P., et al., *Targeted Delivery of Diagnostic Agents by Surface-Modified Liposomes*. Journal of Controlled Release, 1994. 28(1-3): p. 45-58.
132. Woodle, M.C. and D.D. Lasic, *Sterically Stabilized Liposomes*. Biochimica Et Biophysica Acta, 1992. 1113(2): p. 171-199.
133. Woodle, M.C., *Controlling liposome blood clearance by surface-grafted polymers*. Advanced Drug Delivery Reviews, 1998. 32(1-2): p. 139-152.
134. Zalipsky, S., et al., *Long-circulating, polyethylene glycol-grafted immunoliposomes*. Journal of Controlled Release, 1996. 39(2-3): p. 153-161.

135. Blume, G. and G. Cevc, *Molecular Mechanism of the Lipid Vesicle Longevity In vivo*. Biochimica Et Biophysica Acta, 1993. 1146(2): p. 157-168.
136. Woodle, M.C., M.S. Newman, and J.A. Cohen, *Sterically Stabilized Liposomes - Physical and Biological Properties*. Journal of Drug Targeting, 1994. 2(5): p. 397-403.
137. Lasic, D.D. and D. Papahadjopoulos, *Liposomes and biopolymers in drug and gene delivery*. Current Opinion in Solid State & Materials Science, 1996. 1(3): p. 392-400.
138. Ametaj, B.N., et al., *Effect of sample preparation, length of time, and sample size on quantification of total lipids from bovine liver*. Journal of Agricultural and Food Chemistry, 2003. 51(8): p. 2105-2110.
139. Shin, J.H., K. Krapfenbauer, and G. Lubec, *Column chromatographic prefractionation leads to the detection of 543 different gene products in human fetal brain*. Electrophoresis, 2005. 26(14): p. 2759-2778.
140. Chou, C.C., et al., *Solid-phase extraction coupled with liquid chromatography-tandem mass spectrometry for determination of trace rosiglitazone in urine*. Journal of Chromatography A, 2005. 1097(1-2): p. 74-83.
141. Hess, A.V.I., *Digitally enhanced thin-layer chromatography: An inexpensive, new technique for qualitative and quantitative analysis*. Journal of Chemical Education, 2007. 84(5): p. 842-847.
142. Badwan, A.A., et al., *Terfenadine Determination Using Different Analytical Methods*. Analytical Letters, 1991. 24(2): p. 217-232.
143. Stokes, G.G., *On the Change of Refrangibility of Light*. Philosophical Transactions of the Royal Society of London, 1852. 142: p. 463-562.
144. Kasha, M., *50 Years of the Jablonski Diagram*. Acta Physica Polonica A, 1987. 71(5): p. 661-670.
145. Chu, B., *Laser Light Scattering*. Annual Review of Physical Chemistry, 1970. 21: p. 145
146. Berne, B.J. and R. Pecora, *Laser Light-Scattering from Liquids*. Annual Review of Physical Chemistry, 1974. 25: p. 233-253.
147. Einstein, A., *The motion of elements suspended in static liquids as claimed in the molecular kinetic theory of heat*. Annalen Der Physik, 1905. 17(8): p. 549-560.

148. Lomakin, A. and D.B. Teplow, *Quasielastic light scattering study of amyloid beta-protein fibril formation*. Protein and Peptide Letters, 2006. 13(3): p. 247-254.
149. Buckler, K.J. and R.D. Vaughanjones, *Application of a New Ph-Sensitive Fluoroprobe (Carboxy-Snarf-1) for Intracellular Ph Measurement in Small, Isolated Cells*. Pflugers Archiv-European Journal of Physiology, 1990. 417(2): p. 234-239.
150. Seksek, O., et al., *Snarf-1 as an Intracellular Ph Indicator in Laser Microspectrofluorometry - a Critical-Assessment*. Analytical Biochemistry, 1991. 193(1): p. 49-54.
151. Blank, P.S., et al., *Cytosolic Ph Measurements in Single Cardiac Myocytes Using Carboxy-Seminaphthorhodafluor-1*. American Journal of Physiology, 1992. 263(1): p. H276-H284.
152. Austin, C. and S. Wray, *Extracellular Ph Signals Affect Rat Vascular Tone by Rapid Transduction into Intracellular Ph Changes*. Journal of Physiology-London, 1993. 466: p. 1-8.
153. Wieder, E.D., H.Y. Hang, and M.H. Fox, *Measurement of Intracellular Ph Using Flow-Cytometry with Carboxy-Snarf-1*. Cytometry, 1993. 14(8): p. 916-921.
154. Cody, S.H., et al., *Intracellular Ph Mapping with Snarf-1 and Confocal Microscopy . I. A Quantitative Technique for Living Tissues and Isolated Cells*. Micron, 1993. 24(6): p. 573-580.
155. Hunter, R.C. and T.J. Beveridge, *Application of a pH-sensitive fluoroprobe (C-SNARF-4) for pH microenvironment analysis in Pseudomonas aeruginosa biofilms*. Applied and Environmental Microbiology, 2005. 71(5): p. 2501-2510.
156. Ding, A.G. and S.P. Schwendeman, *Acidic Microclimate pH Distribution in PLGA Microspheres Monitored by Confocal Laser Scanning Microscopy*. Pharmaceutical Research, 2008. 25(9): p. 2041-2052.
157. Jin, J. and A.T. Jones, *The pH sensitive probe 5-(and-6)-carboxyl seminaphthorhodafluor is a substrate for the multidrug resistance-related protein MRP1*. International Journal of Cancer, 2009. 124(1): p. 233-238.
158. Ribou, A.C., J. Vigo, and J.M. Salmon, *C-SNARF-1 as a fluorescent probe for pH measurements in living cells: Two-wavelength-ratio method versus whole-spectral-resolution method*. Journal of Chemical Education, 2002. 79(12): p. 1471-1474.

159. Boldt, F.M., et al., *Real-time pH microscopy down to the molecular level by combined scanning electrochemical microscopy/single-molecule fluorescence spectroscopy*. Analytical Chemistry, 2004. 76(13): p. 3473-3481.
160. Li, L. and S.P. Schwendeman, *Mapping neutral microclimate pH in PLGA microspheres*. Journal of Controlled Release, 2005. 101(1-3): p. 163-173.
161. Kreft, O., et al., *Polymer microcapsules as mobile local pH-sensors*. Journal of Materials Chemistry, 2007. 17(42): p. 4471-4476.
162. Parton, R.G. and A.A. Richards, *Lipid rafts and caveolae as portals for endocytosis: New insights and common mechanisms*. Traffic, 2003. 4(11): p. 724-738.
163. Vecer, J., A. Holoubek, and K. Sigler, *Fluorescence behavior of the pH-sensitive probe carboxy SNARF-1 in suspension of liposomes*. Photochemistry and Photobiology, 2001. 74(1): p. 8-13.
164. Frangos, J.A., L.V. McIntire, and S.G. Eskin, *Shear-Stress Induced Stimulation of Mammalian-Cell Metabolism*. Biotechnology and Bioengineering, 1988. 32(8): p. 1053-1060.

Bibliography

1. Rene P. Schwarzenbach, P.M.G., Dieter M. Imboden, *ENVIRONMENTAL ORGANIC CHEMISTRY*. Second ed. 2003, Hoboken, New Jersey: John Wiley and Sons, Inc. 1313.
2. C.G. Caro, T.J.P., R.C. Schroter, W.A. Seed, *The MECHANICS of the CIRCULATION*. 1978, Walton Street, Oxford OX2 6DP: Oxford University Press. 527.
3. Saltzman, W.M., *Drug Delivery*, ed. K.E. Gubbins. 2001, 198 Madison Avenue, New York, New York 10016: Oxford University Press. 372.
4. B. Bonavida, G.R.G., H. Kirchner, L.J. Old, *TUMOR NECROSIS FACTOR/CACHECTIN and RELATED CYTOKINES*. 1988, P.O. Box CH-4009 Basel, Switzerland: S. Karger AG. 276.
5. D.L. Nelson, M.M.C., *Lehninger PRINCIPLES OF BIOCHEMISTRY*. Fourth ed. 2005, 41 Madison Avenue, New York, New York 10010: W.H. Freeman and Company.
6. M.P Lefranc, G.L., *THE IMMUNOGLOBULIN FactsBook*. 2001, 525 B street, Suite 1900, San Diego, California 92101-4495: Academic Press. 457.
7. Cazes, J., *Handbook of Thin-Layer Chromatography*. Second ed, ed. B.F. J. Sherma. Vol. 55. 1996, 270 Madison Avenue, New York, New York 10016: Marcel Dekker, Inc. 1104.
8. Hamley, I.H., *INTRODUCTION TO SOFT MATTER*. 2000, Baffins Lane, Chichester, West Sussex PO19 UD, England: John Wiley and Sons. 342.
9. J.H. Fuhrop, J.K., *MEMBRANES and MOLECULAR ASSEMBLIES: THE SYNKINETIC APPROACH*. Monographs in Supramolecular Chemistry, ed. F. J.F. Stoddart. Vol. 5. 1994, Thomas Graham House, Science Park, Milton Road, Cambridge CB4 4WF, UK: The Royal Society of Chemistry. 227.
10. Huglin, M.B., *LIGHT SCATTERING FROM POLYMER SOLUTIONS*. Physical Chemistry, ed. M.B. Huglin. Vol. 27. 1972, 111 Fifth Avenue, New York, New York 10003: Academic Press Inc. 885.
11. D.A. Lauffenburger, J.J.L., *RECEPTORS*. 1996, 198 Madison Avenue, New York, New York 10016: Oxford University Press, Inc. 365.

12. Hunter, R.J., *INTRODUCTION to MODERN COLLOID SCIENCE*. 1993, New York, New York: Oxford University Press Inc. 338.
13. J.M. Harris, S.Z., *POLY(ethylene glycol) CHEMISTRY and BIOLOGICAL APPLICATIONS*. ACS SYMPOSIUM SERIES, ed. S.Z. J.M. Harris. Vol. 680. 1997, 1155 16th Street, N.W., Washington DC 20036: American Chemical Society. 489.
14. B. Alberts, A.J., J. Lewis, M. Raff, K. Roberts, P. Walter, *MOLECULAR BIOLOGY OF THE CELL*. Fourth ed. 2002, 270 Madison Avenue, New York, New York 10016: Garland Science.

Appendices

Appendix A: Transmission Electron Microscopy Notes

note 1: Embedding resin is made by combining 13.75 grams of Embed 812, 8.5 grams

Araldite502 and stirring thoroughly without introducing bubbles. Then the resin is activated by stirring in as before 27.5 grams of DDSA and 0.7-0.9 grams of DMP-30.

note 2: The grids are prepared by sonicating them in technical grade acetone for one

minute followed by reagent grade acetone for one minute and finally in 95% ethanol. Decant ethanol and invert petri dish over filter paper until grids fall from the dish and have completely dried.

note 3: To make 50 ml of UA stain heat 50 ml DiH₂O to 60 degrees Celsius. Under fume

hood add 0.5 grams of UA (CAUTION) to the heated DiH₂O. Allow to cool and do not agitate before use.

note 4: Simple lead citrate is prepared by adding 0.01-0.04 grams of lead citrate to 10ml

of freshly boiled and cooled H₂O in a screw top vial. Then add 0.1ml of 10N NaOH and shake until lead dissolves.

About The Author

John Elliott received an AA in Computer Science from Saint Petersburg College in 2002. He continued his education and received a B.S. and M.S. in Chemical Engineering from the University of South Florida, in 2006. He then enrolled in the PhD program and has worked as a member of a multidisciplinary team working on a project entitled; “Diagnostic and Treatment Innovations for Mass Casualties” funded by the Department of Defense. He has presented his work at several conferences during his undergraduate and graduate studies. He presented at the 3rd and 4th Annual USF College of Engineering Undergraduate Research Symposium, 2005 and 2006. He has presented at the 16th and 19th USF Health Research Day, 2006 and 2009. He presented his graduate work at the Central Society for Clinical Research and Midwestern Section American Federation for Medical Research (CSCR/MWAFMR) Joint Meeting, 2009. He also presented at the Association of American Physicians and the American Society for Clinical Investigation, American Physicians Scientists Association (ASCI/AAP), (APSA) 2009, and at the 25th Southern Biomedical Conference, 2009. He plans to continue his research in targeted drug delivery after graduation.